PhD degree in Molecular Medicine

European School of Molecular Medicine (SEMM)

University of Milan and University of Naples "Federico II"

Faculty of Medicine

Disciplinary sector: Bio/11

New approaches to study DNA double-strand breaks genome-wide and in single-cells

Alessandro Galbiati

IFOM, Milan

Matricola n. R10784

Supervisor	Dr. Fabrizio d'Adda di Fagagna IFOM, Milan
Internal co-supervisor	Prof. Gioacchino Natoli Humanitas University, Milan
External co-supervisor	Prof. Jan Hoeijmakers Erasmus University MC, Rotterdam

Academic year 2017-2018

Table of contents

Figures Index

Notes about the figures

Figures 11-16 include my original work that has been published, so they are considered as adapted from Iannelli, Galbiati et al., Nature Communication, 2017.

Figures 22-31, 33-34, 37-49 describe my original work that has been published, so they are considered adapted from Galbiati et al., Aging Cell, 2017

Table Index

Note about the tables

Table 1 is my original work that has been published, so it is considered as adapted from (Vitelli et al. 2017).

List of Abbreviations

4-OHT	4-hydroxytamoxifen
53BP1	p53-binding protein 1
AGS	Aicardi-Goutières syndrome
AID	Activation-induced Cytidine Deaminase
ALT	alternative lengthening of telomeres
a-NHEJ	alternative non homologous end joining
APOBEC3B	Apolipoprotein B MRNA Editing Enzyme Catalytic Subunit 3B
ATM	ataxia-telangiectasia mutated
ATRIP	ATR-interacting protein
BER	base excision repair
BIR	Break-induced replication
BLESS	breaks labeling, enrichment on streptavidin, and next-generation sequencing
BLISS	Breaks Labeling *In Situ* and Sequencing
BrdU	5-bromodeoxyuridine
Bru-seq	bromouridine labeling and sequencing
CAGE	cap analysis gene expression
CCF	cytosolic chromatin fragments
CDC25	Cell Division Cycle 25A
CDK	cyclin-dependent kinase
CFS	common fragile site
ChIP	chromatin immunoprecipitation
CHK1	Checkpoint Kinase 1
CHK2	Checkpoint Kinase 2
c-NHEJ	classical non-homologous end joining
CRISPR-Cas9	clustered regulatory interspaced short palindromic repeats/CRISPR-associated protein 9
CYREN	cell cycle regulator of NHEJ
DAPI	4',6-diamidino-2-phenylindole
DDR	DNA damage response
DDRNA	DNA-damage response RNA
DI-PLA	DNA damage in situ ligation followed by proximity ligation assay
diRNA	DSB-induced RNA
DIvA	DSB Inducible via AsiSI
DNA-PKcs	DNA-PK-catalytic subunit
DNA-SCARS	DNA segments with chromatin alterations reinforcing senescence
DSB	double-strand break
EM	Electron microscopy
FBS	fetal bovine serum

GLB1	Galactosidase Beta 1
HJ	Holliday Junction
hnRPA	and heterogeneous nuclear ribonucleoprotein A
HP1	heterochromatin protein-1
HR	homologous recombination
IL-1	Interleukin-1
IL-6	Interleukin-6
IL-8	Interleukin-8
IR	ionizing radiation
KAT5	lysine acetyl transferase 5
MDC1	Mediator Of DNA Damage Checkpoint 1
MEF	mouse embryonic fibroblast
MMEJ	microhomology-mediated end joining
MMR	mismatch repair
MRN	Mre11-Rad50-Nbs1
mTOR	mechanistic target *of rapamycin*
NCS	neocarzinostatin
NER	nulceotide excision repair
NET-seq	native elongating transcript sequencing
NfKB	nuclear factor kappa-light-chain-enhancer of activated B cells
NGS	next generation sequencing
NHEJ	non-homologous end joining
NMDA	N-methyl-d-aspartate
OG	7,8-dihydro-8-oxo-2'-deoxyguanosine
OIS	oncogene induced senescence
PARP-1	*poly (*ADP ribose) polymerase 1
PDGF	Platelet-derived growth *factor*
PFA	paraformaldehyde
PIKK	phosphatidylinositol 3-kinase-like protein kinase
PLA	proximity ligation assay
POT1	Protection of telomeres protein 1
PRC1	Protein Regulator Of Cytokinesis 1
qPCR	quantitative PCR
qRT-PCR	quantiative Real Time PCR
RBP	RNA binding protein
RNA POLII	RNA polymerase II
RNA-seq	RNA sequencing
ROS	reactive oxygen species
RT	room temperature
SAHF	Senescent-associated heterochromatin foci
SASP	secretory phenotype of senescent cells
SA-β-gal	Senescence-associated-β-galactosidase
SDSA	synthesis-dependent strand annealing

SIPS	Stress-induced premature senescence
sncRNA	small non-coding RNA
SSB	single-strand break
TALEN	transcription activator-like effector nucleases
tDDRNA	telomeric DDRNA
TdT	terminal deoxynucleotidyl transferase
TERRA	Telomeric Repeat Containing RNA
TGFβ	Transforming growth factor beta
TIN2	TRF1-interacting nuclear factor 2
TLS	translesion synthesis
TOP1	topoisomerase I
TOP2B	topoisomerase IIβ
TPP1	POT1 and TIN2 organizing protein
TRF1	Telomeric Repeat Binding Factor 1
TRF2	Telomeric Repeat Binding Factor 2
TUNEL	terminal deoxynucleotidyl transferase dUTP nick end labeling
UV	ultraviolet
VEGF	Vascular endothelial growth facto
XLF	XRCC4-like factor
XRCC1	X-ray repair cross-complementing protein 1
XRCC4	X-ray repair cross-complementing protein 4
ZFN	Zinc-finger nuclease

1 Abstract

Genome integrity is constantly threatened by several stimuli either of exogenous or endogenous origin. Cells have evolved several DNA repair mechanisms to maintain their genetic information unaltered and a DNA damage response pathway (DDR) coordinates DNA repair with several cellular events including a cell-cycle arrest (checkpoint) until damaged DNA is repaired. When cells fail to repair DNA lesions, they undergo either apoptosis or cellular senescence, a permanent cell cycle arrest. DNA damage accumulation in cells has been linked to several events, such as cancer initiation and progression, organismal aging, cellular differentiation and reprogramming. More recently, it was also suggested to be a key event in transcriptional activation in response to specific stimuli or hormone-sensing.

Despite a clear role for DNA damage in several cellular processes, direct and sensitive tools for DNA damage detection have not been available until very recently, leaving important questions unanswered. The most used tools to detect DNA lesions rely on indirect, antibody-based recognition of DDR markers, either chromatin modifications or proteins accumulating at the damaged site. One of the main drawbacks of these tools is their low resolution: in fact, DNA damage-induced chromatin modifications spread for several kilobases around the lesion, preventing precise localization of the break position. This feature has hampered, in particular, studies on the impact of DNA damage on transcription. Here, I show the validation and optimization of BLESS and BLISS, two recently developed methods that allow genome-wide single-nucleotide resolution mapping of DNA double strand breaks (DSBs). Using these techniques, in combination with a multi-layered transcription profiling, I studied the impact of DSBs on transcription: in particular, I characterized a DDR-dependent transcription inhibition around the breaks. Differently, exploiting these same methods but in a distinct experimental setup, I observed that following macrophages LPS-stimulation, a transient wave of DSBs is induced at LPS-specific enhancers and it correlates with their transcription activation, thus suggesting a new molecular mechanism for LPS-induced macrophages activation that involves controlled DNA damage generation.

While representing an advancement over the commonly used methods to detect DNA damage, the recently developed tools such as BLESS and BLISS do not allow single-cell studies. Instead, here I describe a new method that I have developed, named DI-PLA, for the detection and imaging of DSBs in fixed cells and tissues. I applied this tool to address a long-standing question in the senescence field. Cellular senescence is fuelled by persistent DDR activation, however, due to the lack of direct DNA damage detection tools, it could not be distinguished whether it is associated with stable chromatin modifications or physical DSBs. Here I show that two types of senescent cells and cells in aged tissues retain physical DSBs associated with activated DDR markers. This observation is in agreement with data available in literature, that I could also recapitulate here, showing that senescent cells accumulate DNA damage at telomeres, where DNA repair is impaired.

Finally, I describe a modification of BLESS to discriminate between DSB bearing telomeres and deprotected telomeres; this approach has the potential to address important questions on the mechanisms of DDR activation at telomeres.

2 Introduction

Cells genomes are constantly subjected to a pletora of stimuli that can lead to DNA damage, which, in turn, alters the genomic structure and the genetic information encoded within. Although in the big scheme of things these modifications drive evolution, genome mantainance is needed for individual organisms survival and especially in stem cells, where genomic mutations are transferred to daughter, or differentiated cells. Genomic mutations emerging in non-dividing somatic cells may have less negative impact on individual survival compared to those happening in germ and stem cells, however it is well established that DNA mutations including DNA recombination events can drive oncogenesis and cancer progression (Hoeijmakers 2009, Jackson & Bartek 2009).

2.1 Types of DNA damage

It has been estimated that each cell in the human body can undergo up to ten thousands DNA lesions per day (Lindhal & Barnes 2000). Sources of genomic instability can be both endogenous and exogenous to the cell.

Exogenous sources can be divided in two main groups: physical and chemical insults. Physical genotoxic agents are ionizing radiation (IR) such as X-rays used for medical diagnoses, and the ultraviolet (UV) component of sunlight. Genotoxic chemical compounds are various, from food components, to cigarette smoke and anti-cancer drugs (Ciccia & Elledge 2010).

Endogenous damage to DNA can be either a random event, caused by by-products of cellular metabolism, or a scheduled event, such as that induced by a class of enzymes known as topoisomerases, that induce transient DNA breaks to release localized topological stress, or during meiosis, where genomic recombination is critical for a correct chromosome segregation in daughter cells (Borde & de Massy 2013).

This heterogenous plethora of stimuli can induce different types of DNA lesions. Informational DNA damage can be induced, for example, by oxidation reactions, and results

in nitrogen bases loss and mutation of the genetic information, as it is the case for cytosine deamination that is converted to uracil. DNA structural damage can be generated by single-strand breaks (SSBs) which are nicks in the sugar-phosphate backbone of one strand, by double-strand breaks (DSBs) which consist of breakages of both strands, and by DNA crosslinks, which are covalent links between the two strands. Structural damages are generated by UV, IR, programmed enzymatic cleavage and reactive oxygen species (ROS). Given the number and the variety of DNA lesions threatening the genome integrity every day, cells evolved complex mechanisms to detect, signal and repair damaged DNA. The study of these mechanisms, that were first discrovered in the 1960s, has generated an entire branch of research in the life sciences and has been highlighted in 2015 with a Nobel Prize for work in this field.

2.2 DNA damage repair

In order to repair different kind of lesions, cells have developed several DNA repair mechanisms.

2.2.1 Informational DNA damage repair

Informational DNA damage, is usually quickly repaired with fairly simple processes, well conserved from bacteria to human.

DNA alkylation damage is repaired by direct reversal, through enzymatic removal of the adduct (Mishina et al. 2006). DNA mismatch repair pathway (MMR) is responsible for correcting base substitutions, insertions and deletions occurring during DNA replication (Kunkel & Erie 2005): dedicated sensors recruit endonucleases, at the site of damage, to excise the mismatched region in the newly synthethized strand; then DNA polymerases fill-in the single strand DNA gap and finally DNA ligases seal the repaired DNA strand. A similar mechanism is employed by two other DNA repair mechanisms: nucleotide excision

repair (NER) and base excision repair (BER). NER is involved in the repair of bulky DNA adducts such as thymidine dimers induced by UV light, through removal of a tract of single strand DNA surrounding the lesion, which is then newly synthesized and sealed (Marteijn et al. 2014). Differently, BER takes care of single base oxidative damage, such as 7,8-dihydro-8-oxo-2'-deoxyguanosine (OG), which if not repaired, yields a transversion mutation (G:C to T:A) after DNA replication (David et al. 2007). BER acts through DNA glycosylases that remove the damaged base generating an abasic site, which is later cleaved by endonucleases, that induce a SSB, in turn repaired with the contribution of DNA polymerases and DNA ligases.

Another tool that cells have to deal with single-strand DNA lesions, is translesion synthesis (TLS). This is a DNA damage tolerance pathway that allows DNA replication past DNA lesions such as thymidine dimers or abasic sites, through the switch between the canonical DNA polymerases and specialized translesion polymerases that have low-fidelity on undamaged templates, but are particularly efficient at pairing nucleotides to the damaged bases (Waters et al. 2009).

2.2.2 Structural DNA damage

Breaks in the DNA backbone, in particular, DSBs, are particularly deleterious, because if unrepaired before cell division, can lead to the loss of critical amounts of genetic information and to dramatic chromosomal rearrangements. This type of lesion is repaired either with non-homologous end joining (NHEJ) or by homologous recombination (HR).

NHEJ is highly efficient and acts through a simple mechanism of DNA ends re-ligation, however, it is prone to mutations (Chang et al. 2017, Lieber 2010). DNA ends are recognized by KU proteins that recruit DNA-PK catalytic subunit (DNA-PKcs) which phosphorylates itself and several targets. One of DNA-PKcs targets is Artemis, a 3'-5' exonuclease that contributes to DNA ends blunting, to generate compatible DNA ends; to ensure proper DNA blunting, also specialized DNA polymerases (DNA pol X) are active to fill-in protruding

DNA ends. Notably, it has been reported that microhomology domains (<4 nucleotides protruding ends), may favour DNA ligation of DNA ends. Finally, DNA ligase IV, which is phosphorylated by DNA-PKcs, together with its binding partners X-ray repair cross-complementing protein 4 (XRCC4) and XRCC4-like factor (XLF), ligates DNA ends. NHEJ is active throughout the entire cell cycle and it is the most used mechanism to repair DSBs in mammals. There is also a redundant pathway, the alternative NHEJ (a-NHEJ), also known as backup NHEJ or microhomology-mediated end joining (MMEJ) (Bennardo et al. 2008), that is active in the absence of the proteins needed for the classical NHEJ and requires 2-20 nucleotides protruding DNA ends. This mechanism relies on a different subset of proteins, among which DNA ligase 3, XRCC1 and DNA polymerase θ seem to play a major role.

Differently from NHEJ, HR is an error-free mechanism that uses a sister chromatid as template for repair, thus it can occur only during the S and G2 phases of the cell cycle (Heyer et al. 2010, San Filippo et al. 2008). The HR process begins with the endonuclease activity of the MRE11-RAD50-NBS1 (MRN) complex in cooperation with CtIP (Clerici et al. 2005, Sartori et al. 2007). This initial step generates short 3' protruding ends that are further processed by the 5'-3' exonuclease activity of exonucleases such as BLM and Exo1 (Mimitou & Symington 2008). Once DNA ends have been resected, ssDNA is immediately coated by the RPA complex, which is then displaced by RAD51 which, in cooperation with BRCA2, coats the DNA generating a nucleoprotein filament (White & Haber 1990). RAD51 is able to catalyse the invasion of the intact homologous duplex DNA, which is used as a template to repair the DSB: the invading filament generates a structure known as D-loop. According to the canonical HR pathway, the free DNA end of the invading DNA is then extended by a DNA polymerase and, finally, the invading DNA end is ligated to the other end of the DSB generating a structure named Holliday Junction (HJ): this is resolved by endonucleases and helicases to obtain two intact and repaired DNA molecules. Alternatively to the pathway just described, synthesis-dependent strand annealing (SDSA) and Break-

induced replication (BIR), are other HR sub-types that lead to the resolution of the D-loop but do not require endonuclease activity.

The repair pathway choice is a fine-tuned mechanism, still not completely understood (Gobbini et al. 2013, Symington & Gautier 2011). However, it is clear that the Ku70/Ku80 heterodimer plays a major role, promoting c-NHEJ and inhibiting the recruitment of HR components to the DNA ends. The 5'-3' resection is also very well regulated and is inhibited by RIF1 and 53BP1 in G1 phase (Clerici et al. 2014, Daley & Sung 2013, Panier & Boulton 2014), while it is promoted by CtIP and BRCA1 in G2 to favour HR (Cruz-García et al. 2014). Recently, a new protein named CYREN, has been described as negative regulator of NHEJ in S/G2 (Arnoult et al. 2017).

2.3 The DNA damage response pathway

The DNA Damage Response (DDR) pathway is a complex signalling cascade that coordinates the DNA repair process with a broad set of events (Figure 1) (Ciccia & Elledge 2010, Polo & Jackson 2011). In the presence of DNA breaks, the DDR is activated and transiently arrests cell-cycle progression to prevent the propagation of altered genomic information to the daughter cells.

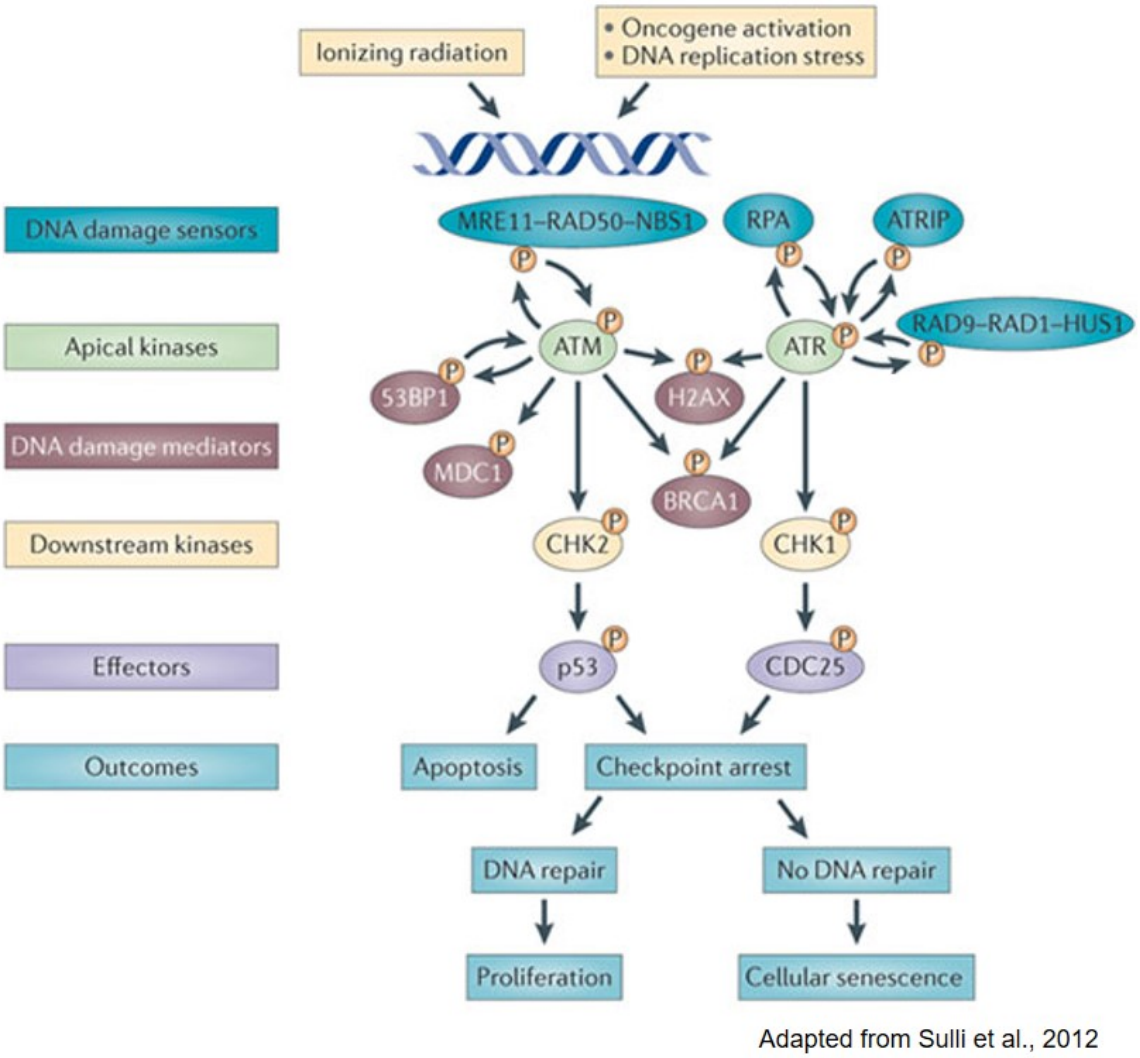

Figure 1 - The DNA damage response pathway.

DNA breaks are recognized by DNA damage sensors including the MRN complex and the RPA complex. These sensors recruit the apical kinases ATM and ATR, which is also bound by ATRIP and the RAD9-RAD1-HUS1 complex. The apical kinases, in turn, phosphorylate (P) the histone variant H2AX on Ser139 (γH2AX) to recruit DNA damage mediators such as MDC1, 53BP1, BRCA1, which boost the signal, providing a positive feedback loop on the apical kinases. The diffusible downstream kinases CHK2 (mainly phosphorylated by ATM) and CHK1 (mainly phosphorylated by ATR) spread the signal to several effectors including p53 and CDC25, which coordinate several cellular events to ensure that the DNA damage is not propagate to daughter cells. The first response is a transient cell cycle arrest until DNA is repaired (DNA damage checkpoint); failing to repair DNA damage, and prolonged DDR activation leads, instead, to cell death by apoptosis or cellular senescence.

The DDR is triggered by DNA damage sensors recognizing the lesion, mainly the MRE11-NBS1-RAD50 (MRN) complex, poly (ADP ribose) polymerase 1 (PARP-1), KU and RPA (that coats ssDNA). Once the lesion has been recognized by sensor proteins, these activate three key protein kinases of the phosphatidylinositol 3-kinase-like protein kinase (PIKK) family: ATM and DNA-PK, mainly in response to DSBs, and ATR, which is activated in

response to ssDNA, which might be generated by SSBs, or by resection at DSBs in S/G2 phase, or under replication fork stalling. In particular, ATM is recruited to DSBs by MRN, where it is acetylated by lysine acetyl transferase 5 (KAT 5) (Sun et al. 2005), and then undergoes an autophosphorylation reaction on serine 1981, causing its activation and monomerization (Shiloh 2006). DNA-PKcs is instead recruited to the break site by KU and undergoes an activating autophosphorylation on the five residues within the PQR cluster (also known as the S2056 cluster). ATR activation relies on the presence of ATR-interacting protein (ATRIP) and ssDNA bound to RPA. In addition to ATR, other protein complexes are recruited to ssDNA, including the RAD17 containing complex, which loads the heterotrimeric 9-1-1 complex (RAD9, RAD1, HUS1) on the DNA, where it contributes to boosting ATR kinase activity (Parrilla-Castellar et al. 2004).

One of the first targets of the three apical kinases is the histone variant H2AX, which is locally phosphorylated in *cis* at serine 139 (named γH2AX): this phosphorylation can spread up to 1Mb away from the DNA lesion site (Iacovoni et al. 2010). γH2AX acts as recognition mark for the DSBs and promotes the retention of other DDR proteins at the site of damage (Martin et al. 2009, Rogakou 1998). This also results in the formation of cytologically detectable nuclear foci that contain the DDR proteins recruited to the site of damage (Lukas et al. 2011). Thus, immunostaining or chromatin immunoprecipitation (ChIP) with antibodies against γH2AX and other DDR proteins are commonly used tools to detect the presence of DSBs in cells or at specific genomic loci. However, this indirect way to detect DSBs is associated with several drawbacks, as discussed in the section 2.5.

It is well established that γH2AX plays a key role in the DDR cascade, and it fuels the signal amplification by recruiting the DDR mediator MDC1 (mediator of DNA-damage checkpoint 1). MDC1 directly binds γH2AX through its C-terminal domain and further promotes MRN and ATM accumulation at the DSB (Spycher et al. 2008), leading to an increase in the concentration of several DDR proteins at the DSB site, thus generating a positive feedback

loop that amplifies DDR signalling. MDC1 also recruits chromatin re-modellers which favour DDR signal amplification and DNA repair. Really Interesting New Genes (RING) domain-containing E3 ubiquitin ligases enzymes, RNF8/RNF168, target H2Ak15 (Mailand et al. 2007) and favour the recruitment of methyltransferases, which in turn target the histone H4k20 (Mallette et al. 2012). These chromatin modifications promote the recruitment of the DNA damage mediators p53 binding protein 1 (53BP1) and BRCA1 to the site of break (Bekker-Jensen et al. 2005, Meerang et al. 2011, Panier et al. 2012, Wang & Elledge 2007). Moreover, the SWI/SNF histone re-modelling complex has been found to be quickly recruited to the DSBs, where it relaxes chromatin and evicts nucleosomes in the immediate vicinity of the exposed DNA ends, promoting resection and repair (Dong et al. 2015, Morrison et al. 2004).

Ultimately, the activated apical kinases, phosphorylate CHK2 (the main target of ATM) and CHK1 (the main target of ATR), which are downstream protein kinases, that can diffuse in the nucleoplasm, where they target their substrates, among which are the cyclin-dependent kinases (CDKs), responsible for the so-called DNA damage checkpoints (see next section). In case of unrepairable DNA damage, prolonged activation of the DDR checkpoints can induce cell death (apoptosis) or a permanent cell cycle arrest known as cellular senescence (see section 2.6).

2.3.1 DNA damage checkpoints

DNA damage checkpoints are transiently activated to arrest cell cycle proliferation until the DNA lesion has been repaired. To do so, DDR modulates cyclin-dependent kinases (CDKs) that are responsible for transitions between cell cycle phases (Branzei & Foiani 2008, Sancar et al. 2004). There are three distinct checkpoints regulating cell cycle progression: the G1/S, the intra-S, and the G2/M.

2.3.1.1 G1/S checkpoint

The G1/S checkpoint prevents the transition to S phase in the presence of DNA damage, by inhibiting the initiation of DNA replication. In the presence of DNA damage in G1, CHK2 and CHK1 phosphorylate the phosphatase CDC25A, which is consequently activated and inhibits CDK2, preventing, in this way, the CDK2-dependent phosphorylation of CDC45, that is necessary to initiate replication.

Moreover, ATM, ATR, CHK1 and CHK2 target p53 at different phosphorylation sites as well as the ubiquitin ligase MDM2: this leads to inhibition of p53 nuclear exportation and inhibition of MDM2-dependent p53 degradation (Sancar et al. 2004). The accumulation of p53 in the nucleus leads to activation of p53 targets, including p21, which binds to and inhibits the S-phase-promoting CDK2-cyclinE complex, thus contributing to the maintenance of G1/S arrest. Furthermore, p21 binds to the CDK4-cyclinD complex, thus preventing pRB phosphorylation, which is necessary for the activation of E2F, a transcription factor which promotes cell cycle progression (Bartek et al. 1996).

2.3.1.2 The intra-S checkpoint

The intra-S checkpoint is triggered by unrepaired DNA damage that escapes the G1/S checkpoint and generates a block in replication or by DNA damage encountered during the S phase.

The intra-S checkpoint acts by slowing down replication forks and by blocking replication origin firing. This is obtained by multiple pathways, one being the CDC25-dependent CDK2-CyclinE inhibition, as described for the G1/S checkpoint, while another is the ATR-dependent Cdc7/Dbf4 inhibition: both pathways ultimately lead to the inhibition of Cdc45, which is necessary to promote the replication origin firing (Costanzo et al. 2003).

2.3.1.3 The G2/M checkpoint

The G2/M checkpoint prevents the entrance in mitosis in the presence of DNA damage encountered during G2 phase or escaped from the previous checkpoints. ATM and ATR, through phosphorylation of CHK2 and CHK1, inhibit the entry into mitosis by down-regulating CDC25A and up-regulating Wee1, which together control CDK1-Cyclin B activity, responsible for G2/M transition (Yarden et al. 2002).

2.4 DNA damage and RNA

Transcription is the cellular function that converts the genetic information of the DNA in RNA molecules: protein-coding RNAs are then translated into functional proteins, while noncoding-RNA directly exert their functions (Shandilya & Roberts 2012).

DNA damage and RNA metabolism are intertwined at several levels (Capozzo et al. 2017, D'Alessandro & d'Adda di Fagagna, 2016). Transcription has classically been considered an endogenous source of genomic instability, however recent reports have suggested a role for RNA in DDR signalling and DNA repair and even a role for DDR proteins and DNA damage in transcription modulation.

2.4.1 RNA as a source of DNA damage

Transcription can cause DNA damage in several ways, although, compared to traditional sources of DNA damage, transcription-induced damage is less frequent. The transcriptional machinery can collide with the DNA replication machinery either when they are moving in opposite directions or when they are moving in the same direction (Helmrich et al. 2013). To limit the collision events, transcription levels are reduced during the S phase, however, genes larger than 800kb require more than one complete cell cycle to be transcribed and exhibit DNA damage hotspots known as common fragile sites (CFS) (Helmrich et al. 2011). The collision between DNA replication and transcription bubbles results in localized

torsional stress, which can cause DNA polymerases to stall or collapse, resulting in a DNA lesion. Moreover, as consequence, also RNA polymerases get stalled, favouring the formation of so-called R-loops: hybrid duplexes formed between the nascent RNA and the template DNA strand, that leave the non-transcribed DNA strand in a single-stranded state, which can undergo DNA damage (Reaban et al. 1994). Moreover, single strand DNA can form noncanonical structures depending on its sequence and base content, such has single-stranded hairpins or loops in genes containing stretches of the same trinucleotide repeat (Petruska et al. 1996, Zhao & Usdin 2015), and G-quadruplex in GC-rich regions (Duquette et al. 2004), which are stable structures that induce RNA polymerase II (RNA POL II) pausing and promote the stability of the R-loops, in a positive feedback loop (Belotserkovskii et al. 2010). Prevention of R-loops formation is necessary to avoid the negative effects of their accumulation. Under physiological conditions, the nascent RNA is promptly bound by several proteins that control its nuclear export and splicing, impeding the formation of RNA:DNA hybrids. Moreover, prokaryotes and eukaryotes have RNAseH enzymes, which are specialized in degrading RNA hybridized to DNA molecules; mutations in the RNAseH2 enzymes have been linked, in humans, to the Aicardi-Goutières syndrome (AGS), a neurological inflammatory disorder, which resembles a congenital viral infection and is associated with accumulation of ribonucleotides in the DNA (Crow et al. 2006).

2.4.2 RNA contribution to DNA repair and DDR signalling

Besides the detrimental effects of transcription-induced torsional stress and DNA:RNA hybrids on genome integrity, several reports show a positive role of transcription in DNA repair and genome maintenance. In fact, it has been reported that actively transcribed regions, are repaired faster than non-transcribed regions, despite being DNA damage hotspots (Aguilera 2002, Mellon et al. 1986). Indeed, transcription-coupled repair, is a conserved NER pathway, that actively removes DNA lesions which block RNA POL II (Hanawalt & Spivak 2008). Moreover, in mammalian cells, high-resolution mapping of

proteins bound to regions surrounding the DSBs showed that RNA POL II is not disengaged from the DNA upon damage (Iacovoni et al. 2010). Intriguingly, occupancy peaks of the main subunit of RNA POL II, POLR2A, spatially exclude histone occupancy (including γH2AX), which could be due to the transcription machinery ability to evict nucleosomes, thus favoring DNA repair (Iacovoni et al. 2010). As additional evidence for a role of transcription machinery in DNA repair, it has been reported that DSBs falling in actively transcribed regions are preferably repaired by homologous recombination, possibly because the chromatin modifications normally associated with transcription favor DNA end resection (Aymard et al. 2014).

Several transcription factors and RNA binding proteins (RBPs) have also been reported to localize at DNA damage sites, where they are phosphorylated by ATM or ATR (Izhar et al. 2015). One example, is the splicing regulator FUS, that is recruited to DSBs, where it seems to play a role in promoting DNA repair by both HR and NHEJ (Mastrocola et al. 2013). This hypothesis is supported by the observation that amyotrophic lateral sclerosis patients harboring familial mutations in FUS genes have increased genomic instability (Wang et al. 2013).

Recently, a role for RNA itself, has been integrated into the canonical model of DDR signaling.

Upon DNA damage, small non-coding RNAs (sncRNAs), named DNA-damage response RNAs (DDRNAs) and DSB-induced RNA (diRNA), have been reported to accumulate at DSBs in humans, drosophila, plants and mice (Sharma & Misteli 2013). DDRNAs are generated by DROSHA and DICER cleavage of a longer precursor RNA, and together with the RNA precursor participate in DDR signaling (Francia et al. 2012), favoring 53BP1 and MDC1 recruitment (Francia et al. 2016). Recent evidence shows that the long precursor RNA is produced at the site of damage by RNA POLII, that is recruited to the DSB through the interaction with MRN complex (Michelini et al, in press). Another group, independently

identified a role for diRNAs in promoting DNA repair by HR (Gao et al. 2014, Wei et al. 2012).

2.4.3 The impact of DNA damage on transcription

Despite the recent observations reporting that noncoding RNAs are produced at site of break, it has also been known for a while an overall inhibitory effect of DSBs on pre-existing transcription. This mechanism prevents aberrant transcripts to be produced at DNA damaged loci, which could alter cell homeostasis (Adam & Polo 2014, Svejstrup 2010).

Recent reports have shown some apparently contrasting data on the mechanism of DSBs-dependent transcription inhibition. In particular, it has been reported that generation of a DSB within a gene body, results in transcription inhibition of the damaged gene, in a DNA-PK dependent manner, through the exclusion of RNA POLII from the gene body and promoter (Pankotai et al. 2012). However, the transcription inhibition affects only the damaged locus and not the neighboring genes, and this observation was also recapitulated *in vivo*, in mice, through the genome-wide analysis of transcriptome alterations induced by the endonuclease I-PpoI (Kim et al. 2015). Differently, a cluster of DSBs induced in an exogenous sequence, repressed the activity of a distal promoter in *cis*, in an ATM-dependent manner, through chromatin condensation, for several kilobases (Shanbhag et al. 2010). ATM was reported to promote H2A ubiquitination, which in turn promotes PRC1 recruitment at DSBs, which is a well-known repressor of gene expression. The contrasting views of these two reports might be explained by the peculiar features of DNA loci where DNA damage was induced: in fact, while Shanbag and colleagues induced several breaks close to an exogenous sequence, Kim and colleagues, generated single DSBs at endogenous loci mainly within ribosomal genes. As it is also described in the Results section, in collaboration with Dr. Iannelli and colleagues, I have contributed to show that DSBs induced at endogenous sites promote an ATM-dependent transcription inhibition of the gene bearing the DSB and

of the neighbouring genes, although the transcription inhibition is progressively weaker at increasing distance from the DSB (Iannelli et al. 2017).

ATM-dependent transcription inhibition has also been reported for RNA polymerase I upon DNA damage induced in rDNA (Harding et al. 2015, Kruhlak et al. 2007).

Although the effect of DNA damage on transcription inhibition is in apparent contrast with the observation of RBPs recruitment at DSBs and *de novo* transcription involved in DDR signaling and DNA repair, it has been proposed that a first PARP-dependent chromatin relaxation, required for the accessibility of DDR proteins at the DSBs sites, might lead to the recruitment of RNA POLII and transcription factors at DNA damage sites (D'Alessandro & d'Adda di Fagagna 2016). This event may precede the ATM-dependent chromatin condensation required for further amplification of DDR signalling and transcription silencing.

In support of a role for DSBs in chromatin relaxation and consequent transcription activation, several observations emerged in the last few years showing stimuli-dependent, scheduled, transient DNA damage in several physiological processes, leading to transcription of specific promoters or enhancer.

One of the first observations connecting DNA damage to transcription activation was topoisomerase IIβ (TOP2B) accumulation in β-estradiol-sensitive pS2 promoter following hormone stimulation, along with proteins associated with DDR such as PARP1, KU, and DNA-PK (Glass & Rosenfeld 2006). Here, TOP2B induces transient DNA breaks that are necessary for transcriptional activation of the genes activated by the hormone.

DNA damage-mediated transcription activation has also been reported in cultured primary neurons stimulated by various molecules that induce synapses-like signals, such as *N*-methyl-D-aspartate (NMDA), potassium chloride, and bicuculline (Madabhushi et al. 2015). Also in this case, transcription activation depends on transient DSBs induced by TOP2B

activity at gene promoters and enhancers, that leads to RNA POLII releasing from a paused state.

Another report showed TOP1-induced SSBs at androgen-receptor binding sites, in prostate cancer cells activated by dihydrotestosterone to activate enhancers and promoters (Puc et al. 2015b). Here, TOP1 induces nicks that are readily recognized and repaired by the DDR and DNA repair pathways. Indeed, knockout of the DDR or DNA repair pathways abolishes androgen-induced transcription activation. Similarly, in estrogen-sensitive breast cancer cells, hormone-induced gene activation is mediated by APOBEC3B. This enzyme, is part of the AID/APOBEC family and catalyzes the cytidine to uracil conversion on DNA, which is recognized by the BER pathway: a transient DSB is generated to remove the lesion and this is required to recruit RNA POL II at promoters (Periyasamy et al. 2015).

Several models could explain the role of DNA damage-mediated transcription activation (Vitelli et al. 2017). The simplest explanation is that DSBs are needed to release topological stress that accumulates in actively transcribed genes, in order to promote RNA polymerase processivity: this is in agreement with the observations that TOP1 and TOP2B are involved in most of the cases described here. Another hypothesis is that DSBs are needed to induce chromatin reorganization and modifications that favour transcription, as it has been observed in the case of APOBEC3 (Periyasamy et al. 2015). Nevertheless, while the appearance of transient breaks, leading to nucleosome-free zones and chromatin modifications may favour transcription initiation, prolonged and unrepairable DNA damage is detrimental and can lead to transcription inhibition. In collaboration with Dr. Vitelli, as described in the Result section, I have contributed to find a new molecular basis for LPS-induced macrophage activation through transient DSB induction at specific enhancers.

2.5 DNA damage detecting methods

The most commonly used methods to detect DNA damage rely on antibody recognition of chromatin modifications associated with DNA damage or proteins involved in DDR signalling. With this strategy, it is possible to detect, by immunostaining, the accumulation of DDR foci or map, by ChIP, the genomic regions enriched with the DDR marker of choice. However, an increasing amount of evidence suggests that H2AX is not uniformly distributed in the genome, and heterochromatin is, to an extent, resistant to H2AX phosphorylation (Cowell et al. 2007, Kim et al. 2007, Lafon-Hughes et al. 2013). These observations, suggest the existence of genomic regions where DNA damage is repaired with low efficiency, which might bear "invisible" DNA damage. Moreover, in a particular cell type, astrocyte, our group has observed the lack of a full DDR response upon IR-induced DNA damage generation (Schneider et al. 2012). On the other hand, other labs reported the accumulation of γH2AX in the absence of DSBs (de Feraudy et al. 2010) and some groups have suggested DNA damage-independent functions for γH2AX (Fernandez-Capetillo et al. 2003, Rybak et al. 2016a, Tu et al. 2013). Thus, the use of DDR markers as a proxy for DSB marker might be biased or misleading. As an additional drawback, ChIP against DDR markers provide low resolution in DNA damage mapping, since DNA damage markers spread away from the lesions for up to 1 Mb, preventing precise identification of the DNA breaks positions. This feature has negatively impacted the studies on the correlation between DSBs and transcription events. In fact, differently from DNA damage mapping methods, several tools widely used by the scientific community to study transcription alterations, such as differential expression of genes with RNA sequencing (RNA-seq) (Wang et al. 2009), different genome-wide transcription start activities with cap analysis gene expression (CAGE) (Shiraki et al. 2003), bromouridine labeling and sequencing (Bru-seq) (Paulsen et al. 2014), and native elongating transcript sequencing (NET-seq), generate high sensitivity, single-nucleotide resolution maps of the transcriptome.

To circumvent the problem of DNA damage mapping, several studies exploited the generation of controlled DSBs at known loci. This approach was pioneered in the budding yeast *Saccharomyces cerevisiae* by inducing DNA cleavage in the *MAT* gene locus with the endogenous endonuclease HO (Kramer et al. 1994) and was subsequently implemented in mammalian cells through the use of restriction enzymes (Massip et al. 2010, Monnat Jr et al. 1999) or engineered nucleases (such as zinc-finger nucleases (ZFNs), transcription activator–like effector nucleases (TALENs), or clustered regulatory interspaced short palindromic repeats/CRISPR-associated protein 9 (CRISPR/Cas9) (Ghezraoui et al. 2014)) to introduce DSBs at specific sites in the genome. Although these studies have provided valuable insights into DDR mechanisms, they had the great disadvantage of being limited to individual loci—often within an ectopic DNA sequence, limiting their impact on transcriptomic studies.

However, in the last five years, prompted by the limitations of DNA damage detection methods mentioned above, by an increasing interesting in DSB mapping associated with gene editing methods, and by the reduced costs of next-generation sequencing (NGS), several groups have independently developed techniques to map different types of DNA lesions at genome-wide level (**Table 1**). All of these methods provide high-resolution information about the genomic locations of the lesions (most of them at a single-nucleotide level), making them particularly suitable for use in conjunction with established methods of transcriptomic analysis. The recently developed DSB-mapping methods have been used to profile genome-wide CRISPR/Cas9-induced DSBs (Kim et al. 2015a, Shi et al. 2016, Wang et al. 2015), to generate genome-wide maps of DNA lesions induced by genotoxic drugs such as etoposide (Baranello et al. 2014) and aphidicolin (Crosetto et al. 2013a) and to map DSBs that occur during physiological processes such as B cell development (Chiarle et al. 2011), or transcription-associated DSBs in neural stem/progenitor cells (Schwer et al. 2016).

Although each method has its own peculiarities, they can be divided into two main categories based on their main purposes: those used to map unrepaired (and thus exposed) DNA ends, and those used to track repaired DSBs (either in situ or by translocation).

2.5.1 Genome-Wide Mapping of exposed DNA Ends

Several methods have been developed to map exposed DNA in a population of fixed cells, thus generating a snapshot of any DNA breaks at a given moment.

The general strategy adopted by these methods is to enzymatically tag DNA ends in fixed cells, either by adding biotinylated dNTPs by terminal deoxynucleotidyl transferase (TdT) (Baranello et al. 2014, Grégoire et al. 2016, Hoffman et al. 2015, Leduc et al. 2011) or by DNA ends blunting and ligation to a biotinylated DNA oligonucleotide (Canela et al. 2016, Crosetto et al. 2013b, Lensing et al. 2016). Once DNA ends have been tagged, genomic DNA is recovered, fragmented and enriched with streptavidin beads that bind the biotinylated tags ligated to DSBs. The enriched material is then suitable for NGS sequencing. All these methods, are affected by general drawbacks, being prone to background signals (which may also be artificially induced while performing cell manipulations), and are limited by the efficiency of DNA ends tagging. Few experimental data are available to compare the different methods, although, as described in the Results section, I have contributed to compare the BLESS method with other published tools. Moreover, I developed a strategy to analyze the DNA captured by BLESS, by quantitative PCR (qPCR), which was neither implemented in the originally published protocol (Crosetto et al. 2013a), nor in any of the other published methods so far.

Among these methods, a special mention goes to BLISS (Iannelli et al. 2017, Yan et al. 2017), which is a development of the original BLESS protocols, and allows DSB mapping starting with a few thousand cells, 1.000 times less than the number of cells required by all the other methods developed so far: this is a great advancement since it allows DSB mapping

on precious samples and reduces the background signals generated by random DNA breaks in a population of cells.

2.5.2 Genome-Wide Mapping of Repaired DNA Double-Strand Breaks

The other approach to map DSBs at high resolution is to track their repair. The simplest strategy is to perform whole-genome sequencing at high coverage, assuming that a repaired DSB will result in a mutation (Veres et al. 2014). However, this is a very indirect strategy, that cannot distinguish bewteen SSBs and DSBsm and it is expensive due to the requirement of very high sequencing coverage. Two other methods (Tsai et al. 2014, Wang et al. 2015), instead, track *in-situ* the rejoining of two broken ends: cells are transfected with short double-stranded oligonucleotides that can be ligated by the endogenous DNA repair machineries at the DSBs sites. The genomic DNA is then recovered and sequenced and the exogenous DNA sequence marks the position of the DNA breaks. A third strategy to track the repair of DSBs has been developed by Dr. Frederick Alt lab, at Harvard, that applied it to study DSB generation and repair in a number of biological problems including transcription-associated breaks and development of mature lymphoid cells (Dong et al. 2015, Hu et al. 2015, Meng et al. 2014, Schwer et al. 2016). It requires cells transfection with an engineered nuclease that induces “prey” DSBs which can recombine with “bait” endogenous DSBs. Then, genomic DNA is recovered and sequenced: junction points between the prey sequence and other genomic regions mark the DSBs (Chiarle et al. 2011, Hu et al. 2016).

These techniques, while having lower sensitivity compared with methods mapping exposed DNA ends, are less prone to background signals and are unlikely to detect low-frequency random DNA breaks, since they can only map DNA repaired regions. Clearly, the drawback of these techniques is that they cannot be used for precise time-course experiments (for example to monitor the DSBs induced by a stimulus) or to study unrepairable DSBs. Moreover, these methods require cell transfection, thus limiting their application to a subset of experimental setups.

The techniques mentioned here will certainly be applied in the future to further characterize the links between DNA damage and transcription, due to the possibility to map at single nucleotide resolution both DSBs and transcription events. As described in the result section, I have applied BLESS and BLISS to study the inhibitory role of DSBs in transcription (Iannelli et al. 2017) and a positive role of transient DSBs in the LPS-induced enhancer activation in macrophages (Vitelli et al., in preparation).

Method	Applied to map breaks induced by:	Strategy	Key steps	Advantages	Disadvantages
dDIP/DBrIC	Restriction enzyme	Map unrepaired DSBs	Fixing/embedding of cells in agarose plugs Enzymatic tagging of DNA ends Purification of DNA Enrichment and PCR amplification (or in vitro transcription) of tagged DNA fragments Sequencing	Have the highest sensitivity among methods for mapping DNA breaks Provide snapshots of unrepaired DSBs (possibility to perform time-course experiments)	Are prone to background signals Require efficient tagging of DSBs May induce DSBs by cell manipulation
Break-seq	Hydroxyurea				
DSB-seq (SSB-seq)	Etoposide				
End-seq	Endonucleases, RAG				
BLESS	Aphidicolin, endonucleases				
DSBCapture	Endonucleases, RAG				
BLISS	Etoposide, CRISPR/Cas9				
Digenome-seq	CRISPR/Cas9	Map unrepaired DSBs in vitro	Digestion of genomic DNA in vitro with the endonuclease of interest Sequencing	Endonuclease cut sites are not masked by the epigenomic context	Has high sequencing costs
Whole-genome sequencing	Endonucleases	Map the repaired DNA lesion that produced a mutation	Sequencing at high coverage	Maps any DNA lesion that produces a mutation	Has high sequencing costs
GUIDE-seq	CRISPR/Cas9	Map repaired DSBs in situ	Cell transfection with DNA oligonucleotides Purification of genomic DNA PCR amplification of insertion points Sequencing	Has the highest sensitivity among methods for mapping DNA breaks Has less background signal than other methods	Require cell transfection dsODN/IDLV sequence and length are critical for efficient insertion Require cells proficient in DNA repair
IDLV	CRISPR/Cas9				
HTGTS/LAM-HTGTS	Endonucleases, RAG, AID, transcription-associated breaks	Map repaired DSBs that produced rearrangements	Transfection with endonucleases to generate bait DSBs Purification of genomic DNA PCR amplification of translocated bait DSBs Sequencing	HTGTS is the method applied in most studies Have high sensitivity in proximity to the bait DSB	Are biased by bait DSB position Require cell transfection or a highly recurrent DSB
TC-seq	AID				

Table 1 - Methods for high-resolution mapping of DNA damage.

Techniques are grouped on the basis of the strategy used. Because of space limitations, when one method was used to map DSBs induced by different types of exogenous nucleases (such as restriction enzymes, ZFNs, TALENs, and CRISPR/Cas9), we did not list all of them. Abbreviations: AID, Activation-induced deaminase; BLESS, breaks labeling, enrichment on streptavidin, and next-generation sequencing; BLISS, breaks labeling in situ and sequencing, CRISPR/Cas9, clustered regulatory interspaced short palindromic repeats/CRISPR-associated protein 9; DBrIC, DNA break immunocapture; dDIP, damaged DNA immunoprecipitation; DSB, double-strand break; dsODN, double-stranded DNA oligodeoxynucleotide; GUIDE-seq, genome-wide

unbiased identification of DSBs enabled by sequencing; HTGTS, high-throughput genome-wide translocation sequencing; IDLV, integrase-defective lentiviral vector capture; LAM-HTGTS, linear amplified-mediated high-throughput genome-wide translocation sequencing; PCR, polymerase chain reaction; RAG, recombination-activating gene; SSB, single-strand break; TALEN, transcription activator–like effector nuclease; TC-seq, translocation capture sequencing; ZFN, zinc-finger nuclease.

2.5.3 DNA damage detection in single cells

The general drawback of the methods described above to map DSBs position on the genome is their sensitivity limit, and the impossibility to apply them to single-cells studies, as in the case of DNA repair kinetics after random DNA damage induction.

For long time, the only alternatives to immunofluorescence for DNA damage detection have been terminal deoxynucleotidyl transferase dUTP nick end labeling (TUNEL), which allows DNA ends labeling with fluorescent nucleotides and detection (Shmuel 1992), and COMET assays (Olive et al. 1991).

TUNEL relies on the enzymatic modification of DNA exposed ends, with the addition of biotinylated dNTPs: this allows physical detection of DSBs, by imaging, with fluorophore-conjugated anti-biotin antibodies.

In the COMET assay, a suspension of single cells is mixed with agarose and spread onto a microscope glass slide. Cells are then lysed and DNA unwinding by electrophoresis is carried out at a specific pH. When subjected to an electric field, the DNA fragments migrate out of the cell, towards the anode, appearing like a 'comet'. The size and shape of the comet and the distribution of DNA within the comet correlate with the extent of DNA damage. However, heterogenous types of DNA lesions migrate differently, confounding the results and resulting in unreliable comparisons between comets induced from different DNA damaging stimuli (Olive & Banath 2006).

Since, both methods have low sensitivity and are prone to artifacts, their application is usually limited to study massive DNA damage, such as that induced by apoptosis. Here, I will describe a method that I have developed to detect physical DNA breaks in single-cells (see Results section) (Galbiati et al. 2017).

2.6 Cellular senescence

Cellular senescence was first formally described more than half a century ago, by Hayflick and colleagues, as the progressive and permanent loss of proliferative potential of human somatic cells (Haflick & Moorhead 1961). Cellular senescence has been connected since long ago to cancer suppressor and aging (Campisi 2013, Deursen 2014), and more recently, it has implicated in cellular reprogramming (Mosteiro et al. 2016), embryonic development (Muñoz-Espìn et al. 2013), wound healing (Demaria et al. 2015), and a wide range of diseases, often associated with aging (Erusalimsky & Kurz 2005, Martin & Buckwalter 2003, Noureddine et al. 2011, Schafer et al. 2017). In addition to the permanent growth arrest, several features and molecular markers are used to identify senescent cells. However, no single characteristic is uniquely associated to the senescent state. Vice versa, not all senescent cells display the whole array of markers that have been identified so far. Thus, senescent cells are generally identified by a constellation of characteristics.

2.6.1 Senescent-associated features

2.6.1.1 Growth arrest

The senescent growth arrest is the first feature that identifies cellular senescence. The senescent arrest is sustained and maintained by at least two major tumor suppressor pathways: the p53/p21 and p16INK4a/pRB pathways. It is indeed distinct from quiescence, because it cannot be reverted by appropriate mitogenic stimuli and changes in culturing conditions. However, senescent cells that do not express p16INK4A can resume growth after inactivation of p53 (Beauséjour et al. 2003). Cellular growth arrest can be detected by measuring the incorporation rate of 5-bromodeoxyuridine (BrdU) in replicating DNA (see section 3.10), or by monitoring the expression levels of proliferation markers, such as Ki-67.

2.6.1.2 Morphology

The morphology is altered when cells undergo senescence: cells are flattened and the size is increased, sometimes enlarging more than two-fold compared to non-senescent cells (Hayflick 1965).

2.6.1.3 Senescent-associated β-galactosidase

Lysosomal β-galactosidase, encoded by the GLB1 gene, is normally active at acidic pH 4.5. Its expression level increases during senescence, so its activity can be detected also in suboptimal conditions, at pH 6 (Dimri et al. 1995). Senescence-associated-β-galactosidase (SA-β-gal) was the first marker to permit the detection of senescent cells in tissues, and it is still one of the most used to markers for senescent cells (see section 3.11).

2.6.1.4 Senescent-associated DNA damage foci

The DDR activation can be detected in the form of persistent DNA damage foci, which contain proteins that are associated with the DDR, like γH2AX, the MRN complex, 53BP1, ATM pS1981 and MDC1 (Di Micco et al. 2006, Fagagna et al. 2003, Rodier et al. 2011, Sedelnikova et al. 2004). These foci lack ssDNA and DNA repair proteins associated with HR, such as RPA and RAD51 (Rodier et al. 2011). It has been hypothesized that these structures might not be sites of damaged DNA per se, rather stable chromatin alterations resulting from damage (without an underlying lesion), which are necessary to reinforce senescence, termed DNA-SCARS (Rodier et al. 2011). This hypothesis could not be verified due to the lack of tools to detect physical DNA breaks, however with the method that I developed, and here described (DI-PLA), I could prove that these persistent DDR foci correspond to physical DNA breaks (Galbiati et al. 2017). This is consistent with the observation that DNA damage in senescent cells preferentially accumulates at telomeres (Fumagalli et al. 2012, Hewitt et al. 2012), where DNA repair is inhibited (see section 2.7).

DDR plays an essential role in both senescence initiation and maintenance (d'Adda di Fagagna et al., 2003; Herbig et al., 2004; Sedelnikova et al., 2004; von Zglinicki et al., 2005). Indeed, transient inactivation of ATM, alone or together with ATR, and combined CHK1 and CHK2 inactivation, leads to escape from senescence and re-entry into the S-phase of the cell cycle. Several stimuli that induce senescence also induce DDR activation (see section 2.6.2), such as ROS, produced by mitochondria (Correia-Melo & Passos 2015, Correia-Melo et al. 2016). Moreover, long term activation of the checkpoint gene p21 induces mitochondrial dysfunction and production of highly reactive ROS, which are well known inducers of DNA lesions (Passos et al. 2010). In particular, telomeric DNA, being rich in guanine is be particularly susceptible to oxidative modifications, and, being resistant to DNA repair, leads to a persistent activation of the DDR checkpoint, enforcing cell senescence through a positive feedback loop.

2.6.1.5 Senescent-associated secretory phenotype

Senescent cells undergo widespread changes in protein expression and secretion, developing what is known as secretory phenotype of senescent cells (SASP) (Coppé et al. 2010). SASP signature can vary depending on stimuli and tissue type, however it includes cytokines (such as IL-1, IL-6), chemokines (IL-8), growth factors (such as TGFβ and VEGF) and extracellular proteases (such as matrix metalloproteinases). These components can bind receptors on the same cell that secreted them (autocrine effect) or on the surrounding cells (paracrine effect), fuelling the senescence state (Acosta et al. 2013).

Cytokines that are part of the SASP facilitate the removal of senescent cells by attraction of phagocytic immune cells. This function proved to be particularly important for tissue repair: wounding induces senescence in resident fibroblasts and endothelial cells; consequently senescent cells secret PDGF, which promotes myofibroblasts differentiation and favour the kinetics of wound closure (Demaria et al. 2015). Senescent induction and subsequent macrophage-dependent clearance also elicits tissue remodelling, explaining the role of senescence-induction during embryonic development (Muñoz-Espìn et al. 2013).

However, when senescent cells accumulate, such as during aging or in age-associated diseases, the chronic pro-inflammatory environment induced by SASP appears to be detrimental. This model is strongly supported by the observation that organisms that do not display a typical aging phenotype, are highly efficient in the clearance of senescent cells, such as salamander (Yun et al. 2015). Moreover, genetically engineered mice where it is possible to selectively induce clearance of senescent cells, display a delay in the onset of age-associated disorders (Baker et al. 2011), extended median lifespan (Baker et al. 2016) and show reduced chemotherapy side effects (Baar et al. 2017, Demaria et al. 2016).

Despite a growing interest in modulating the SASP to uncouple the tumour-suppressor role of senescent-associated growth arrest from the detrimental pro-inflammatory response induced by the senescent-associated secretory phenotype (Birch & Passos 2017), it is not yet clear what are the key regulators involved in SASP modulation. DDR is certainly involved in SASP regulation: in particular ATM signalling has been linked to NFkB activation, one of the major transcription factors regulating SASP-associated components (Fumagalli & d'Adda di Fagagna 2009, McCool & Miyamoto 2012, Rodier et al. 2009). mTOR activity has also been connected to SASP production (Laberge et al. 2015). Furthermore, recent evidence suggests that cytosolic chromatin fragments (CCF) that are extruded from the nucleus in senescent cells (Ivanov et al. 2013), induce the activation of the cGAS-STING pathway, an innate immune response pathway which senses double-stranded DNA in the cytosol, and leads to secretion of SASP components (Glück et al. 2017).

2.6.1.6 Senescent-associated heterochromatin foci (SAHF)

In some types of senescent cells, the heterochromatin is reorganized into discrete foci, that are proposed to enforce cellular senescence by suppressing the transcription of genes involved in proliferation (Narita et al. 2003, Zhang et al. 2007). SAHFs are detected by the preferential binding of DNA dyes, such as 4',6-diamidino-2-phenylindole (DAPI), and the presence of heterochromatin-associated histone modifications like H3K9me3 and

H3K27me3, and proteins, like heterochromatin protein-1 (HP1). SAHFs are mainly generated as a consequence of spatial reorganization of the existing heterochromatin, rather than expansion of heterochromatin domains (Chandra et al. 2012). Chromatin reorganization is facilitated by the senescent-associated reduction in nuclear lamin B1 that is normally associated with heterochromatin domains (Sadaie et al. 2013).

2.6.2 Cellular senescence inducers

There are several stimuli that are known to induce cellular senescence, most of them leading to DNA damage, although with different mechanisms. Interestingly, it has been recently reported that most of the genes that are transcriptionally altered when cells undergo senescence, are specific for cell type and the senescence inducer (Hernandez-Segura et al. 2017).

Mechanism leading to cellular senescence activation in the embryo, and involved in tissue repair and cell reprogramming will need further investigation, although it is known that they rely on p21 (Muñoz-Espìn et al. 2013) or p16 (Demaria et al. 2015, Mosteiro et al. 2016) to enforce the senescence phenotype. Differently, much more studies are available on other types of cellular senescence.

2.6.2.1 Replicative senescence

Replicative senescence was the first cell senescent phenotype described as the result of in vitro replicative exhaustion of human fibroblasts (Hayflick 1965). During DNA replication, telomeres are incompletely replicated, losing between 50 and 200 bp during each S phase (see section 2.7.4). Therefore, in the absence of specialized telomere maintenance mechanisms (which, indeed, are normally absent in somatic cells), each DNA replication cycle, reduces the number of telomeric repeats (see further discussion in section 2.7.4). Telomere attrition limits the proliferative lifespan of many human cells types and causes

cells to undergo replicative senescence with short telomeres (Harley et al. 1990). In fact, progressive telomere shortening ultimately leads to the recognition of the DNA ends by ATM and ATR, with the consequent appearance of DDR foci. Interestingly, it is not the average length of telomeres, rather the presence of a single (or few) critically short telomere that triggers senescence (Hemann et al. 2001, Joice et al. 2014). Indeed, ectopic expression of the enzyme telomerase, which is capable of elongating telomeres, bypasses the replicative senescence arrest (Bodnar et al. 1998).

2.6.2.2 Stress-induced premature senescence

The Stress-induced premature senescence (SIPS) is a response to an external stress coming from the cell environment (Toussaint et al. 2000). Repeated or acute non-lethal doses of these stresses are required to efficiently induce accumulation of stress-induced senescent cells. However, cells undergoing SIPS share many cellular and molecular features with replicative senescent cells.

UV and IR-induced senescence. UV light, and in particular UVB (280-320 nm), is known to provoke oxidative stress through the generation of highly reactive ROS that could be the cause of UV-induced SIPS (De Magalhães et al. 2002). Indeed, free radical scavengers were shown to remove ROS and reduce the harmful effects of UVB irradiation, resulting in a significant delay in senescence establishment (Ho et al. 2005). IRs are also inducers of SIPS: IR-treatment creates DSBs resulting in the activation of the ATM-p53-p21 pathway within few hours from treatment (Fumagalli et al. 2012). Differently from replicative senescence, SIPS is not associated with telomeric shortening and IR does not appear to accelerate telomere erosion. Moreover, telomerase expression in different types of normal diploid cells exposed either to high doses of IR, UV or hydrogen peroxide, did not prevent senescence induction. Cumulatively, these data indicate that DNA lesions can induce senescence and that telomere dysfunction can occur irrespectively of length (Gorbunova et al. 2002). Additional support to this hypothesis comes from length-independent telomere

damage observed in post-mitotic tissues such as neurons of aged baboon (Fumagalli et al. 2012) and mice (Chow & Herrup 2015, Jurk et al. 2012).

Culture shock-induced senescence. Another interesting example of SIPS comes from the biological behaviour of primary mouse embryonic fibroblasts (MEFs). Explanted MEFs stop dividing after only 15-30 cell divisions when placed in culture: this observation is not consistent with the replicative senescent onset, since MEF telomeres are too long to become critically short in so few replication cycles. However, it has been shown that oxygen sensitivity can trigger SIPS: in fact MEFs do not senesce in physiological (3%) oxygen levels, but do so in 20% oxygen (Parrinello et al. 2003). Moreover, mild hyperoxia has been correlated with enhanced telomere shortening, likely due to accumulation of ROS-induced DNA damage at telomeres (Saretzki et al. 2003, von Zglinicki et al. 1995).

DNA damaging drug-induced senescence. Several chemiotherapic drugs used to treat cancer, can induce SIPS, without affecting telomere length (Schmitt 2003). Notable examples are the DNA-intercalating doxorubicin, the topoisomerase I inhibitor camptothecin, the topoisomerase II inhibitors Adriamycin and etoposide, the cross-linking agent cisplatin and the anti-metabolite cytarabin. Recent observations connected chemotherapic drugs-induced senescence to chemotherapy side-effects such as fatigue and cancer relapse (Demaria et al. 2016).

2.6.2.3 Oncogene-induced senescence

Oncogenes are particular genes that have the potential to transform cells when they accumulate mutations or their expression level is altered. Normal cells respond to many oncogenes by triggering the so-called oncogene-induced senescence (OIS). This results in the generation of a biphasic response: activated oncogenes prompt an initial burst of cellular hyperproliferation, that is followed by senescence (Di Micco et al. 2007). Indeed, OIS has been shown to prevent cancer development *in vivo* both in humans and in mouse models

(Dankort et al. 2007, Grandori et al. 2003, Lazzerini Denchi et al. 2005, Michaloglou et al. 2005)

OIS was first described in cells expressing the constitutively activated form of RAS, which is responsible for transducing mitogenic signals and promoting cell growth, proliferation and survival (Serrano et al., 1997). Similarly, activation or upregulation of other components of the RAS signalling cascade, such as RAC1, RAF, MOS, MEK or the loss of the inhibitor of the RAS pathway, PTEN, can induce cellular senescence (Evan & d'Adda di Fagagna 2009). At the molecular level, upregulated expression of oncogenes leads to aberrant DNA replication, which in turn generates DNA lesions due to discontinuous replicative fork progression and altered single-stranded DNA generation, which eventually triggers DDR activation (Bartkova et al. 2006). Moreover, RAS activation induces re-replication, an event known to cause DNA damage and DDR activation, and to increase the number of active origins (Di Micco et al., 2006). Similarly, upregulation of MYC oncogene boosts the number of contemporary active DNA replication origins leading to DNA replication-associated DNA damage (Dominguez-Sola et al. 2007). Oncogene activation in proliferating cells, also induces formation of SAHFs, dependent on p16 upregulation and DNA replication-stress associated ATR activation (Di Micco et al. 2011, Narita et al. 2003, Serrano et al. 1997, Sulli et al. 2012).

Despite a clear role for OIS senescence in tumour suppression, by preventing the proliferation of cells bearing an activated oncogene, more and more reports show a role for cellular senescence in favouring tumour onset and progression (Campisi 2013). This "dark side of senescence", is fuelled by some, but not all (Wang et al. 2011), components of the SASP, such as VEGF (Coppé et al. 2006) which promotes tumor-driven angiogenesis, or IL-6 and IL-8 that promote epithelial-to-mesenchymal transition in pre-malignant epithelial cells and nonaggressive cancer epithelial cells (Laberge et al. 2012).

Thus, as already discussed above, cellular senescence has a dual role in preventing uncontrolled proliferation leading to cancer, but also in favouring tumour growth of surrounding cells.

2.6.3 Cellular senescence and aging

Cellular senescence is considered a major hallmark of organismal aging *in vivo* (López-Otín et al. 2013, Rossiello et al. 2014). Senescent cells have been reported *in vivo* in human skin fibroblasts (Dimri et al. 1995), in mouse stem and somatic cells (Hewitt et al. 2012, Sedelnikova et al. 2004) and in baboons skin, brain and liver (Fumagalli et al. 2012, Herbig et al. 2006). Moreover, cells that express senescence markers are also found in age-related pathologies, including osteoarthritis, atherosclerosis and chronic lung diseases (Birch et al. 2015, Erusalimsky & Kurz 2005, Martin & Buckwalter 2003, Noureddine et al. 2011, Price et al. 2002, Schafer et al. 2017).

At a molecular level, telomere shortening is certainly involved in tissue aging in various tissues (Tümpel & Rudolph 2012). Consistently, loss of telomerase function, in mice, causes senescence and aging in various tissues (Ferrón et al. 2004, Rudolph et al. 1999, Satyanarayana et al. 2004). Moreover, elongation of telomeres by reactivation of telomerase is sufficient to eliminate the degenerative phenotypes in multiple organs observed in telomerase knockout mice (Jaskelioff et al. 2011).

However, as discussed above, dysfunctional telomeres can induce senescence irrespectively of their length: in support of this, accumulation of chronic DNA damage has been shown to mimic tissue aging by White and colleagues (White et al. 2015).

The causative effect of senescence on ageing is supported by different observations. In fact, p16 expression increases with age in the stem and progenitor cells of the mouse brain, bone marrow and pancreas, where it suppresses stem-cell proliferation and tissue regeneration. Consistently, the age-related tissue regeneration decline can be prevented by the lack of p16 expression (Janzen et al. 2006, Molofsky et al. 2006). Similarly, a genetically engineered

mouse model in which p16-expressing cells are specifically cleared, shows a delay in age-related pathologies, delayed tumorigenesis and preserved organ function, leading to a longer median lifespan (Baker et al. 2011, 2016). The role of senescence in aging is believed to be related to the chronic inflammation induced by the SASP.

These observations have led the scientific community to identify new interventions to target senescence as a therapy against ageing and age-related diseases (Chang et al. 2016, Soto-Gamez & Demaria 2017, Zhu et al. 2015). Effort has been put by both companies and academics to identify anti-ageing drugs, also called senolytics: 14 compounds have been described so far, including small molecules, antibodies and peptides, and have been successfully applied in mouse models of physiological ageing (Baar et al. 2017), osteoarthritis (Jeon et al. 2017), fibrotic pulmonary disease (Schafer et al. 2017), and more. However, caution is necessary since, while these senolytic drugs selectively kill senescent cells, they are not effective against all types of senescent cells. Moreover, the long-term effects on young tissues have not yet been adequately investigated.

2.7 Telomeres

2.7.1 Telomere structure

Telomeres are nucleoprotein structures at the end of the linear chromosomes (Figure 2). They are made of three main components: long stretches of DNA tandem repeats (TTAGGG in vertebrates), telomere-associated proteins (known as the shelterin, a six-subunits complex) and non-coding RNA (Telomeric repeat-containing RNA, TERRA). The length of human telomeres is typically 9-15 Kb, whereas laboratory mice strains chromosomes have longer telomeres, ranging from 10 to 60 Kb. Chromosome ends have a 3'-protruding single-stranded G-rich overhang, typically 50-300 nucleotides long, also named G-tail or G-overhang (O'Sullivan & Karlseder 2010). The overhang is generated through post-replicative 5'-3' resection of the C-rich strand by APOLLO and EXO1 nucleases (Wu et al.

2012) and it has a key role in telomere maintenance. In fact, it functions as a primer for the telomerase complex, which adds newly synthesized repeats to the telomere end (Greider & Blackburn 1987, see section 2.7.4). Moreover, the G-tail can invade the preceding double-stranded DNA region in a lasso-like structure, known as the T-loop. The formation of T-loop is mediated by the DNA binding protein TRF2, and it contributes to telomere protection as a cap that masks the telomeric DNA ends to the DDR machinery (Griffith et al. 1999). T-loops were first detected by electron microscopy (EM) analysis *in vitro* (Griffith et al. 1999), however, *in vivo* detection of T-loops has been hampered by technical challenges. Only recently, super-resolution microscopy allowed imaging of T-loops in cells (Doksani et al. 2013), although with steep requirements in the imaging machinery required for the experiments. In the Result section, I will describe how DI-PLA can be adapted to easily assess T-loop formation *in situ*. Moreover, with a complementary approach based on BLESS, I will suggest an unprecedented strategy to distinguish between intact telomeres, DNA damage bearing telomeres, and uncapped telomeres (see Results section 4.4.2).

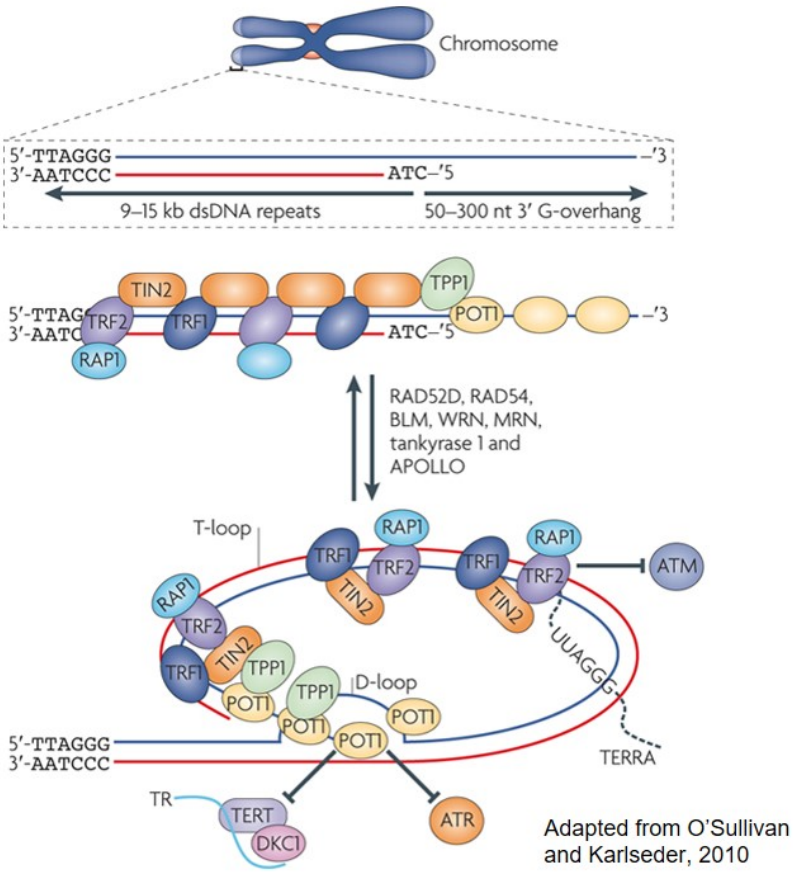

Figure 2 - Structure of the human telomeres. Structure of the human telomeres.

Human telomeres are nucleoprotein complexes consisting of kilobases of TTAGGG repeats, with a 3' G-rich overhang, an RNA component called TERRA and the shelterin proteins TRF1, TRF2, RAP1, TIN2, TPP1 and POT1. These factors help the formation of a protective structure at chromosome ends, the T-loop. Activation of ATM is inhibited by TRF2, while ATR is inhibited by POT1. Telomerase (TERT-DKC1-TR) is probably inhibited by the shelterin proteins.

2.7.2 Telomeric binding proteins

Telomeres are associated to a protein complex named shelterin (Palm & de Lange 2008), consisting of six components: TRF1 and TRF2 (telomeric-repeat-binding factor 1 and 2), POT1 (protection of telomeres 1), RAP1 (also known as TERF2IP, telomeric repeat binding factor 2 interacting protein), TIN2 (TRF1-interacting nuclear factor 2) and TPP1 (POT1 and TIN2 organizing protein). However, besides the shelterin complex, which represents the core of key proteins involved in telomere maintenance, almost 200 proteins have been associated with different aspects of telomere biology (Déjardin & Kingston 2009, Grolimund et al. 2013)

TRF1 and TRF2 directly associate as homodimers with the double-stranded telomeric DNA, through their MYB domain. TRF1, has been proposed to allow efficient replication of telomeres (Sfeir et al. 2009). In fact, the G-rich telomere strand is a substrate prone to fold into four-stranded G-quadruplex structures, that interfere with DNA replication. In the absence of TRF1, replication stress induced by G-quadruplex activate an ATR dependent checkpoint. TRF1 prevents ATR signalling and in cooperation with the helicases BLM and RTEL1 allows DNA replication at telomeres. Moreover, TRF1 acts as a negative regulator of the telomere length, probably by controlling the access of telomerase, together with several partners including Tankyrase I, TIN2 and TRF2 (Ancelin et al. 2002, Kim et al. 1999, Smith & de Lange 2000, Smogorzewska et al. 2000, van Steensel & de Lange 1997). Recently, another protein associated with telomeres, but not part of the shelterin complex, named TZAP has been discovered as a new regulator of telomere length, independent from TRF1 functions (Li et al. 2017).

TRF2 maintains the T-loop structure and is mainly implicated in chromosome end protection, by preventing DNA repair activity at telomere ends, which would result in ATM activation and end-to-end fusions (Doksani et al. 2013, Griffith et al. 1999, van Steensel et al. 1998). However, it has been proposed that telomeres may adopt an intermediate state where the T-loop is lost and DDR is activated without leading to end-to-end fusions due to the presence of sufficient shelterin proteins (Cesare et al. 2009)

POT1 coats the single-stranded overhang using two oligonucleotide/oligosaccharide binding folds and inhibits the ssDNA recognition by the ATR-dependent DDR. Moreover, it acts as a regulator of telomere length, switching between an inhibitory and a promoting role in telomerase recruitment at DNA ends (Baumann & Cech 2001, Baumann & Price 2011, Colgin et al. 2003).

RAP1 binds to TRF2 and is involved in the silencing of subtelomeric genes and telomere-length regulation (Lustig et al. 1990, Martinez et al. 2010).

TIN2 is essential to the overall integrity of the shelterin complex as it links TPP1/POT1 heterodimer to TRF1 and TRF2, and stabilizes TRF1 and TRF2 association to telomeric DNA (Frescas & De Lange 2014; Ye et al. 2004a,b).

Telomeres and subtelomeres are enriched for heterochromatic markers, such as H3K9me3, H4K20me3 (Benetti et al. 2007). In addition, human and mouse subtelomeres are heavily methylated through the activity of DNA methyltransferases (Schoeftner and Blasco, 2009). This chromatin context has an inhibitory role on telomerase activity, and contributes to subtelomeric gene silencing. However, in contrast with these observations, recent evidence has shown that telomeres are transcribed by RNA POL II, giving rise to a class of long noncoding RNAs containing telomeric repeats called TERRA.

2.7.3 Telomeric transcripts

TERRAs molecules are transcribed from the subtelomeric regions toward the chromosome ends and consist of subtelomeric-derived sequences and G-rich telomeric repeats (Azzalin & Lingner 2008, Schoeftner & Blasco 2008). TERRAs are transcribed by RNA Polymerase II starting from promoters located in the subtelomeric regions through the telomeric repeats (Nergadze et al. 2009), although it has also been suggested that TERRAs are mainly produced at a single promoter on chromosome 18 (de Silanes et al. 2014). TERRAs are polyadenylated and very heterogenous in size (Porro et al. 2010). Their expression level is cell cycle regulated, with a decrease in S phase to allow DNA replication, it is positively regulated by TRF1, which interacts with RNA POL II, and negatively regulated by heterochromatin and telomere length (Schoeftner and Blasco, 2008).

A physiological role for TERRAs has been described in regulating telomere length, by functioning as a telomerase inhibitor (Redon et al. 2010), and in promoting heterochromatinization (Deng et al. 2010). It has also been proposed that TERRA promotes telomere protein composition changes during cell cycle: TERRA regulates the RPA-to-POT1 switch during S phase to allow DNA replication and subsequently telomere protection (Flynn et al. 2011). TERRAs are also involved in favouring DNA ends processing: at deprotected telomeres RNA promotes the physical interaction between the lysine demethylase LSD1 and MRE11, thus favouring MRE11 nucleolytic processing of uncapped telomeres (Porro et al. 2010). Furthermore, TERRAs transcripts are upregulated in the absence of TRF2 (Porro et al. 2014)

Recently, it has been reported that dysfunctional telomeres are transcribed to generate telomeric DDRNAs (tDDRNAs) and their precursors, that are necessary for DDR activation at deprotected telomeres (Rossiello et al. 2017).

2.7.4 Mechanisms of telomere maintenance

DNA replication of linear chromosomes suffers from the end-replication problem: at the end of the chromosome, on the lagging strand the DNA replication machinery is unable to copy the last bit of DNA sequence. Thus, at each cell division telomeres are shortened by 100-300bp due to the so-called end-replication problem, combined with the exonucleolytic processing needed to generate the G-rich overhang (Harley et al. 1990). This progressive telomere shortening leads to critically short telomeres that lose their protective structure and induce replicative senescence (see section 2.6.2.1), although it is not yet clear what is the critically short length necessary to activate the DDR signalling (O'Sullivan & Karlseder 2010).

In most cases, the telomere shortening is counteracted by the telomerase complex, which consists of the reverse transcriptase catalytic subunit (TERT), the RNA component (TERC) that is used as a template to elongate the G-rich telomeric DNA strand, dyskerin that helps the assembly of the complex and TCAB1, involved in the localization of telomerase to the Cajal Bodies, where the telomerase complex is assembled (Cohen et al. 2007, Greider & Blackburn 1987, Mitchell et al. 1999, Venteicher et al. 2009). In humans, telomerase is not active, with the exception of activated lymphocytes, adult stem cells, germ line, and embryonic cells (Wright et al. 1996). Telomerase inactivation, despite possibly reducing the organism longevity (Tomás-Loba et al. 2008), is an important tumour suppressor mechanism: indeed, most cancer need to activate telomerase to survive.

Recently, non-telomeric functions for mammalian TERT have been suggested, which include the regulation of global chromatin dynamics, stem cell proliferation and transcription of developmentally regulated genes (Masutomi et al. 2005, Park et al. 2009). Moreover, telomerase is excluded from the nucleus upon oxidative stress and it has been proposed a role for telomerase in mitochondria protection under mild oxidative stress (Ahmed et al. 2008).

Approximately 10–20% of human cancers maintain their telomeres by a telomerase independent pathway known as the alternative lengthening of telomeres, or ALT (Cesare & Reddel 2010, Lovejoy et al. 2012). ALT is essentially dependent on HR: when the 3′ overhang is recognized by the HR machinery, it can invade other telomeric DNA, which can be used as a template for DNA replication. Telomeres in ALT cells are heterogeneous in length; some of them are very short, but they can reach up to 100 kb. A particular feature of ALT cells, is the presence of extrachromosomal telomeric DNA, predominantly in the form of partially single stranded circles (C-circles) (Henson et al. 2009).

2.7.5 Telomeres and the DDR

Telomeres resemble, at their essence, a single DSB end, however they are not recognized by the DDR machinery. This is mostly due to the shelterin complex, since the activation of the DDR apical kinases ATM and ATR is inhibited by TRF2 and POT1, respectively (Denchi & de Lange 2007, Karlseder et al. 2004). TRF2 knockout leads to DDR activation, including H2AX phosphorylation, ATM activation, 53BP1 recruitment at telomeres and activation of downstream kinases CHK2 and p53 (Bae & Baumann 2007, Benarroch-Popivker et al. 2016, Takai et al. 2003) and results in dramatic end-to-end fusions by c-NHEJ (van Steensel et al. 1998). Paradoxically, a component of the c-NHEJ pathway, the Ku70–Ku80 complex, is constitutively present at telomeres (d'Adda di Fagagna et al. 2001), where its main function is to inhibit both a-NHEJ and HR events (Sfeir & de Lange 2012). However, POT1 plays the main role in preventing ATR activation at telomeres, by coating the ssDNA and excluding RPA binding (Gong & de Lange 2010), apparently with the help of TERRA and heterogeneous nuclear ribonucleoprotein A (hnRNPA) (Flynn et al. 2011).

This view of irreparable DNA damage at telomeres has been recently challenged by a HR-dependent and an a-NHEJ-dependent mechanisms for DSB repair at telomeres (Doksani & de Lange 2016, Mao et al. 2016). Internal telomeric DSBs generated by engineered nucleases were reported to activate DDR signaling in mice and human cells, and undergo DSB repair.

However, repair was observed only in proliferating cells, while senescent cells with persistent DDR activation failed to repair the endonuclease-induced damage (Mao et al. 2016), possibly as a consequence of senescence-associated heterochromatinization which inhibits DNA repair.

3 Materials and Methods

3.1 Cell culture

All cell lines used here were grown under standard tissue culture conditions (5% CO_2, 37°C). BJ cells (human diploid fibroblasts, The American Type Culture Collection, ATC) were grown in MEM supplemented with 10% foetal bovine serum (FBS), 1% L-glutamine, 1% non-essential amino acids, 1% sodium pyruvate. BJ hTERT cells, are a BJ-derived cell line that stably expresses human telomerase reverse transcriptase (Fumagalli et al. 2012).

MEFs CRE-ER TRF2$^{flox/flox}$ GFP-TRF1 (Rossiello et al. 2017), were grown in DMEM supplemented with 10% foetal bovine serum and 1% glutamine; they are MEF-derived cell line which stably express the fusion protein TRF1-eGFP, both TRF2 alleles are loxP-flanked, and that stably expresses the CRE recombinase fused to the oestrogen receptor (ER); for induction, cells were grown in the presence of 4-hydroxytamoxifen (600 nM, 4-OHT Sigma cat. no. H7904) for 48 hours, to allow CRE-ER to translocate into the nucleus and to generate the TRF2$^{-/-}$ cells.

DIvA (AsiSI-ER-U20S) cells were cultured in Dulbecco's modified Eagle's medium (DMEM, Gibco) without phenol red, supplemented with glutamine, pyruvate, HEPES and 10% foetal bovine serum (FBS). Cells were selected on a semi regular basis with puromycin at a final concentration of 1 μg/ml. For AsiSI-dependent DSB induction, cells were treated with 300 nM 4-OHT for 4h.

Hela111, a kind gift of Dr. Evi Soutoglou were cultured in DMEM without phenol red, supplemented with 10% Fetal Calf Serum TET system, 1% Glutamine, 0.1mM sodium pyruvate. These cells contain an I-SceI site stably integrated in the genome, flanked on one side by on array of 256 repeats of the LacO sequence, and on the other side by a unique sequence.

Raw 264.7 were grown in DMEM supplemented with 10% FBS, 1% glutamine. To induce the inflammation response Lipopolysaccharides from E. coli (100ng/mL LPS, Sigma L2654) was added to the cell culture medium.

U2OS NBS1-GFP (Lukas et al. 2004), a kind gift from Jiri Bartek, were cultured in DMEM supplemented with 10% FBS, 1% Glutamine. Cells were selected with puromycin at a final concentration of 1 μg/ml.

3.2 Animal and treatments

Mice used to generate Figures 37-38 were bred and maintained under pathogen-free condition at the Scripps Research Institute and were handled according to Institutional Animal Care and Use Committee guidelines. After exposure to ionizing radiation, tissues were collected and freshly frozen in dry ice, embedded in OCT (Sakura), a cryprotective embedding medium. Tissues were then sectioned, mounted on glass slides and stored at -80 °C until use.

Mice used to generate Figures 48-49 (C57BL/6J) were purchased from Charles River Laboratories (Saint-Constant, Quebec), by Christian Beausèjour at Canadian Institute of Health Research, Montreal; *in vivo* manipulations were approved by the Comité Institutionnel des Bonnes Pratiques Animales en Recherche (CIBPAR) of CHU-Ste-Justine. Immediately after sacrificed, mouse tissues were freshly frozen on dry ice and embedded in OCT compound. Cryosections of 10μm thickness were mounted on glass slides previously treated with 1% gelatin and 0.05% chromo alum, dried at ambient temperature and then stored at −80 °C until use.

3.3 Ionizing radiation

Ionizing radiation (IR) was used to generate DNA damage exogenously in several experiments. IR refers to highly energetic particles or waves that can detach (ionize) at least one electron from an atom or molecule. This event leads to DNA damage in the form of base damage, single strand breaks (SSB), double strand breaks (DSB) and DNA crosslinks. Here, to induce DNA damage with IR in cells, an X-ray generating machine (Faxitron, X-Ray

Corporation) was used. The Gray (Gy) is the International System of Units of absorbed radiation dose, where 1 Gy is the absorption of 1 joule of radiation energy by 1 kilogram of matter.

Mice used to generate Figures 37-38 were subjected to 5Gy total body irradiation at the Scripps Reasearch Institute, San Diego.

3.4 Laser-induced DNA damage

Laser micro-irradiation is an alternative tool to ionizing irradiation used to induce DNA damage, that allows sub-nuclear resolution of DNA damage distribution. It has been broadly exploited to study the dynamics of protein recruitment at the site of DNA damage (Lukas et al. 2003). Cells were cultured in glass-bottom dishes (Mattek P35G-1.5-14-C) and pre-sensitized to DNA damage induction by incubation for 72 h in 10 μM BrdU. Laser micro-irradiation was carried out using a 50 mW 405 nm diode laser with a 100% power output. At 2× digital magnification, multiple regions of interest (ROI) of the same size were selected in each nucleus and the 405nm laser was used to scan the ROIs for 50 iterations (total dwell time per pixel 490μs).

Live-cell imaging was carried out with a Leica TCS SP5 point scanning confocal microscope equipped with a Leica HCX PL APO 63×/1.4NA oil immersion objective and an environmental microscope incubator (OKOLab) set to 37°C and 5% CO_2 perfusion. The Leica TCS SP5 confocal microscope was driven by Leica LAS AF software.

3.5 Neocarzinostatin treatment

Neocarzinostatin (NCS) is a macromolecular chromoprotein antibiotic, which can bind and react with the DNA, inducing DNA damage. Here, cells were incubated NCS 50ng/mL in cell culture medium for 20 minutes at 37°C, to induce an amount of DNA damage

comparable to that generated by 2-3Gy. Cells were immediately fixed after 20 minutes of incubation with the drug.

3.6 Transfection of plasmid DNA in Hela cells and Mouse Embryonic Fibroblasts

Cell transfection was used to obtain transient expression of particular DNA sequences in target cells. Hela111 were transfected with the plasmid pCMV5 or pCMV5-ISceI-HA, to induce a single cut at a specific locus. MEFs were transfected with the plasmid pLPC-TRF1-FokI, to induced DSBs at telomeres or with the nuclease dead version pLPC-TRF1-FokID405A, as control. Cells were plated in 10 cm dishes and transfected at 70% confluency. For each transfection reaction 1.5mL of serum-free medium (Opti-MEM) were mixed with 12µg of plasmid DNA and 1.5mL of Opti-MEM with 36µl Lipofectamine 2000 transfection reagent (Life technologies). The two solutions were incubated 5 minutes at RT, then mixed and incubated for 20 minutes at RT to allow the formation of lipid complexes. The growth medium was removed from the cells and substituted with the transfection mix. After 6h incubation, the transfection reaction was removed, and fresh culture medium was added to the cells.

3.7 Immunofluorescence in cultured cells

One of the techniques used in this work to study protein sub-cellular localization (mostly DDR foci formation) at single-cell level is immunofluorescence (IF). This technique allows visualization by fluorescent microscopy of target proteins that are recognized by antibodies. Cells were grown on coverslips, washed twice for 5 minutes with PBS and fixed with 4% paraformaldehyde (PFA) for 10 minutes at RT. To allow accessibility of the target epitopes to the antibodies, cells were permeabilized with 0.2% Triton X-100 for 10 minutes at RT.

Cells were incubated for 1 hour in blocking solution (PBG, 0.5% BSA, 0.2% cold water fish gelatin, Sigma) and then incubated with primary antibodies diluted in PBG for 1 hour at RT or overnight at +4°C, in a dark humidified chamber. Cells were washed twice for 5 minutes with PBG and incubated with fluorophore-conjugated secondary antibodies diluted in PBG for 1 hour at RT in a dark humidified chamber. The incubation with secondary antibodies was followed by 3 minutes incubation with 4'-6-Diamidino-2-phenylindole (DAPI, 1µg/ml, Sigma-Aldrich, excitation wavelength 358nm, emission wavelength 461nm). DAPI binds preferentially to AT clusters of DNA minor groove and it was used to visualize nuclei. Cells were briefly washed with PBS and water. Finally, coverslips were mounted with mowiol mounting medium (Calbiochem), which is a polyvinyl alcohol solution containing an "anti-fade" agent, capable of reducing photobleaching of the fluorophores conjugated to the secondary antibodies. Coverslips were air dried before microscope analyses.

3.8 Immunofluorescence in mouse tissue sections

In this work, immunofluorescence was also used to detect sub-cellular protein localization in tissue sections. Tissue sections mounted on glass slides were fixed with 4% PFA in PBS for 20 minutes. Slides were washed twice for 5 minutes at RT in washing buffer (0.1% Tween in PBS for 5 minutes). Tissues were blocked in 2% BSA, 0.1% Tween in PBS for 1 hour at RT and incubated with primary antibodies diluted in blocking buffer, overnight at +4°C in a dark humidified chamber. Tissues were then washed twice for 5 minutes at RT with the blocking buffer and incubated for 1 hour at RT with fluorophore-conjugated secondary antibodies in a dark humidified chamber. Nuclei were stained with DAPI (1 µg/ml, Sigma-Aldrich). Samples were mounted with glycerol mounting medium (50%glycerol, 50mM Tris, pH 8), which provides an “anti-fading” function similar to mowiol, but also allows better conservation of the 3D-structure of the sample. Finally, the coverslips were sealed with nail-polish and air-dried before imaging.

3.9 BrdU incorporation assay

The BrdU incorporation assay was used as a tool to monitor cell proliferation. 5-bromodeoxyuridine (BrdU) is a synthetic analogue of thymidine, which is incorporated into DNA during replication. Cells were plated on coverslips, incubated with cell culture medium in the presence of BrdU (Sigma-Aldrich, 10 µg/ml) for 6 hours, then washed twice and fixed with 4% PFA. Incorporation can be evaluated by immunofluorescence after DNA denaturation. Denaturation was achieved by a mild treatment with a DNA nuclease that digests DNA to allow antibody access, simultaneously with antibody incubation. Cells were permeabilized with 0.2% Triton X-100 for 10 minutes at RT. After blocking with PBG for 1 hour, cells were incubated with a 50uL reaction mix containing primary antibody (anti-BrdU, 1:20), DNaseI (Promega, 0.1 U/µl,), DNase buffer and $MgCl_2$ (3 mM) for 45 minutes at RT in a dark humidified chamber. Cells were washed twice in PBG and the immunofluorescence was continued following the protocol previously described.

3.10 Senescence-associated-β-galactosidase assay

The activity of β-galactosidase enzyme is a widely used biomarker for cellular senescence, because β-gal is overexpressed in lysosomes of senescent cells and it is specifically active at pH 6.0 in senescent cells (Lee et. Al, 2006), while its activity at this pH is poorly detectable in pre-senescent, quiescent or immortal and transformed cells (Dimri et al., 1995). Cells were grown on coverslips, washed in PBS, fixed in 4% PFA for 10 minutes at RT, washed again and incubated at 37°C in the dark with fresh SA-β-gal stain solution (1 mg/ml 5-bromo-4-chloro-3-indolyl beta-D-galactopyranoside, 0.5 M phosphate buffer at pH 6.0, 5 mM potassium ferrocyanide, 5 mM potassium ferricyanide, 150 mM NaCl, 2 mM $MgCl_2$). After 16h of incubation, cells were washed with PBS, fixed with 4% PFA for 10 minutes at RT, permeabilized with 0.2% Triton X-100 for 10 minutes at RT, washed with PBS, incubated with DAPI for 2 minutes, washed with PBS and mounted with mowiol. Cells were imaged

with a brightfield microscope. β-gal staining led to the formation of detectable blue perinuclear precipitates, specifically in senescent human fibroblasts.

3.11 PLA

Proximity Ligation Assay is a tool commonly used to detect with high sensitivity proximity interactions between two proteins of interest at single-cell level (Söderberg et al. 2006, Jarvius et al. 2007). Briefly, the proteins of interest are recognized by two primary antibodies raised in two different species, then cells are incubated with a pair of different secondary antibodies, each conjugated to a DNA oligo (also called probe, in the commercially available Duolink In Situ PLA kit, Sigma). In a subsequent reaction two connector oligo are ligated forming a DNA circle which can hybridize with the probes; however, the hybridization with the probes can take place only if the two target proteins are in close proximity (< 40nm). In the final reaction, the DNA circle works as the template and one of the probes as the primer for a rolling circle amplification reaction (RCA); the amplified product is recognized by fluorescent oligonucleotides, leading to the formation of a signal detectable by fluorescent microscopy. Here, PLA was performed using Duolink In Situ PLA reagents from Sigma, according to manufacturer's instructions, with minor modifications. Cells grown on coverslips were fixed, permeabilized, blocked with PBG and incubated with primary antibodies as described for immunofluorescence. Then coverslips were washed twice for 5 minutes at RT in PBG and incubated with 35µL of probes (typically 1:5 Duolink In Situ PLA Probe Anti-Mouse Plus and Anti-Rabbit Minus, diluted in Duolink Antibody Solution 1x) for 1 hour at 37°C in a sealed humidified chamber. After two 5 minutes washes with Duolink Wash buffer A (Sigma) at RT, coverslips were incubated with 35µL of Ligation reaction (1:5 Duolink Ligation Buffer, 1:40 Duolink Ligase, diluted in pure water), for 30 minutes at 37°C in a sealed humidified chamber. Afterwards, coverslips were washed twice for 2 minutes and then incubated with 35uL of Amplification reaction (1:5 Duolink Orange

buffer, 1:80 Duolink polymerase, diluted in pure water). Finally, coverslips were washed twice with Duolink Wash buffer B for 10 minutes at RT, then incubated for 3 minutes with DAPI and finally mounted with mowiol.

To perform PLA on tissue sections, the samples mounted on glass slides were fixed, permeabilized, blocked and incubated with primary antibodies as described for immunofluorescence on tissue sections (section 3.8). The volumes used for PLA reactions were scaled up to completely cover the tissue sections.

3.12 DI-PLA

The development of this method, to study physical DSBs in proximity to a DDR marker, has been one of the main points of my thesis work and it is extensively described in the Result section.

Adherent cells grown on coverslips were fixed in 4% PFA for 10 minutes at RT and permeabilized in 0.2% Triton X-100 for 10 minutes at RT, as described for immunofluorescence. Then, coverslips were washed twice for 5 minutes in NEB 2 buffer (NEB) 1x and once in blunting buffer 1X (Quick Blunting kit, NEB) at RT. Afterwards, exposed DNA ends were blunted, the reaction was performed at RT for 60 minutes, in a final volume of 50 µL for each coverslip using: 38.5 µL H2O, 5 µL Blunting Buffer 10x (NEB), 5 µL dNTP 1mM (NEB), 0.5 µL BSA, Molecular Biology Grade 20mg/mL (NEB), 1 µL Blunting Enzyme Mix (NEB), in sealed humidified chamber. Coverslips were then washed twice in NEB 2 buffer 1X and twice in T4 Ligase buffer 1X (NEB). Then, *in situ* ligation was performed overnight at 16°C in a sealed humidified chamber, in 100 µL final volume per coverslip using: 2 µL T4 Ligase (NEB), 5 µL 10 uM biotinylated linker (Table S1), 10 µL T4 Ligase Buffer 10X (NEB), 1 µL ATP solution 100mM (NEB), 1 µL BSA, Molecular Biology Grade 20mg/mL (NEB), 81 µL H2O. Coverslips were washed twice in PBS, and

then blocked for 1 hour in PBG, before incubation with primary antibodies. This step was followed by the standard PLA, described above.

To perform DI-PLA on tissue slides, fixation, permeabilization, blocking and primary antibody incubations were performed as described for immunofluorescence on tissues (section 3.8). Moreover, reaction volumes were scaled up, in order to completely cover the tissue section and the concentration of biotinylated linker was doubled.

3.13 Imaging

Immunofluorescence, PLA and DI-PLA were acquired using a wide field Olympus Biosystems Microscope BX61 or a Leica TCS SP2 confocal laser microscope. To allow accurate signals discrimination, confocal images were obtained by sequential scanning of several planes along the z-axis. Comparative immunofluorescence analyses were performed in parallel, with identical acquisition parameters. Number of foci per cell were analysed by the imaging software CellProfiler (Carpenter et al. 2006), using the same pipeline for each sample in the same experiment. To identify foci or dots, I used as template the "Speckle counting" pipeline that can be found at http://cellprofiler.org/examples/#Tracking. In particular, I set an allowed diameter for foci and dots, in order to help the program exclude image artifacts and I used a global thresholding strategy with the RobustBackground method. Percentages of PLA-positive and DI-PLA-positive nuclei were scored manually. For cells experiments I defined: %positive cells = 100* fraction of nuclei with ≥ 2 foci/dots, %negative nuclei = 100* fraction of nuclei with < 2 foci/dots. For tissue experiments I scored nuclei as positive if they had at least 1 focus/dot.

3.14 Quantitative PCR

The Real Time PCR (RT-PCR) instrument allows real time detection of PCR products as they are generated at the end of each elongating step of the PCR cycles. In qPCR experiments

Sybr Green based- reaction mix were used. Sybr Green is an intercalating agent that has the property to emit fluorescent signal only when bound to dsDNA. With this strategy, the Real time qPCR instrument (Roche LightCycler 480) measures the fluorescence of each reaction, which is directly correlated to the quantity of dsDNA PCR products in each sample. In the first cycles of PCR, the low fluorescence defines the baseline for the plot of fluorescence signal vs cycle number. A fixed fluorescence threshold can be set above the baseline: when the fluorescence in a sample exceeds the set threshold, the threshold cycle (Ct) is called. Thus, the Ct is defined as the cycle number at which the fluorescence becomes higher than the fixed threshold: the higher the initial amount of the sample, the sooner the accumulated product is detected in the PCR process as a significant increase in fluorescence, and the lower the Ct value.

Ct values are reproducible in technical replicates because the Ct are detected in the exponential phase of the PCR (in the first 35 cycles), where there is a linear relation between the log change in fluorescence and the cycle number. When the Ct values were higher than 35, PCR results were classified as undetermined. Here, Real time qPCR was mainly used to quantify the amount of specific genomic DNA regions enriched in BLESS and BLISS experiments.

3.15 Antibodies

Anti-γH2AX (mouse, Millipore, 05-636, 1:2000), Anti-γH2AX (rabbit, Cell Signaling, 9718, 1:2000), Anti-53BP1 (rabbit, Novus Biological, NB100-304, 1:2000). Anti-biotin (mouse, Sigma, B7653, 1:2000), anti-biotin (rabbit, Abcam, AB53494, 1:2000), anti-BrdU (Becton Dickinson, 347580, 1:20), Anti-GFP (rabbit, Abcam, ab290, 1:2000), Anti-TRF2 (mouse, Millipore, 05-521, 1:1000), anti-cyclinA (1:800, BD transduction laboratories).

3.16 Statistical analyses

Results are shown as mean ± standard error of the mean (s.e.m) where the number of biological replicates was ≥ 3, if nothing else is specified. Results are shown as mean ± 95% confidence interval where the number of biological replicates was ≥ 3, if nothing else is specified. P-values were calculated by Student's two-tailed t-test or chi-squared test, respectively, using Prism software.

3.17 BLESS

BLESS (direct *in situ* breaks labeling, enrichment on streptavidin and next-generation sequencing) is a technique to detect and map DSBs at genome-wide level in a population of cells (Crosetto et al. 2013). BLESS testing and development has been one of the main point of this work, thus extensive discussion on the method can be found in the Results section. Here, the version used for most experiments is reported: a modified version of the protocol published by Crosetto and colleagues in 2013. For a typical BLESS experiment 5-10 million cells, for each condition, were crosslinked with 2% formaldehyde for 30 minutes at RT. The crosslinking reaction was then quenched with the addition of 125mM Glycine. Fixed cells were rinsed twice in 1X cold PBS, collected by scraping and centrifuged at 2000 rpm for 5 min at 4°C. Cells were washed twice in cold PBS and the pellet was flash-freezed at -80°C and stored until use. Pellets were resuspended in 1mL of Lysis buffer (Tris HCl pH 8 10mM, NaCl 10mM, EDTA 1mM, EGTA 1mM, NP-40 0.2%, DTT 1mM, Proteases inhibitors (Roche)), and incubated for 90 minutes on a rotating wheel at 4°C. Cells were then collected by centrifugation (2000rpm for 5 minutes at 4°C) and resuspended in 1mL Nucleus break buffer (Tris HCl pH 8 10mM, NaCl 150mM, EDTA 1mM, EGTA 1mM, SDS 0.3%, DTT 1mM) and incubated in a thermomixer at 37°C shaking at 800 rpm for 45 minutes. Cells were then collected by centrifugation (2000rpm for 5 minutes at RT) and resuspended in 500µL NEB Buffer 2 (Tris HCl pH 8 10mM, NaCl 50mM, $MgCl_2$ 10mM,

DTT 1mM, 0.1% Triton) + 10µg/mL Proteinase K (Roche) and incubated in a thermomixer at 37°C shaking at 800 rpm for 45 minutes. Samples were quickly transferred to ice and 500uL NEB Buffer 2 + Protease Inhibitor was added to each sample. Isolated nuclei were centrifuged (3000rpm for 10 minutes at 4°C) and washed twice in NEB buffer 2 and once in Blunting buffer (Tris HCl pH 7.5 100mM, NaCl 50mM, $MgCl_2$ 10mM, DTT 5mM, 0.025% Triton X-100). The pellet of isolated nuclei was then subjected to a blunting reaction (42µL Blunting buffer 1X, 5µL dNTP 1mM, 2µL Blunting enzyme mix (Quick blunting kit, NEB) for 45 minutes at RT. After blunting, nuclei were resuspended in 1mL NEB Buffer 2, centrifuged (3000rpm for 10 minutes at 4°C) and washed twice. Then the pellet was washed twice in T4 Ligase buffer and finally the nuclei were subjected to the Ligation step with the biotinylated proximal linker which would tag each exposed DSB in the nuclei (18.5µL T4 Ligase buffer 1x, 5µL of 10µM Linker P1B in T4 Ligase buffer 1x, 1.5 Ligase 400.000 U/µL (NEB)). *In situ* ligation was performed overnight as described in the published BLESS protocol, followed by DNA de-crosslinking and extraction. After ligation, the pellets were washed twice in 1mL Wash&Bind buffer (W&B, 5mM Tris HCl pH 7.5, 1mM EDTA, 1M NaCl, 0.1% Triton X-100); after each wash, the samples were centrifuged 10 minutes at 3000rpm, at RT). Then, the pellets were resuspended in 500uL of NEB Buffer 2 + 200µg/mL Proteinase K and incubated for 45 minutes in a thermomixer set at 55°C, shaking 800rpm. Afterwards the incubation was continued for 45 minutes at 65°C.

The samples were spinned for 1 minute and transferred in ice. Potassium Acetate (0.3 M), Glycogen and 0.7 volumes of ice-cold Isopropanol. After mixing the solution, samples were incubated for 1 hour at -20°C and later centrifuged 13000rpm for 20 minutes at 4°C. Pellets were washed twice with 70% ethanol and finally resuspended in 130 µL of pure water.

Purified genomic DNA was fragmented with Covaris S220 (10% duty factor, 175W peak incident power, 200 Cycles/burst, 150s) to obtain a pool of 250 bp fragments. Covaris machines utilize the Adaptive Focused Acoustics™ (AFA) process to shear DNA,

exploiting bursts of ultrasonic acoustic energy at very high frequency that lead to a strictly regulated fragment size distribution.

Next, the sheared DNA fragments were diluted with 180 µL of pure water: 10µL of this solution was stored and used as Input for further analyses. The remaining sheared DNA fragments were captured on streptavidin beads (Dynabeads MyOne Strepdavidin C1, ThermoFisher Scientific): the samples were incubated for 30minutes with 10µL of beads on a rotating wheel at 4°C in W&B buffer.

Magnetic beads were then washed twice in W&B buffer and resuspended in 37.5µL pure water. The sheared fragments underwent a blunting reaction (5 µL Blunting buffer, 5 µL dNTP 1mM, 2 µL Quick blunting enzyme mix, 0.5 BSA 20mg/mL) for 45 minutes at RT, shaking at 1200rpm for 15 seconds every 15 minutes.

Afterwards, the sheared DNA fragments were washed twice in W&B buffer and resuspended in 33 µL pure water. Next, they were ligated to the distal linker (LinkerD3): they were incubated overnight in 5µL Ligase buffer 10X, 10µL Linker D3 100mM, 2 µL T4 Ligase (400.000 U/µL, NEB), in a thermomixer set at 16°C, shaking for 45 seconds at 1200rpm every 45 minutes.

The ligation product was washed twice in W&B buffer and resuspended in 21 µL pure water. BLESS linkers have a hairpin-like structure: the stem is composed of a barcode sequence, the I-SceI target site then there is the loop containing the biotinylated nucleotide. Digestion of the ligation product with I-SceI allowed linearization of the linkers, thus recovery of the fragments from the magnetic beads, followed library preparation. The digestion was performed by adding 2.5 µL Cut Smart Buffer 10x, 0.5 µL BSA 20mg/mL, 1 µL I-SceI (NEB): the samples were incubated at 37°C for 4 hours. In parallel, also input samples were digested with I-SceI using the same reaction mix. Finally, the supernatants were recovered and subjected to PCR amplification. Each sample was split in 5 PCR reactions: 5 µL I-SceI digested DNA, 1 µL PCR primer 1, 1 µL PCR primer 2, 1 µL dNTP 1mM, 5 µL 10x Q5 buffer, 0.5 µL Q5 polymerase (NEB). Each reaction was subjected to

18 cycles of PCR reaction. PCR products were recovered and the ones coming from the same sample were pooled together. Finally, both input samples and PCR products were purified with Wizard SV gel and PCR clean-up system (Promega) and resuspended in 35 µL pure water.

The purified samples were either subjected to Next Generation Sequencing (NGS) library preparation with Truseq Nano LT kit (Illumina) or analyzed with BLESS-quantitative PCR (BLESS-qPCR).

3.18 BLESS-qPCR

To quantify the enrichment of DNA sequences at specific genomic regions, captured by BLESS, I developed an approach inspired by ChIP-qPCR analyses. I performed BLESS as described above, but I stopped before preparing the Truseq DNA library for Next Generation Sequencing.

qPCR primers were typically designed in the 500bp surroundings of the site of interested. qPCR with the selected primers was performed on the final BLESS product and on the genomic Input, that corresponds to 1:30 of the material recovered after sonication.

The enrichment was expressed as % of input:

$$\%\ of\ input = \frac{LB}{IN} \times 100$$

LB = 2^{-Ct} Library, corresponding to the BLESS product obtained after the PCR step

IN = 2^{-Ct} Input

In this way, the DNA enrichment for each sample is normalized on the amount of starting material. Note that this calculation does not take into account the input dilution and the PCR cycles used to amplify the material in the final step of BLESS protocol. However, since I always used the same input dilution and number of PCR cycles, different BLESS experiments are comparable.

3.19 BLISS linker preparation

The single-strand oligonucleotides for BLISS, listed in 3.25, were annealed in 100µL of purified water, at a final concentration of 10 µM. The oligonucleotides mix was heated to 95 °C for 5 minutes. Tubes were removed from the heat source and slowly allowed to cool to room temperature.

3.20 BLISS

Breaks Labelling *In Situ* and Sequencing (BLISS) is an evolution of BLESS method, to map DSBs at genome-wide level, that allows low-input samples and higher sensitivity (Yan et al, 2017). Here, I used the same protocol available in Protocol Exchange doi:10.1038/protex.2017.018.

For the experiments presented in this work a range of 1 to 3 coverslips per sample were fixed, with 10.000 to 50.000 cells attached. Briefly, cells were fixed with 4% PFA for 10 minutes, washed with PBS and incubated for 1 hour at 4°C in Lysis buffer (the same described above for BLESS, but with 0.2% Triton X-100). Then, coverslips were washed and incubated with Nucleus break buffer (the same described above for BLESS), for 1 hour at 37°C. Permeabilized nuclei were washed twice with PBS, and twice with Cut Smart Buffer 1x (NEB). Afterwards, DNA ends were blunted by incubating coverslips with 50µL of the blunting mix used for BLESS, for 1 hour at RT. After blunting, coverslips were washed twice with Cut Smart Buffer 1x (NEB) and subjected to ligation with the BLISS adapter (2 µL). The ligation reaction was performed overnight at 16°C in a sealed humidified reaction, with the same ligation reaction described for DI-PLA.

The excess of linkers was removed by washing twice in W&B buffer (as for BLESS) 1 hour at RT. Finally, genomic DNA was extracted by scraping cells in DNA extraction buffer (100mM NaCl, 50mM EDTA, 10mM Tris HCl pH 8, 1% SDS) and Proteinase K

(10mg/mL). The scraped samples were transferred to tubes and incubated overnight at 55°C, shaking at 800 rpm.

DNA was the purified by standard phenol-chloroform protocol and EtOH precipitation: briefly phenol:chloroform:isoamyl alcohol was added 1:1 to the extracted DNA sample, then the mix was centrifuged at 13000rpm for 10 minutes at RT, and the upper phase (containing the DNA) was transferred to a new Eppendorf. Sodium Acetate was added to obtain 0.3M solution, then glycogen and 2.5x volumes of 100% EtOH were added and the mix was incubated at -20°C for 1 hour. The DNA was centrifuged at 13000rpm for 20 minutes at +4°C and washed twice with 70% EtOH.

Finally, the pellet is air dried and resuspend in 130µL pure water and sonicated with Covaris as described for BLESS. The sheared DNA fragments were then concentrated with vacuum to obtain a 16µL solution in pure water: half of the material was saved as Input for further analyses, while 7.5µL were subjected to in vitro transcription using Ambion T7 Megascript kit, with the following reaction mix: 7.5µL Sonicated genomic DNA, 8 µL rNTP mix, 2µL T7 polymerase buffer 10×, 2 µL T7 Polymerase, 0.5 Ribosafe RNase Inhibitor). The reaction was incubated for 14 hours at 37°C and was followed by 15minutes at 37°C DNAseI treatment.

Afterwards, the RNA product of the IVT reaction was purified using Agencourt RNA XP beads, following manufacturer's instruction, and resuspended in 8uL pure water.

Afterwards, the library for NGS is prepared using components from Truseq SmallRNA seq kit (Illumina), performing reaction as advised by manufacturer's instruction. Firstly, the RA3 (3' adapter) is ligated, then the RNA is reverse transcribed using SuperScript III, and finally the library is indexed and amplified for 8-10 cycles of PCR. Agencourt Ampure XP beads were used to purify the PCR product, resuspending the library product in a final volume of 20µL pure water. Library product was then either subjected to NGS or analysed by BLISS-qPCR.

3.21 BLISS-qPCR

Similarly to the approach developed for BLESS, qPCR was used to analyze BLISS libraries, to study whether specific genomic regions were represented in the library.

Differently from the experiments performed for sequencing, the starting material was doubled (2 coverslips per condition). After *in situ* blunting, ligation with linkers and genomic purification, the DNA was fragmented by sonication, according to BLISS standard procedure. Then, the fragmented DNA of each condition was concentrated to 16µL, of which 8µL were used for *in vitro* transcription (IVT), while the remaining 8µL were stored at -20°C. This aliquot was used as Input of genomic DNA, to allow normalization of the genomic material represented in BLISS libraries, on the amount of starting material for each sample. IVT and library preparation were performed according to BLISS workflow.

Primers designed to amplify the regions of interest were used for qPCR analysis of the BLISS libraries, normalized over the input. Following the same formula shown in BLESS-qPCR section.

Fold induction of DSBs for each couple of primers was calculated with this formula:

$$Fold\ induction = \frac{\frac{LB_{Induced}}{IN_{Induced}}}{\frac{LB_{Uninduced}}{IN_{Uninduced}}}$$

LB = 2^{-Ct} Library, corresponding to the final BLISS product

IN = 2^{-Ct} Input

3.22 BLESS and BLISS sequencing, alignment and data analysis

Library quality and quantity was assessed on the 2100 Bioanalyzer (Agilent) using the High Sensitivity DNA kit (Agilent). Clusters were generated on the Illumina flow cell using the

automatic cBot station and the TruSeq PE Cluster Kit v3-cBot-HS. Sequencing was carried out on Illumina HiSeq 2000 using the TruSeq SBS Kit v3-HS chemistry.

For DSB detection in U2OS AsiSI cells, paired-end sequencing reads from each sample were mapped to the human genome (GRCh37/hg19) using BWA. At most one mismatch per read was allowed and duplicated reads were removed using rmdup of SAMtools (Li et al. 2009). All reads uniquely mapping were scanned for the presence of the proximal linker barcode with *ad-hoc* scripts written in bash and R languages. Finally, all reads within ±100 bp of the AsiSI sites identified by BEDtools intersect, were considered on target and retained for further analysis (Quinlan & Hall 2010). The same approach was used for DSB detection in LPS-induced macrophages, with the only difference that only the reads falling in the enhancers (as listed in (Ostuni et al. 2013)), were considered on target and retained for the analysis.

Differently, for DSB detection in IR exposed cells, a different pipeline was developed, in order to do a *de novo* detection of genome-wide DSBs, without a focus on any particular region.

The algorithm involves several steps, briefly summarized as follows. The first stage of analysis consists in filtering the raw sequencing data in order to remove reads with low mapping-quality score. The second step is the normalization of BLISS reads due to the huge discrepancy of their depth of coverage. In the third step, a Discrete Wavelet Transform algorithm, followed by a statistical evaluation according to a Poisson distribution, were used to obtain, for each time point, a list of significant peaks having p-values lower than an arbitrarily-defined threshold of significance, representing DSBs more enriched for reads in treated sample than in normalized control.

3.23 DSBCapture

DSBCapture is a technique to detect and map DSBs at genome-wide level in a population of cells (Lensing et al. 2016). DSBCapture protocol was adapted from the published protocol to make it most comparable with BLESS. All buffers and all steps in the protocol are the same as described for BLESS, however, DSBCapture linkers were used. Since the linkers are T-tailed, a A-tailing step was introduced after *in situ* DNA ends blunting with the following reaction mix: 0.5µL 10mM dATP, 3µL Klenow Fragment exo- (NEB, cat. no. M0212), 46.5µL pure water.

Each sample was incubated for 45 minutes at 37°C, then washed twice with NEB2 buffer and submitted to linker ligation as described for BLESS.

DSBCapture linkers do not have a hairpin structure, thus enzymatic linearization after the second linker ligation was not performed, and the final PCR amplification of the captured DSBs sequences was performed directly on the beads, with the same reaction mix and PCR program described for BLESS: here, in each PCR reaction were used 5µL of DNA bound to beads (instead of 5µL of digested DNA), and primers matching DNACapture linkers were used instead of BLESS PCR primer (see Primers table).

qPCR detection of DSBs sequences detected by DSBCapture was performed with the same strategy described in BLESS-qPCR.

3.24 Primers

ID	Sequence	Figure
PCRP1	CCCTAGCGTAACTCTCGAGGTAGTA	3,4,,57,58
PCRD3	CTAGCGTAACTCTCGAGACGACG	3,4
507_prox_FW	GGATTGACTCTGGGGTTTGC	4,6
507_prox_rev	TCACACTCCACAGCCAATCC	4,6
203up_prox_fw	CCAGTTGATTTGAGTAGGAGACG	4,5,6,10
203up_prox_rev	TCTAGAATTAAGGGACGAGGCC	4,5,6,10
uncut_FW	ACCTGGGATGGGACATATC	4,5,6,10
uncut_rev	TACCAAGCCTGTCCCTGAAC	4,5,6,10
245down_prox_fw	AGAAGGATGGTGGTGTCTGC	4,5,6,10

245down_prox_rev	AATCAGAACTCTCGCTCCCC	4,5,6,10
453_prox_fw	GCCTATGGAACTGACGGTGG	4,5,6,10
453_prox_rev	GCTCCTCCCCTCCTTTCC	4,5,6,10
985_down_Fw	CACCAAACCAAGGAAGCAGC	4,5,6,10
985_down_rev	GGTTCTCTGCCTTCCAAAGC	4,5,6,10
I-sceI_near_F	TTGGGTAACGCCAGGGTTTT	7
I-sceI_near_R	TTCCTCAGCGTGGCCAATTC	7
483_F	TTCTGACAGTGGGGAAAGCA	15
483_R	CTGAGATCTTCGGCAAGCC	15
554_F	GGCACTCACGTAGGCTAGAT	15
554_R	GGGGACTGGCTAGATCTGTG	15
961_F	GATCCATGCCCGCTGAATTT	15
961_R	GCTTGGGGTCGTTGAATCTG	15
1072_F	TGTCACAGACCCACACACC	15
1072_R	GTCAGCAAACCACAGAGAGG	15
E1_F	AGTTCACAGGCTGGCTGTCCAT	17,18
E1_R	CCACACTCAAGCTGCATGCTG	17,18
E2_F	CCACACTCAAGCTGCATGCTG	17,18
E2_R	TTACTGGGCTGTTACAAATGGG	17,18
E3_F	GCCATTACACTTGAAGTTCCTC	17,18
E3_R	CTAAGCAAGCACAGGGACAT	17,18
E7_F	CAGAGTTCAGAAATGAGGGA	17,18
E7_R	CACCCAGCAGTCTAATGCTA	17,18
H3.1 FW	ACCACAATTTCAGGCCCTCT	51
H3.1 REV	CACCACGCCCAGCTAATTTT	51
H3.2 FW	GGGTGACGGAGCATGACT	51
H3.2 REV	AGGATTAGGATGGTGGTGGC	51
H6.1 FW	AAGGCAAGAAAGGAAAGGGC	51
H6.1 REV	ACAAAATGGTATCTGGAGCAAGA	51
No_DSB_F	AGCATCTCCACCACCTCAAA	51
No_DSB_R	CACCACTGCACTTTAGCCTG	51
H9.1 FW	TGCAGAGGAGGTTCTTTGGT	51
H9.1 REV	TGGAAGGAAGGGAGGAAGGA	51
H11.1 FW	TCCTGGGCAAGTCACTTCAG	51
H11.1 REV	CTTTAGCCAATCCTGCCTGC	51
H11.2 FW	GGACGTCATTGAACTGCAGG	51
H11.2 REV	TAGCTTGCACACCTGACTCT	51
H12.1 FW	GTCCCCGACTTAAGATGGTT	51
H12.1 REV	CGTAGCCTTCCTTAAACATGCT	51
H12.2 FW	GTAATGGGGTGGACGAGACA	51
H12.2 REV	TCTGCCTCATTGCCCAACTA	51
H22.1 FW	ATCCACCTAAGTTGGGCTCC	51
H22.1 REV	GTACATCACTGGTGGGAATGT	51
TELO_FW	TAGGGTTAGGGTTAGGGT	52,56,57,58
TELO_REV	CCCTAACCCTAACCCTAA	52,56,57,58
PCR-DSBC_FW	AATGATACGGCGACCACCGAGATCTACACTCTTTCCCTACACGA	10
PCR-DSBC-REV	CAAGCAGAAGACGGCATACGAGATATTGGCGTGACTGGAGTTCAGACGTGT	10

3.25 Linkers

ID	Sequence	Notes
Linker P1B	TACTACCTCGAGAGTTACGCTAGGGATAACAGGGTAATATAGTTT[BtndT]TTTCTATATTACCCTGTTATCCCTAGCGTAACTCTCGAGGTAGTA	Biotinylated linker used for BLESS and DI-PLA
Linker P1	TACTACCTCGAGAGTTACGCTAGGGATAACAGGGTAATATAGTTTTTTCTATATTACCCTGTTATCCCTAGCGTAACTCTCGAGGTAGTA	Non-biotinylated linker used for DI-PLA controls
Linker D3	CGTCGTCTCGAGAGTTACGCTAGGGATAACAGGGTAATATAGTTTTTTTCTATATTACCCTGTTATCCCTAGCGTAACTCTCGAGACGACG	Distal linker used for BLESS
BLISS_FW	GCGTGATGNNNNNNNNGATCGTCGGACTGTAGAACTCTGAACCCCTATAGTGAGTCGTATTACCGGCCTCAATCGAA	Linker FW for BLISS
BLISS_REV	CGATTGAGGCCGGTAATACGACTCACTATAGGGGTTCAGAGTTCTACAGTCCGACGATCNNNNNNNNCATCACGC	Linker Rev for BLISS

4 Results

In this section, I will first describe the optimization of a genome-wide method to map DNA double strand breaks (BLESS) and its comparison with other recently published tools. I will describe the application of one of these tools (BLISS) to map at genome-wide level DSBs induced by a restriction enzyme (Iannelli et al. 2017). Genome-wide data have been analyzed in collaboration with Dr. Fabio Iannelli, a bioinformatician in the lab where I have worked. I will also describe the application of BLESS and BLISS to map DSBs induced in response to LPS activation of macrophages, which is part of a project in collaboration with Dr. Valerio Vitelli, a post-doc in the lab where I carried out my thesis.

In the second part, I will describe a new tool that I developed for DNA doubles strand breaks imaging in fixed cells and its application to study persistent DNA damage in senescent cells and tissues from aged animals (Galbiati et al. 2017).

In the last part, I will describe how DI-PLA and BLESS can be applied to study the integrity of telomeres.

4.1 DSB Mapping

The most commonly used method to map DNA double strand breaks (DSB) is Chromatin Immunoprecipitation (ChIP) using antibodies against chromatin modifications (γH2AX) or their interacting proteins (such as 53BP1), which are used as a proxy for DNA damage. However, these DNA damage markers spread away from the lesions for up to 1 Mb, thus not allowing a precise location of DSBs (see Introduction, section 2.5). Recently, an increasing interest in genome editing, together with the decreasing cost of high-throughput sequencing techniques, prompted the development of several new techniques to map DSBs at genome-wide level, as I recently reviewed in collaboration with other colleagues from our group (Vitelli et al. 2017). At the beginning of my PhD, I started working on the optimization of a recently published protocol, BLESS (Crosetto et al. 2013b, Figure 3), that could be applied to several biological problems.

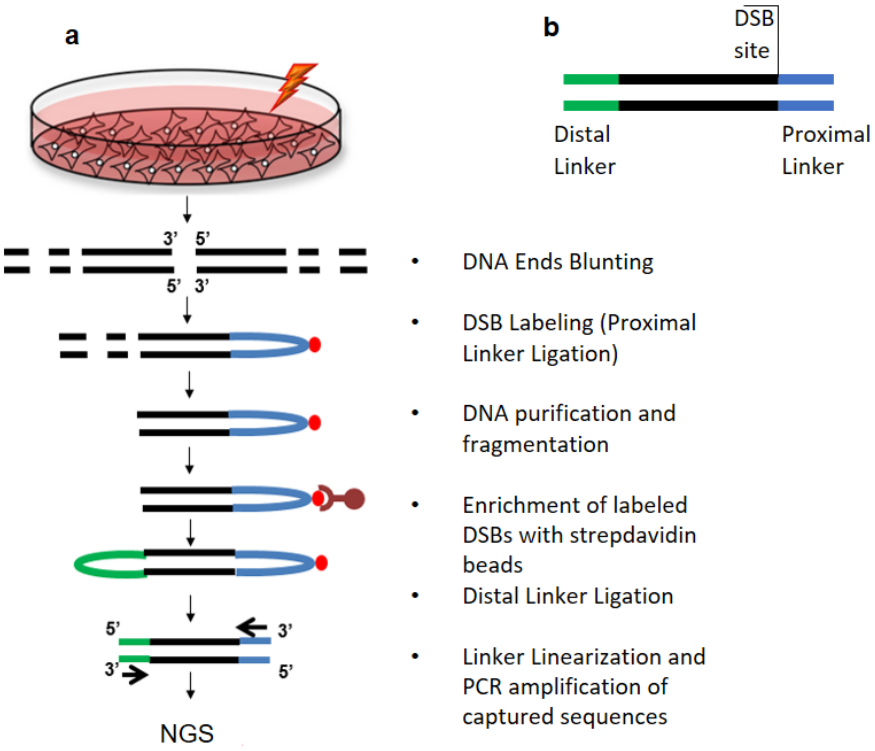

Figure 3 - BLESS workflow.

a. Highlight of the key steps in BLESS workflow. **b.** Scheme of a typical BLESS product: DNA fragment in black, linkers in green (distal) and blue (proximal).

As described in detail in the Material and methods section 3.17, this technique can be applied to fixed cells to map DSBs. It relies on *in situ* DSB blunting and ligation to a biotinylated double-stranded DNA linker which labels the DSB positions. Thus, after DNA extraction and fragmentation, it is possible to pull-down the biotinylated sequences with streptavidin beads. Following a distal linker ligation, it is possible to amplify the enriched sequences using primers matching the linkers and submit the amplified library to sequencing.

To test and optimize BLESS, I first applied it to map DSBs in a human osteosarcoma (U2OS) cell line, stably expressing the fusion protein AsiSI-ER (Iacovoni et al. 2010, Massip et al. 2010), where the restriction enzyme AsiSI is fused to a modified oestrogen receptor (ER) binding domain. The addition of tamoxifen (4-OHT) to cell culture medium induces nuclear translocation of AsiSI-ER, where the restriction enzyme cleaves its target sequences. This cell line has been recently used in several studies on DDR, and published results suggest that

although more than 1.000 genomic loci contain AsiSI target sequence, the endonuclease, *in vivo*, cleaves only a fraction of these, probably due to the varying degrees of accessibility of the genomic regions containing the target sequence. Given the possibility to induce DSBs with varying efficiency at known location in the genome, I thought that this cell line would be an ideal model to test BLESS efficacy in mapping DSBs.

4.1.1 BLESS-PCR

For my own reference, in collaboration with the bioinformatician of our group, Dr. Fabio Iannelli, we generated a map of all putative AsiSI target sequences in the human genome and we assigned an ordered number to each AsiSI site (AsiSI ID) starting from the closest to the start of chromosome 1.

The published BLESS paper lacked any tool to analyze BLESS-captured sequences, besides Next Generation Sequencing (NGS). Thus, I decided to develop a strategy to quickly test by PCR or quantitative PCR (qPCR) whether specific genomic regions were enriched in BLESS libraries. This strategy is also valuable to perform controls on the library preparation steps, prior submitting it to NGS.

To do this, one possible approach was to design one PCR primer in proximity of the putative DSB site to test and another matching the proximal linker (the one that marks the DSB position in BLESS) – Figure 4a. Alternatively, I designed a couple of primers, both matching genomic DNA, in the proximity of the putative DSB sites – Figure 4c. For this experiments I chose arbitrarily 4 AsiSI sites that, according to literature, were enriched in γH2AX (measured by ChIP - (Iacovoni et al. 2010) and 1 site as negative control (uncut), that was not in proximity to an AsiSI target site.

I performed BLESS on U2OS AsiSI cells either uninduced, induced for 4 hours with 4OHT and on parental U2OS cells, that did not contain the construct coding for the fusion protein, to exclude the contribution of a background level of AsiSI cleavage in cells containing the fusion protein.

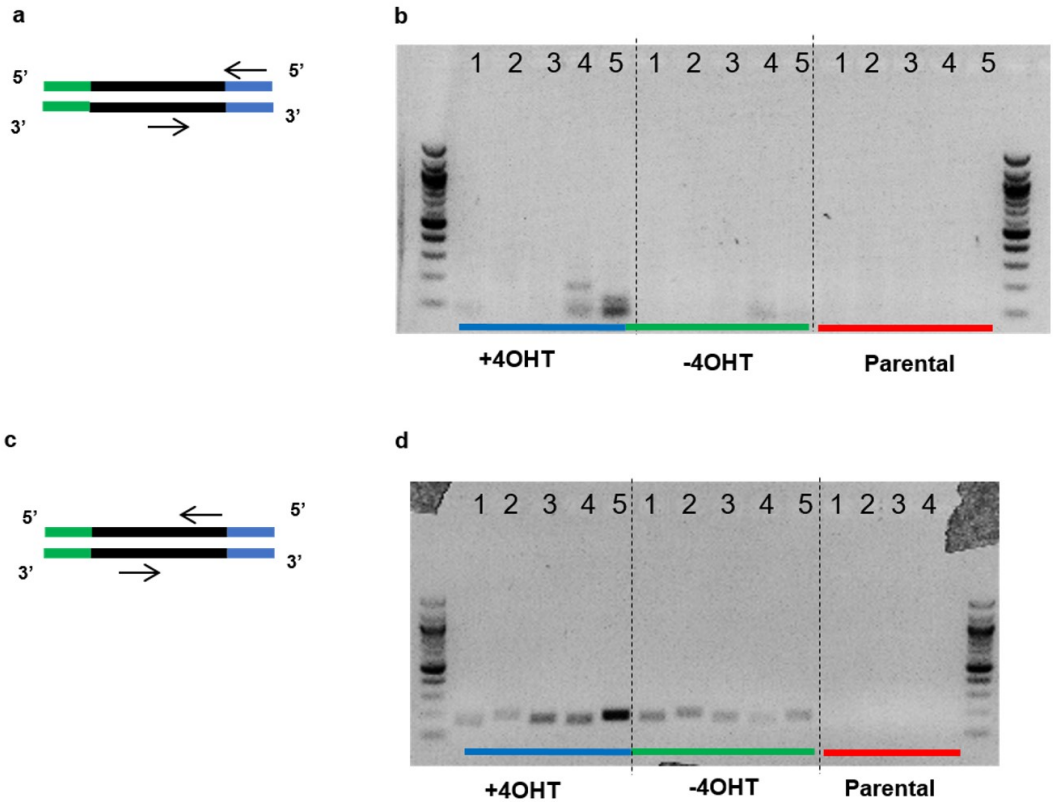

Figure 4 – BLESS-PCR on U2OS AsiSI cells.
Detection of captured DSB sequences by BLESS-PCR in U2OS AsiSI cells either induced (+4OHT), uninduced (-4OHT) and in U2OS cells (Parental) **a.** Forward primer specific for the genomic region, reverse primer specific for BLESS proximal linker **b.** PCR products run on agarose gel. Lane IDs 1: AsiSI_507, 2: Uncut, 3: AsiSI_203, 4: AsiSI_453, 5: AsiSI_985. **c.** Forward and reverse primers are designed on genomic DNA to amplify a specific region. **d.** PCR products run on agarose gel. Lane IDs 1: Uncut, 2: AsiSI_507, 3: AsiSI_203, 4: AsiSI_453, 5: AsiSI_985.

As shown in Figure 4b, d I found that using two primers matching the genomic DNA gave the best specificity in PCR detection, producing a single band, and showing the expected higher amount of captured DSBs, for at least 3 of the 4 AsiSI sites tested, in the induced sample compared to the uninduced, and no enrichment at the uncut site and in parental cells. On the other hand, PCR using one primer matching the genomic DNA and one matching the linker, were less efficient, often producing multiple bands; although I could still observe an enrichment for 3 of the 4 AsiSI sites tested. In Figure 4, as in any other Figure, the AsiSI IDs are the ones that we assigned to each putative AsiSI cleavage site in the genome, when we generated the *in silico* AsiSI cleavage map.

To further confirm that the PCR approach to detect BLESS-enriched DSB was reliable, I repeated the experiment, adding a normalization step on the Input (before streptavidin enrichment, see Material and Methods), to take into account the amount of starting material for each sample, in a similar fashion to the commonly used ChIP-qPCR approach.

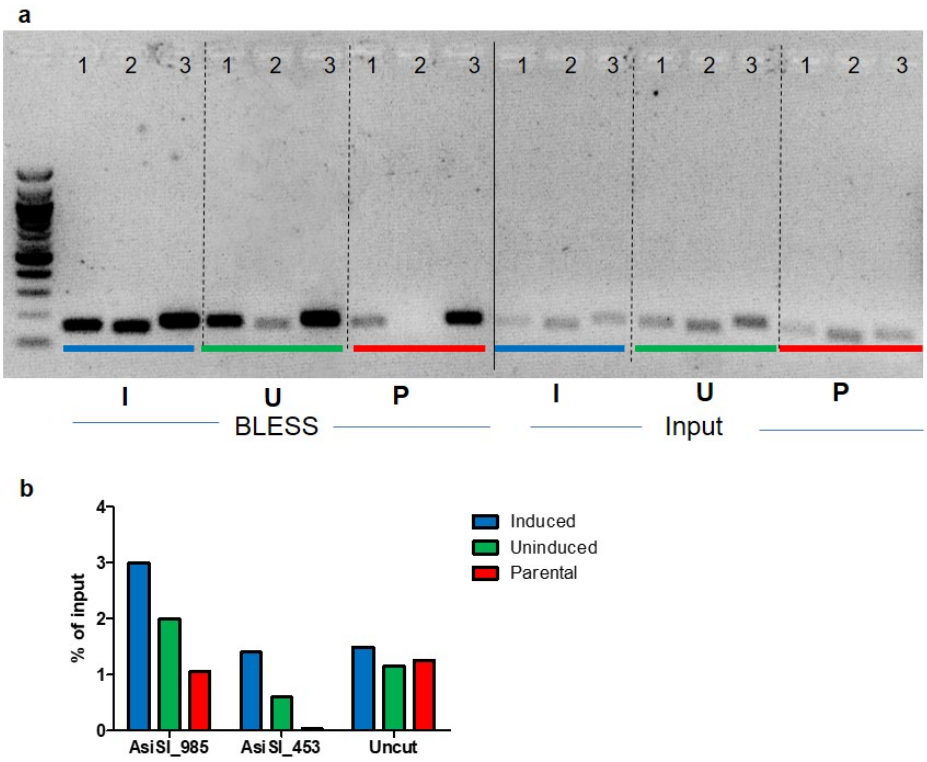

Figure 5 - BLESS-PCR normalized on input in U2OS AsiSI cells.
PCR detection of captured DSB sequences in U2OS AsiSI cells either induced (+4OHT), uninduced (-4OHT) and in U2OS cells (Parental). **a.** PCR products on BLESS libraries and PCR product on Input fragments were run on an agarose gel. Lane IDs 1: AsiSI_985; 2: AsiSI_453; 3: uncut. The ratios of band intensities quantified with (ImageJ Gel Analysis tool) of BLESS products over input, for each primer couple, are plotted in panel **b**.

As shown in Figure 5, I observed that, indeed, even after normalization of the BLESS products on the inputs, I could detect a specific enrichment of genomic material at the AsiSI cut sites in induced cells compared to uninduced cells or parental U2OS, but not at the uncut site, indicating that the approach that I developed was working reliably.

Since PCR is a semi-quantitative technique, and band intensity quantification by digital acquisition, followed by automatic quantification with imaging software (such as ImageJ, here) may not be particularly precise, I decided to use qPCR to have more accurate quantification of BLESS-captured DSBs. As shown in Figure 6, I observed that, using the

strategy validated by semi-quantitative PCR, I could reproducibly detect an enrichment of genomic material at several AsiSI-cleaved sites, specifically in induced cells.

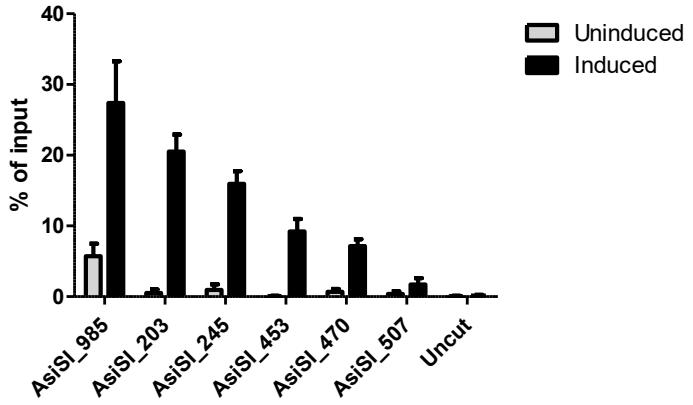

Figure 6 - BLESS-qPCR at several genomic regions in U2OS AsiSI cells either Induced or Uninduced.
Bars represent % of input (n=3).

As further confirmation that BLESS-qPCR was working, I performed BLESS on Hela111, a cell line carrying an exogenous sequence containing the target site for the I-SceI endonuclease (Figure 7a) and transfected the cells with a plasmid coding for I-SceI, to induce one DSB per cell, or with the empty vector as control. As shown in Figure 7b, I could specifically detect the cut at the I-SceI cleavage site only in cells that were transfected with the endonuclease.

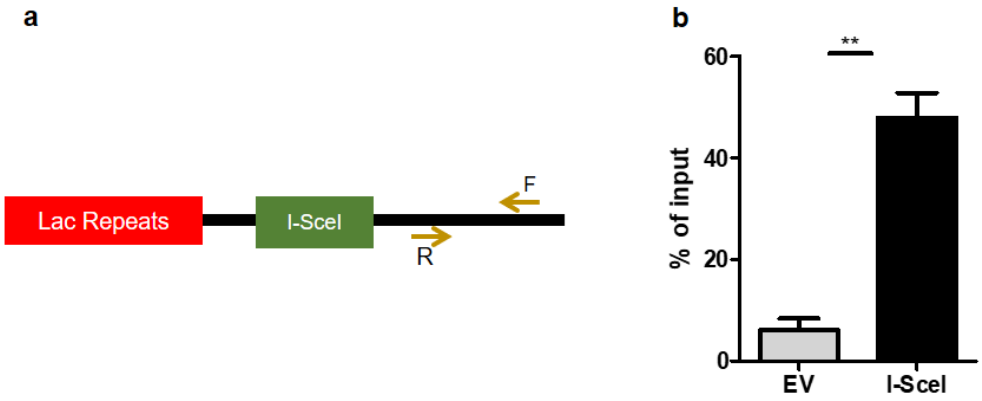

Figure 7 - BLESS in Hela 111.

a. Scheme of the genomic region containing the I-SceI target site and qPCR primer design. **b.** BLESS-qPCR in Hela111 transfected with an empty vector (EV) or a plasmid coding for the endonuclease I-SceI. Bars represent % of input (n=3).

In summary, I assessed that BLESS-qPCR is a reliable strategy to analyze BLESS captured DSBs.

4.1.2 Improvement of BLESS fragmentation step

I was interested in using BLESS to draw a precise genome-wide map of AsiSI cleavage sites in U2OS AsiSI-ER cells, something that was missing when I started this project, and would have been a useful resource for other studies in the laboratory and in the DNA damage field, given the broad application of this cell line.

While I was preparing the library for NGS, I realized that the mean size of library fragments, obtained by HaeIII enzymatic digestion, as reported in the original BLESS protocol (Crosetto et al. 2013a), was between 1000-2000bp (Figure 8a). This fragment size distribution is suboptimal for Illumina sequencing and it is known to yield low efficiency in cluster formation, a key step in Illumina sequencing-by-synthesis: in fact, long fragments have a low chance to stably hybridize to the probes attached to the Illumina flow cells, thus, yielding low efficiency of library sequencing. Instead, the optimal library fragment size distribution should be in the 200bp-600bp range (Bronner et al. 2013).

I was able to solve this problem by substituting the enzymatic fragmentation with a mechanical fragmentation step, using the Covaris sonicator (see Materials and Methods, section 3.17), which yielded smaller mean library fragments size, sharper fragment size distribution (Figure 8b), with the added advantage of being a faster and cheaper step than enzymatic digestion.

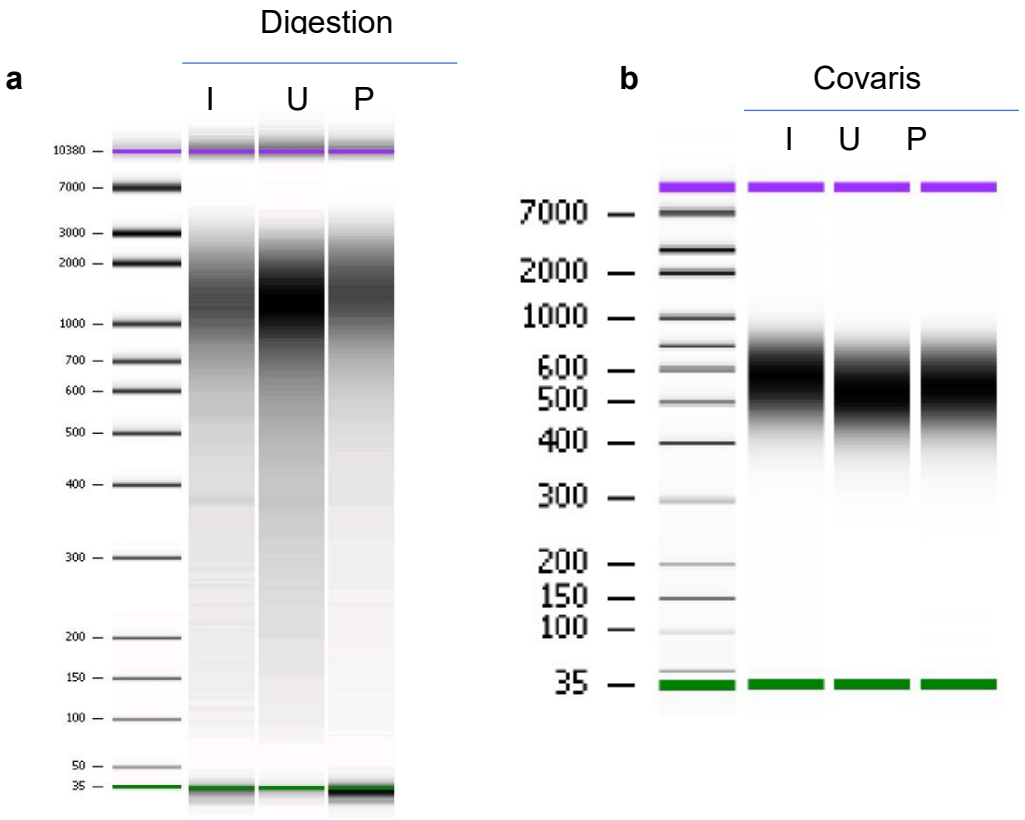

Figure 8 - Bioanalyzer profiles of BLESS on U2OS AsiSI cells.

U2OS AsiSI cells were either induced (I), uninduced (U) on U2OS cells (P). **a.** Fragmentation step performed with enzymatic digestion. **b.** Fragmentation step performed with Covaris.

To confirm the effectiveness of the change that I made to the original protocol I sequenced the BLESS libraries. In collaboration with Dr. Iannelli, we aligned the reads around the AsiSI cleavage sites that we found with the *in silico* AsiSI genome restriction. Figure 9 shows the normalized read counts in proximity (at different window sizes) of the detected AsiSI sites obtained with the two protocols. Strikingly, I found that the Covaris fragmentation yielded more than 10-times higher mean read counts in proximity of cut sites compared with the library prepared with enzymatic fragmentation.

Experiment	Window (bp)	Min	Median	Mean	Max
BLESS Digestion	500	1	1,5	1,89	9
	1000	1	1	1,79	9
BLESS Covaris	500	4	19	19	263
	1000	5,5	23	23	457

Figure 9 - Normalized read counts in the proximity (500bp or 1000bp windows) of AsiSI cut sites in U2OS AsiSI induced cells.

From this point onward, I always performed BLESS with the Covaris fragmentation step, unless otherwise specified. Notably, the latest methods developed to map DSBs, that use strategies similar to BLESS to capture DNA breaks, such as DSBCapture (Lensing et al. 2016) and End-seq (Canela et al. 2016), also include a mechanical fragmentation step, instead of an enzymatic fragmentation step.

4.1.3 Comparison between BLESS, DSBCapture and BLISS

4.1.3.1 DSBCapture

Following BLESS, a number of DSBs mapping methods have been published, as also discussed in the introduction (section 2.5), some with a whole different strategy, while others are improvements of the original BLESS protocol.

I decided to compare BLESS with DSBCapture (Lensing et al. 2016), which shares most of the protocol with BLESS, but uses T-tailed linkers to improve the efficiency of ligation of linkers to the DSBs, thus leading to a more efficient DSB labeling. This modification also requires the introduction of an A-tailing step after the DSBs blunting, to allow the ligation of the T-tailed linker. Another minor modification to the linker design, to include Illumina adapters in the sequence, allows the DSBCapture users to skip some steps in the library preparation for sequencing; however, this improvement is not relevant for the PCR detection of DSBs at specific loci. Lensing and colleagues, reported that DSBCapture mapped genome-wide more endogenous breaks than BLESS in normal human epidermal keratinocytes (NHEK), however they did not provide any control for false positive or background noise.

Thus, I decided to compare DSBCapture and BLESS efficiency in detecting AsiSI-induced DSBs and measure the enrichment of the captured sequences by qPCR.

As shown in Figure 10, and in agreement with the results published by Lensing and colleagues, I observed higher enrichment of DSB detection with DSBCapture compared to

BLESS in induced U2OS AsiSI cells. However, I also observed a higher level of background in uninduced cells and at an uncut sequence (lacking the AsiSI target site): this is particularly obvious when plotting the ratio of induced over uninduced at each AsiSI site (Figure 10b), where BLESS outperformed DSBCapture for most of the sites analysed.

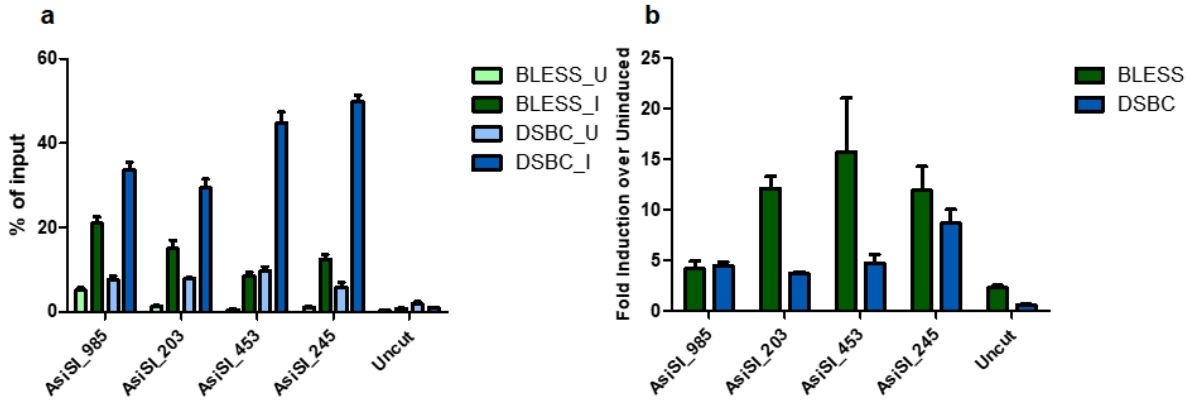

Figure 10 - qPCR comparison of DSBs detected by BLESS and DSBCapture.

a. Bars represent the % of input at each AsiSI site (n=2). **b.** Bars represent the ratio of % of input of Induced over Uninduced for each method of DSB detection.

Although, with this experiment, I could not infer any conclusion on genome-wide DSB detection by NGS with DSBCapture, the results indicate that this method does not significantly outperform BLESS when using a PCR method to detect captured sequences and suggest that DSBCapture might be more prone than BLESS to pick up background signals.

I also tried to repeat the same comparison between BLESS and End-Seq (Canela et al. 2016), but I failed to retrieve any DNA sequence at the end of End-seq process, possibly because the published protocol lacked some key details.

4.1.3.2 BLISS

BLISS technique (Yan et al. 2017) works with a strategy similar to BLESS, producing nucleotide-resolution genome-wide maps of DSBs in fixed cells, however a different linker

design and a different strategy for the enrichment of labeled sequences allows the technique to work on few thousand cells, differently from BLESS and most other DSB mapping methods that require a few million cells as starting material. I was also directly involved with BLISS testing in its unpublished version by spending a short period in Dr. Nicola Crosetto's lab in Karolinska Institutet, Stockholm.

The different strategies for DSB labeling and amplification does not allow a side-by-side comparison between BLESS and BLISS by qPCR, thus I compared the two techniques by NGS.

I used the well-tested U2OS AsiSI system and I compared the performance in mapping DSBs genome-wide of BLESS (with either enzymatic fragmentation – Dig, or Covaris fragmentation – Cov) and BLISS. I performed the analysis of sequencing data in collaboration with Dr. Fabio Iannelli. We focused on 100bp windows around AsiSI putative cut sites, we applied a normalization procedure to account for the number of reads surrounding these windows in induced and uninduced samples and, finally, we called DSBs only when we mapped more reads in the AsiSI window in the induced sample compared to the uninduced one, after normalization (see Materials and Methods – section 3.22).

We compared the sites that we detected as cut with a list of AsiSI sites validated in literature by Ligation Mediated-PCR (LM-PCR) (Aymard et al. 2014b, Chailleux et al. 2014): 15 AsiSI cleaved sites (Positive controls) and 3 AsiSI uncut sites (negative controls). We also compared this list of AsiSI sites with the AsiSI-induced DSBs detected by DSBCapture, as reported in literature (Lensing et al. 2016).

Strikingly, I found that all 15 positive controls were detected by BLISS and all 3 negative controls were not detected as cut (Figure 11). Differently, none of the other methods performed as well, with BLESS Dig clearly setting the lowest efficiency in detecting DSBs.

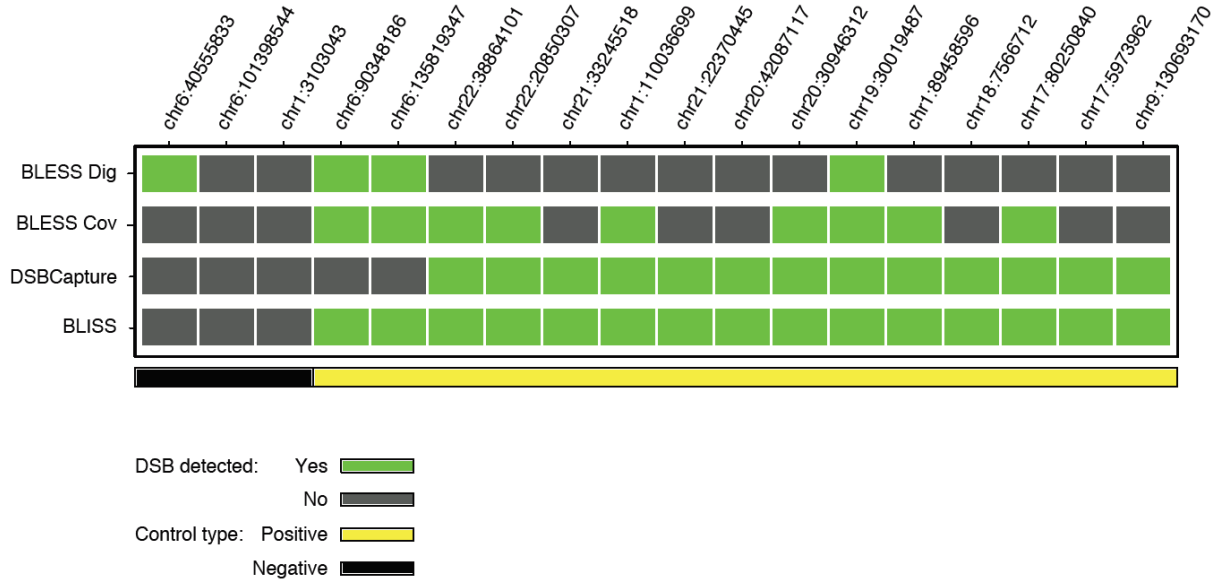

Figure 11 - Comparison between different DSB mapping techniques in mapping breaks at subset of validated AsiSI sites.

Each column represents one AsiSI site, as indicated by the genomic coordinates on top. Yellow sites are cut, Black sites are not. BLESS Dig: fragmentation with restriction enzymes. BLESS Cov: fragmentation with Covaris.

4.1.4 Genome-wide characterization of AsiSI-induced breaks

Next, we characterized the entire set of the 214 cut sites detected by BLISS and we observed that these sites were homogenously distributed along the genome and the coverage of BLISS reads was fairly uniform, as it can be inferred by the fact that most of the detected sites had similar read coverage (Figure 12).

These observations suggest that there were no obvious regions in the genome under- or over-represented due to sequencing errors or sequence-dependent coverage bias.

Figure 12 - Circos plot (http://circos.ca/) showing the AsiSI-induced DSBs detected by BLISS, for each chromosome.

Each dot represents an AsiSI site detected by BLISS, and the circles with different shades of red represent the read coverage of BLISS reads in a 200bp window centered around each AsiSI site (bins of read density from inner to outer circle: 0-0.25, 0.25-0.5, 0.5-0.75, 0.75-1).

To further validate the genome-wide map of AsiSI-induced breaks obtained with BLISS, we compared the detected sites with γH2AX ChIP-seq (Iannelli et al. 2017) performed under the same experimental conditions. We established a subset of the 100 AsiSI cut sites with the highest γH2AX enrichment around the DSB, and we found that 74 of 100 sites were also detected by BLISS (Figure 13).

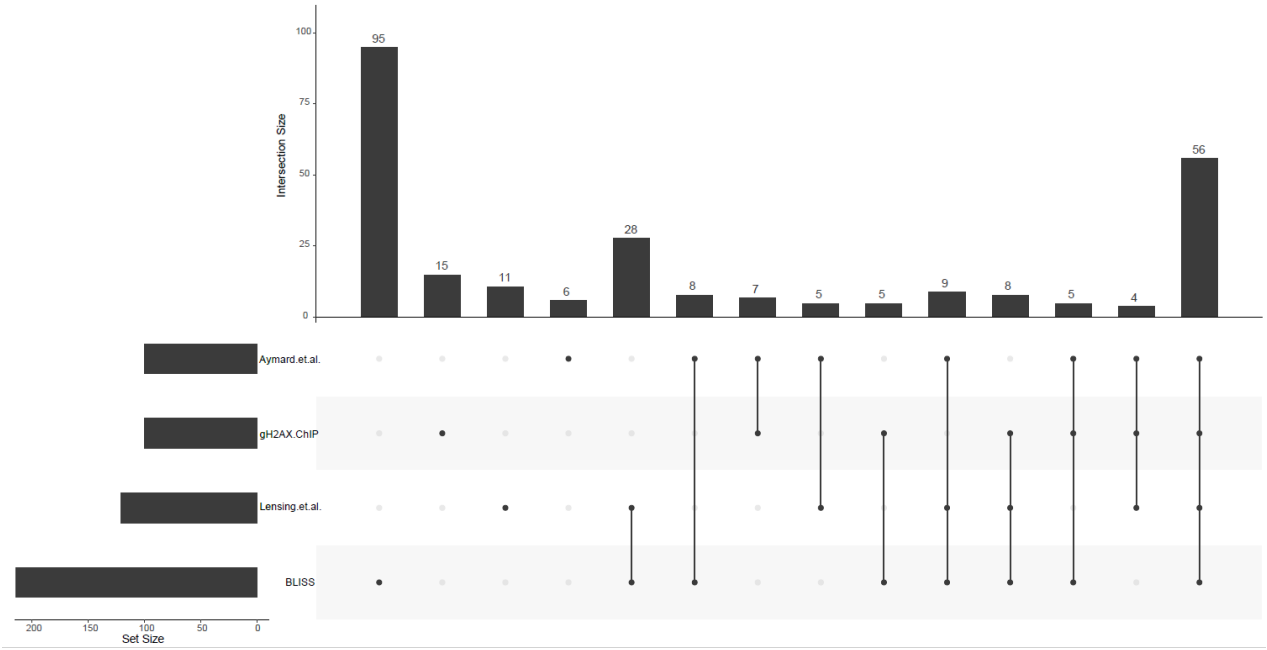

Figure 13 - AsiSI cut sites detection by different DSB mapping techniques.

Bars on the left represent the number of AsiSI sites detected by different techniques: metadata from γH2AX ChIP-seq (Aymard et al. 2014a), γH2AX ChIP-seq (Iannelli et al. 2017), DSBCapture (Lensing et al. 2016) and BLISS. Vertical bars indicate the number of AsiSI cut sites exclusively detected in each intersection among experiments.

Analyses of the 26 sites that were not detected by BLISS, but detected by ChIP-seq, showed that they might be cut with low efficiency, possibly with little reproducibility among biological replicates. In fact, only 4 out of 26 (15%) γH2AX ChIP-seq specific sites were detected consistently in literature (Figure 13), while a strikingly higher number of sites detected by both BLISS and γH2AX ChIP-seq were confirmed also by other reports (56 out of 74, 76%, Figure 13). Extending this analysis to all the 214 sites detected by BLISS, we found that 178 sites were next to genes. Active transcription requires an open chromatin state that could make AsiSI sites particularly accessible to enzyme, thus cut with higher efficiency. Consistently, we noticed that sites detected by both BLISS and γH2AX ChIP-seq were the ones next to genes with significantly higher levels of transcription, compared to the genes in proximity of a AsiSI site that were detected only by one of the two techniques (Figure 14).

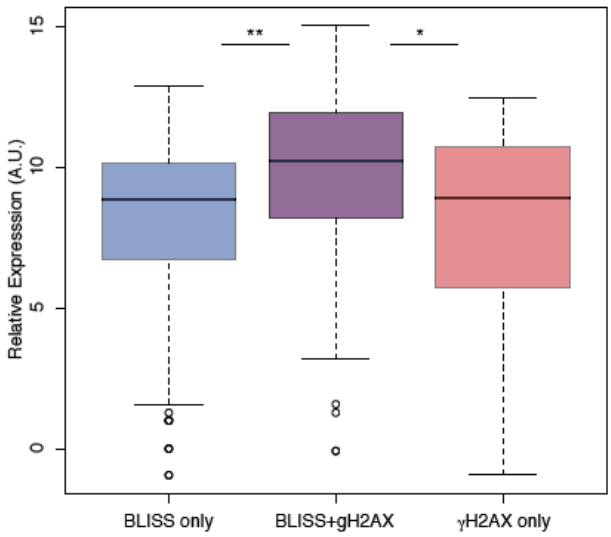

Figure 14 - Transcripts expression in proximity of AsiSI cut sites detected by BLISS and/or γH2AX Chip-seq.

Boxplot representing the relative expression of transcripts in uninduced overlapping or adjacent (± 2 Kb) to the 140 BLISS only sites (blue), to the 74 sites detected by both BLISS and γH2AX ChIP-seq (purple), and to the 26 γH2AX ChIP-seq only sites (red). (* = P<0.05, Wilcoxon test; ** = P<0.01, Wilcoxon test).

As an additional control of BLISS reliability in detecting DSBs, I tested whether a subset of the sites exclusively detected by BLISS, were reproducibly detected in a biological replicate. Indeed, by BLISS-qPCR I found that 4 out of 4 sites that I tested were reproducibly cut, albeit with a low fold induction over uninduced samples (Figure 15).

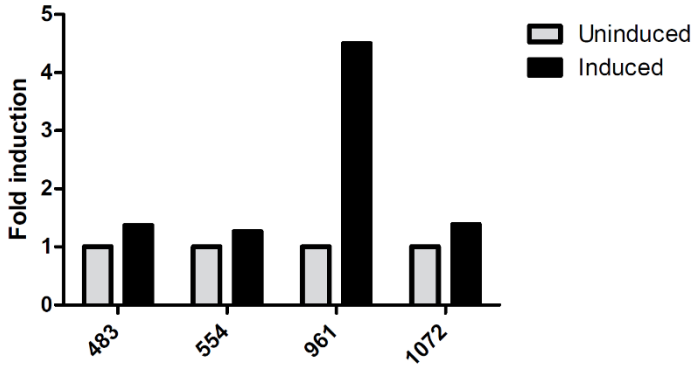

Figure 15 - BLISS-qPCR on U2OS AsiSI either uninduced or induced at a selected subset of AsiSI sites, detected by BLISS sequencing experiment, but not by other techniques.

Bars represent the normalized ratio of % of input for each site in the Induced sample over the uninduced (n=1).

In summary, our analyses indicate that the map of AsiSI-induced breaks generated by BLISS is reliable, it can be used as a resource for other research labs for other studies, and it is likely

to be the most precise map generated so far for this cell line. The fact that not all genomic sequences containing AsiSI sites are not cut according to BLISS is expected, due to different degree of accessibility among different genomic regions, and it is in general agreement with data available in literature.

4.1.4.1 Multi-layered expression profiling around DSBs mapped by BLISS

It is well established that DDR activation leads to global transcription alterations, thus impacting on multiple pathways, including cell cycle arrest, DNA repair, senescence and apoptosis (Riley et al. 2008). More recently, DDR activation has been linked to the local regulation of transcription at the damaged regions (Capozzo et al. 2017). As discussed at length in the introduction, contrasting observations on the impact of DSBs on transcription have been reported. In particular, a cluster of DSBs has been shown to repress the activity of a distal promoter in *cis*, in an ATM-dependent manner (Shanbhag et al. 2010), while another group showed that a single DSBs induces transcription inhibition only at the gene bearing the lesion and not at neighboring regions (Pankotai et al. 2012), in a DNA-PKcs dependent manner.

To address the contrasting views on the impact of DNA damage on transcription, in collaboration with Dr. Fabio Iannelli, we thought to exploit the precise map of AsiSI cleavage sites that we generated by BLISS. We correlated the DSB map with data obtained in our lab and in collaboration with other labs, from four different RNA sequencing technologies: RNA-seq to study steady-state RNA levels, Bru-seq (Paulsen et al. 2014) to study rates of RNA synthesis, Cap analysis gene expression (CAGE, (Shiraki et al. 2003)) to study transcription initiation and RNA POLII ChIP-seq to study levels of total and elongating polymerase (Iannelli et al. 2017). By monitoring transcriptions at genes with AsiSI cut or uncut sites we could observe transcription repression, specifically around AsiSI-cleavage sites (Figure 16).

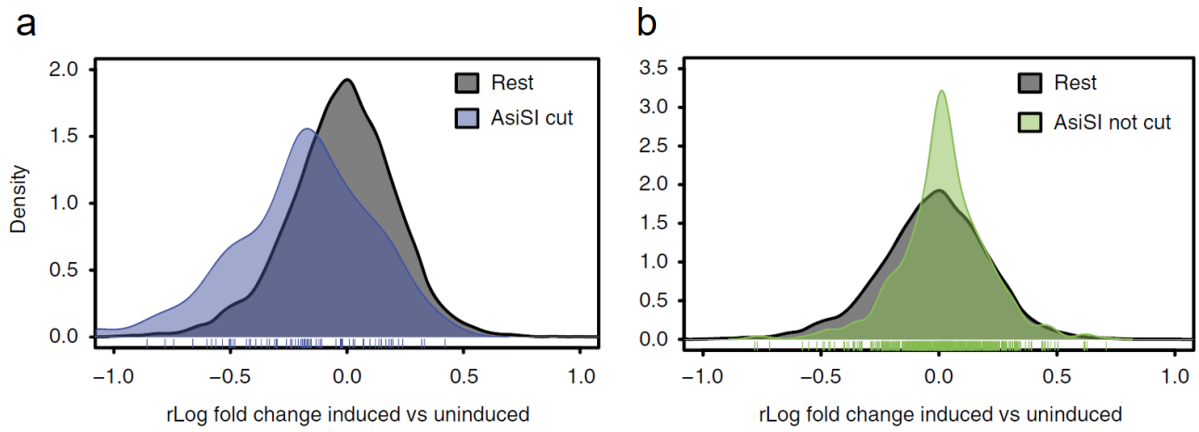

Figure 16 - Impact of AsiSI cleavage on transcription.

a. Distribution of the rlog fold change for transcription at genes with AsiSI cut sites (blue) compared to the rest of the genes (grey). Genes in proximity to AsiSI cut sites show significant shift towards downregulation ($P<0.05$, Wilcoxon test). **b.** Distribution of the rlog fold change for transcription at genes with uncut AsiSI sites (green) compared to the rest of the genes (grey). Genes in proximity to uncut AsiSI cut sites do not show significant shift towards downregulation ($P=0.9996$, Wilcoxon test).

This result was further supported by correlating the data obtained with the other transcriptomic analyses, mentioned above, with DSBs position. With this approach, we could study, for the first time at genome-wide level and single-nucleotide resolution, the impact of DSBs on transcription of endogenous sequences. We could robustly conclude that transcription is inhibited around AsiSI-induced DSBs, but not around AsiSI uncut target sites, in an ATM-dependent manner, and that transcriptional repression is stronger in proximity of the DSBs (Iannelli et al. 2017).

4.1.5 Transient DSBs correlate with LPS-induced macrophages activation

Despite the observation that DSBs induce a local transcriptional repression as reported by our lab and others, there is a growing amount of evidence of functional, transient, site-specific DSBs controlling the activation of transcription programs after exogenous and endogenous stimuli, such as hormone stimulation and neuronal activity, as discussed in the introduction (2.4.3). Here, scheduled, transient DNA breaks may appear at enhancer or promoter regions, possibly inducing chromatin changes, as the accumulation of histone

marks favouring transcription (Hartung et al. 2015, Madabhushi et al. 2015, Periyasamy et al. 2015, Puc et al. 2015b).

Macrophages are one of the best studied models for activation of transcriptional programs upon environmental stimuli. Indeed, comparative analysis of the transcriptional signature of *ex vivo* macrophages derived from different tissues, revealed a striking diversity among them, which is shaped by the presence of different stimuli from the environment of the tissue of origin (Lavin et al. 2014). Here, in collaboration with Dr. Valerio Vitelli, a post-doc in our lab, we asked whether DSBs could be involved in the activation of macrophages proinflammatory response to the recognition of pathogen-produced lipopolysaccharide (LPS). The possibility to apply genome-wide high-resolution DSBs mapping techniques was key to draw a correlation between DSBs generation and transcription activation.

We selected a subset of enhancers, which are silent in normal conditions, but trigger the production of long non-coding enhancer RNAs (eRNAs) upon LPS stimulation (Ostuni et al. 2013). Indeed, all the enhancers tested and their target genes showed a clear induction in transcription starting 20 minutes following LPS stimulation (Figure 17a, b).

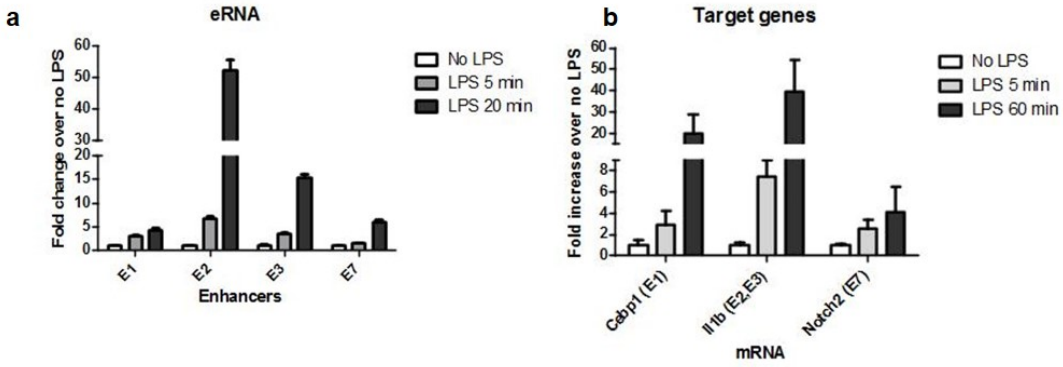

Figure 17 - Transcription activation following LPS stimulation.

RAW264.7 macrophages were either untreated or treated with LPS and harvested 5, 20 or 60 minutes after induction **a**. qRT-PCR of RNA with primer pairs against 4 different enhancer regions (indicated on the x-axis as E1, E2, E3 and E7) (n≥3). The y-axis represents the fold change over the untreated sample which was set at 1. **b.** qRT-PCR performed on the mRNA of the genes under the control of the enhancer analyzed in a BLESS signal determined by qPCR on the same region analyzed in **a.** On the x-axis, the name of the gene is indicated and the name of the controlling enhancer is indicated in parenthesis. The y-axis represents the fold change over the untreated sample which was set at 1 (n=3).

Strikingly, I observed a clear transient DSB formation by BLESS-qPCR, at each of the tested enhancers, as early as 5 minutes after LPS stimulation, which were rapidly resolved and disappeared after 60 minutes (Figure 18).

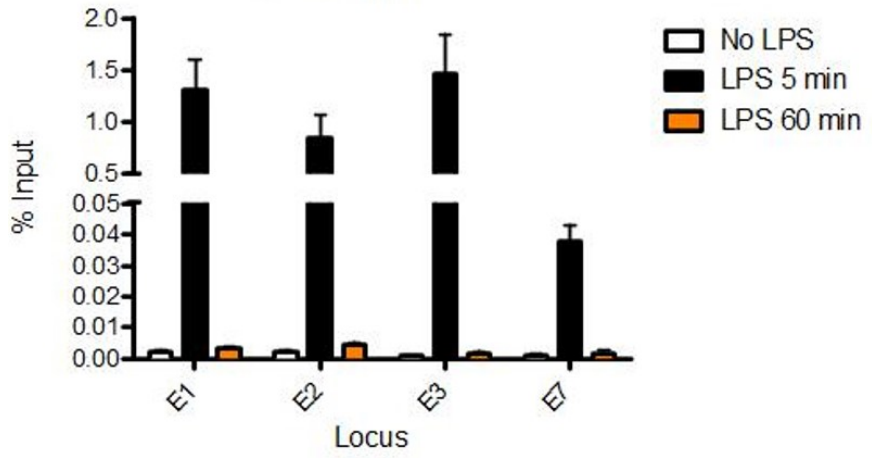

Figure 18 - BLESS-qPCR detection of DSBs at the enhancers analyzed in Figure 17.
RAW264.7 macrophages were either untreated or treated with LPS and fixed 5, 20 or 60 minutes after induction (n≥3).

The observation that I made in a subset of enhancer was later extended by genome-wide mapping of DSBs by BLISS followed by NGS. In collaboration with Dr. Iannelli, we focused on the analysis of BLISS reads in DSBs proximal to the enhancers activated upon LPS treatment, as published by Ostuni and colleagues (Ostuni et al. 2013). We observed that upon LPS stimulation, there is a 2-fold increase in the number of enhancers containing at least one DSBs, as detected by BLISS (Figure 19), showing a significant correlation between LPS administration and DSB formation.

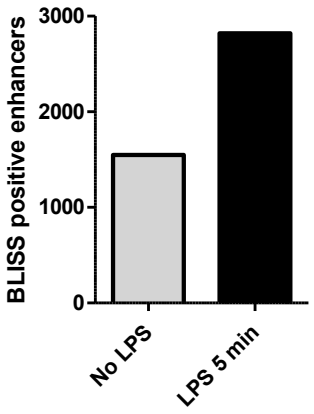

Figure 19 - BLISS genome-wide detection of DSBs induced at enhancers by LPS

Bars show the number of enhancer regions containing BLISS reads. BLISS followed by NGS was performed on RAW264.7 macrophages either untreated or treated with LPS for 5 minutes.

Thus, these results suggest a new role for DSBs in LPS-induced enhancer activation. In particular, LPS might trigger the formation of a transient DSB, which, in turn, can favor transcription activation, similarly to what was already observed in other cell types (Hartung et al. 2015, Madabhushi et al. 2015, Periyasamy et al. 2015, Puc et al. 2015a). These results have set the bases for further investigations to dissect how the DNA damage sensing and resolution are linked to the transcriptional activation of enhancer RNAs (Vitelli et al., *in preparation*).

4.2 DSB detection by imaging

While the most commonly used method to map DSBs in a population of cells is ChIP, immunofluorescence is commonly applied to detect DSBs in individual cells. Both methods, also immunofluorescence relies on antibodies recognizing chromatin modifications (γH2AX) or DNA damage markers (such as 53BP1) accumulating in so-called DDR foci. As discussed in the introduction section 2.5.3 this may represent a considerable source of bias since, since several groups showed or suggested DNA damage accumulation in the absence of DDR or, on the opposite, DDR activation in the absence of DNA damage. Despite the development of several new tools to detect DSBs genome-wide, at high-resolution, there are still some limitations. One is the amount of starting material required by these methods (thousands of cells at least) and another, is their relatively low sensitivity: a DSB has to be generated in the same position in hundreds of cells to be detectable. This implies that they cannot be used to detect randomly distributed DNA damage or with high cell-to-cell variability, or to obtain single-cell resolution of damaged genomes. On the other hand, the only alternatives to immunofluorescence for DNA damage detection in single-cells are

TUNEL, which allows DNA ends labeling with fluorescent nucleotides and detection (Shmuel 1992), and COMET assay (Olive et al. 1991). However, both methods have low sensitivity and are mostly used to detect massive DNA damage, such as that induced by apoptosis.

Inspired by BLESS strategy to label DSBs, I thought to use the same approach to detect DSBs *in situ.* First, I fixed cells with paraformaldehyde and permeabilized them in order to allow enzymes and reagents to enter the cell; then, I performed *in situ* DNA ends blunting by T4 DNA Polymerase (which has both a 3' overhang resection activity and a 5' overhang fill-in activity), followed by ligation to a biotinylated linker (see Material and Methods, section 3.12). Notably, these steps are very similar to the initial steps of BLISS, which was independently developed at later time. Having cells with DSBs labeled by biotin on coverslips, I thought to use an antibody against biotin to detect DSBs in the cells, by canonical immunostaining followed by microscopy. Unluckily, I have not been able to obtain a detectable signal (Figure 20), despite inducing several DSBs in the cells (with the inducible version of AsiSI, already used for DNA damage mapping experiments), probably because the single biotin molecule per DSB is too little abundant to have a robustly detectable signal by immunofluorescence.

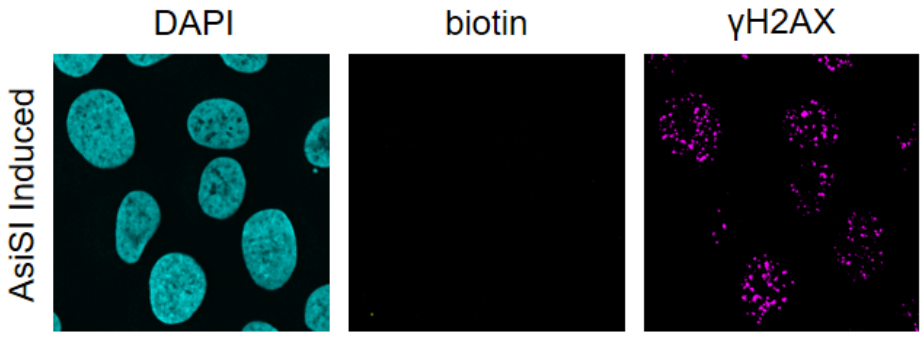

Figure 20 - Immunofluorescence with antibodies against biotin and γH2AX in DNA damaged cells.

U2OS AsiSI-ER cells, DNA damage is induced by the translocation of AsiSI in the nucleus upon 4-OHT treatment. DNA is stained by DAPI. The biotinylated linker has been ligated to exposed DNA ends.

To solve this problem of detection, I first thought to amplify the signal using a chain of secondary antibodies. After DNA end blunting, ligation and blocking with BSA and cold fish gelatin (PBG, see materials and methods, section 3.7), I sequentially incubated cells with a primary antibody against biotin (raised in rabbit), a secondary antibody against rabbit IgG (raised in donkey) conjugated with Cy5, then an antibody against Cy5 (raised in mouse) and finally an antibody against mouse IgG, conjugated with Cy5. However, with this strategy, I was only able to detect, by microscopy, a pan-nuclear background in both damaged and undamaged cells, even in the absence of the biotinylated linkers, probably due to the sum of unspecific binding of the various antibodies (Figure 21).

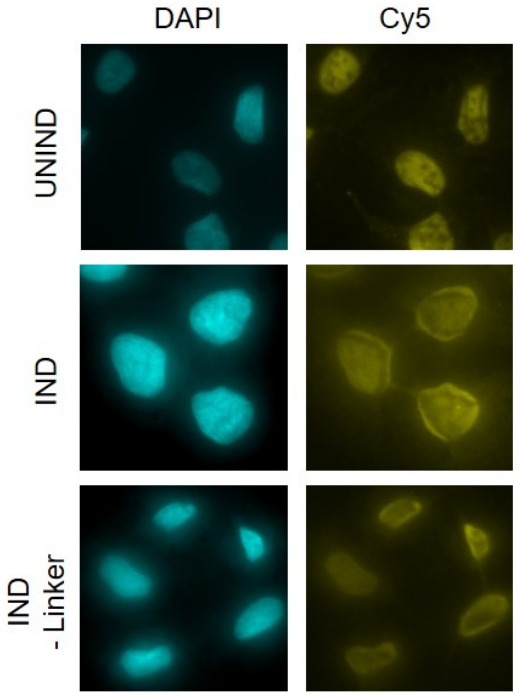

Figure 21 - Multistep immunofluorescence on U2OS AsiSI-ER cells either uninduced or induced with 300nM 4-OHT.

Primary antibody against biotin (raised in rabbit), secondary antibody against rabbit IgG, conjugated with Cy5, tertiary antibody against Cy5 (raised in mouse), quaternary antibody against mouse IgG, conjugated with Cy5. DNA stained by DAPI.

As an alternative way to enhance the signal, I thought to exploit the Proximity Ligation Assay (PLA, see Material and Methods, 3.11) which, through rolling circle amplification (RCA), allows high signal amplification (up to 1000-fold) and high sensitivity (Baner et al. 1998, Larsson et al. 2004, 2010, Ke et al. 2013). By Proximity Ligation Assay, whenever

two proteins of interested come in close proximity (~ 40 nm) and are recognized by two different primary antibodies, an *in situ* RCA reaction can take place, producing a fluorescent signal, dot shaped, detectable by microscopy. PLA reagents are commercialized as kit by Sigma, and this technique has been applied in several studies to study protein-protein interaction both in fixed cells and tissues (Söderberg et al. 2006, Jarvius et al. 2007, Gomez et al. 2013, Leuchowius et al. 2013, Rassoolzadeh et al. 2015). Moreover, it has been modified to work in combination with FISH, to study RNA-protein interaction (Roussis et al. 2016) and it has also been used to study DNA:RNA hybrids formation (Petruk et al. 2016).

I thought to perform PLA, after the ligation of the biotinylated linker to exposed DNA ends, using a primary antibody against biotin and a partner antibody against a marker of DDR activation such as γH2AX or 53BP1. With this strategy, that I named "DNA damage *in situ* ligation followed by Proximity Ligation Assay" (DI-PLA), each signal corresponds to at least one exposed DNA end of a DSB, in close proximity to a DDR factor (53BP1 or γH2AX in most of the following experiments). Importantly, with this strategy, DDR accumulation in the absence of an exposed DNA end is not sufficient to generate a signal by DI-PLA. A flowchart of DI-PLA is shown in Figure 22.

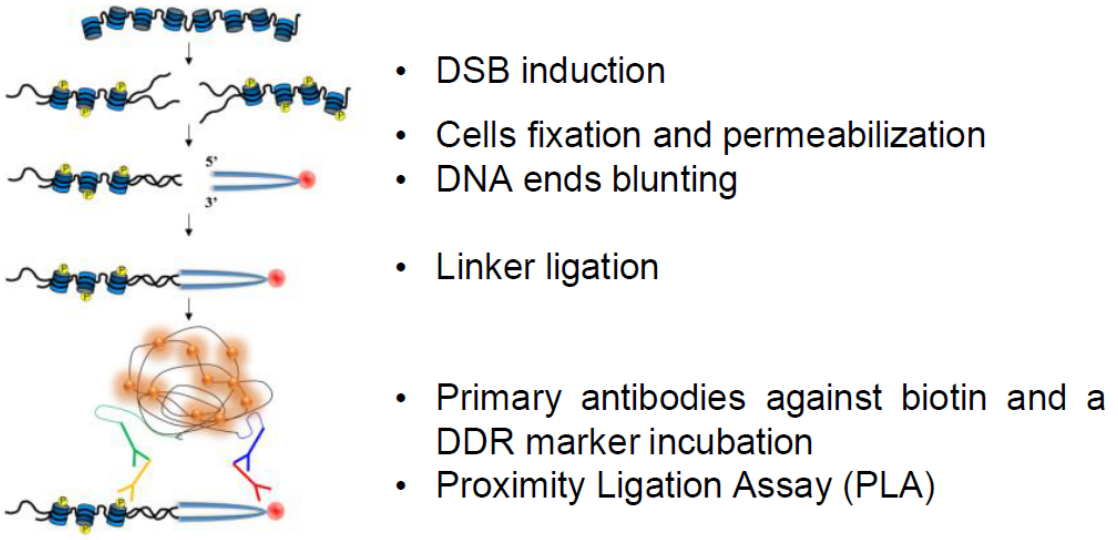

Figure 22 - DI-PLA workflow.

4.2.1 DI-PLA validation

4.2.1.1 DI-PLA detection of DSBs induced different DNA damaging sources.

To validate the efficiency of DSBs detection by DI-PLA, I first tested it on U2OS AsiSI cells either uninduced or induced with tamoxifen as I did for DSB mapping experiments by BLESS.

First, I performed immunofluorescence against the DDR factors 53BP1 and γH2AX (Figure 23) to use as reference for DI-PLA experiment.

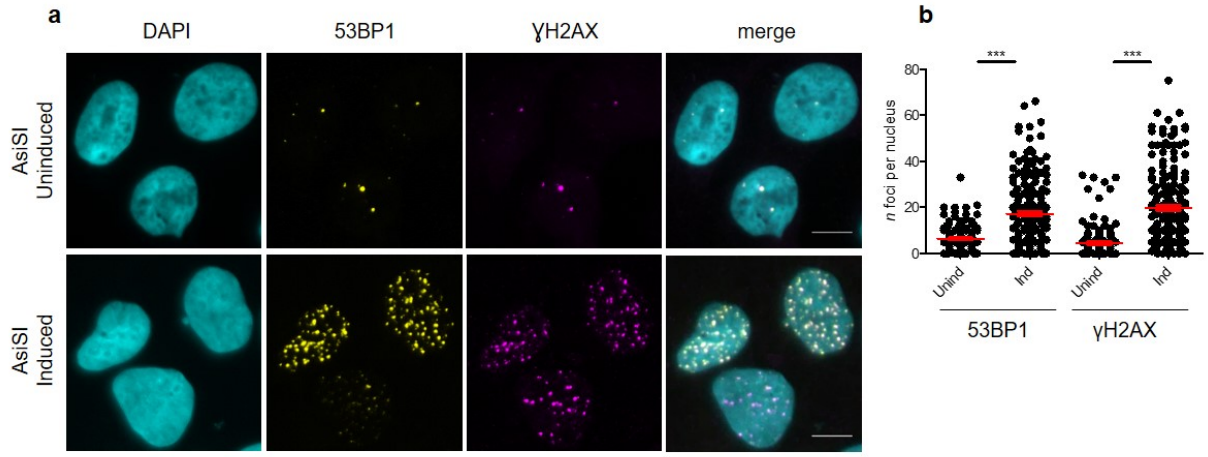

Figure 23 - Immunofluorescence for DNA damage markers in U2OS AsiSI cells.

a. Immunofluorescence for γH2AX and 53BP1 in uninduced (Unind) or induced (Ind) U2OS AsiSI-ER cells. DNA stained by DAPI. Scale bars: 10 µm. Quantification are shown in panels **b** (n=3).

Next, in the same experimental conditions, I performed PLA between γH2AX and 53BP1 and DI-PLA between biotin and either 53BP1 or γH2AX. As shown in Figure 24, both by PLA and DI-PLA, nuclear signals were robustly detected only in induced cells and not in control cells. Importantly, the number of dots measured by DI-PLA was very similar between the two sets of antibodies and comparable to those obtained by PLA between 53BP1 and γH2AX. Additionally, PLA and DI-PLA signals were similar in number to those obtained by immunofluorescence for the individual DDR markers.

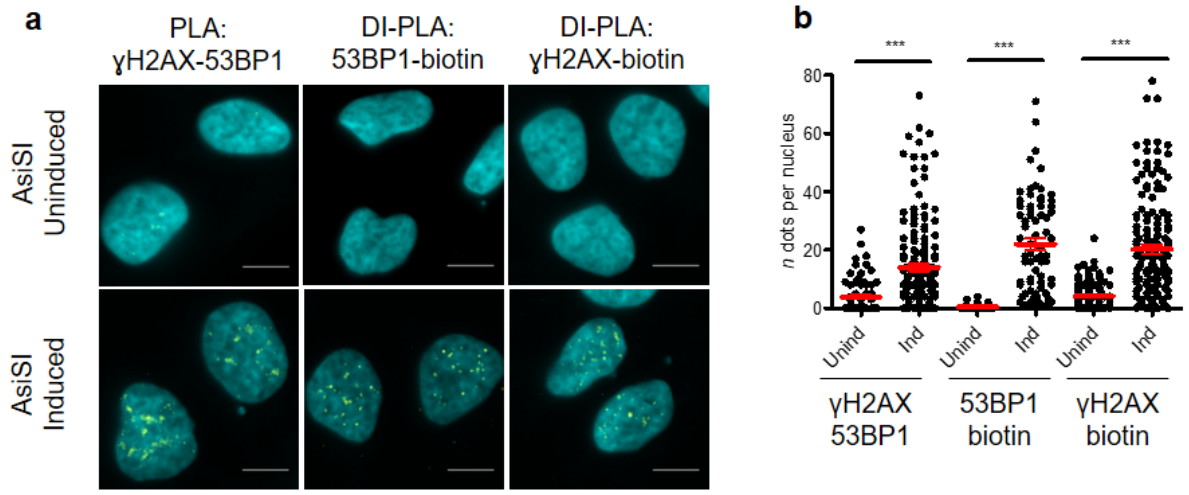

Figure 24 - DSBs generated by AsiSI are detected by DI-PLA in fixed cells.

a. PLA between γH2AX and 53BP1 or DI-PLA between 53BP1 and biotin or γH2AX and biotin, in uninduced (Unind) or induced (Ind) U2OS AsiSI-ER cells (DNA stained by DAPI). Scale bars: 10µm. Quantifications are shown in panel **b** (n≥3).

I reasoned that AsiSI-induced DSBs are particularly "clean", having all the same structure, with 2 protruding nucleotides, thus they are a very suitable substrate to DNA ends blunting and ligation reactions. However, most of the DSBs induced by endogenous stimuli or exogenous genotoxic agents are likely to have complex and heterogenous structures. Thus, I tested the robustness of DI-PLA in detecting DSBs generated by different genotoxic treatments, producing a plethora of different DNA breaks, including DSBs, likely to have heterogenous end structures. For this test, I used human BJ fibroblasts untreated or fixed 1 hour after exposure to ionizing radiations (IR), and I first performed immunofluorescence (Figure 25) for γH2AX and 53BP1, that I later compared with PLA performed between 53BP1 and γH2AX, and DI-PLA using antibodies against biotin and either 53BP1 or γH2AX (Figure 26).

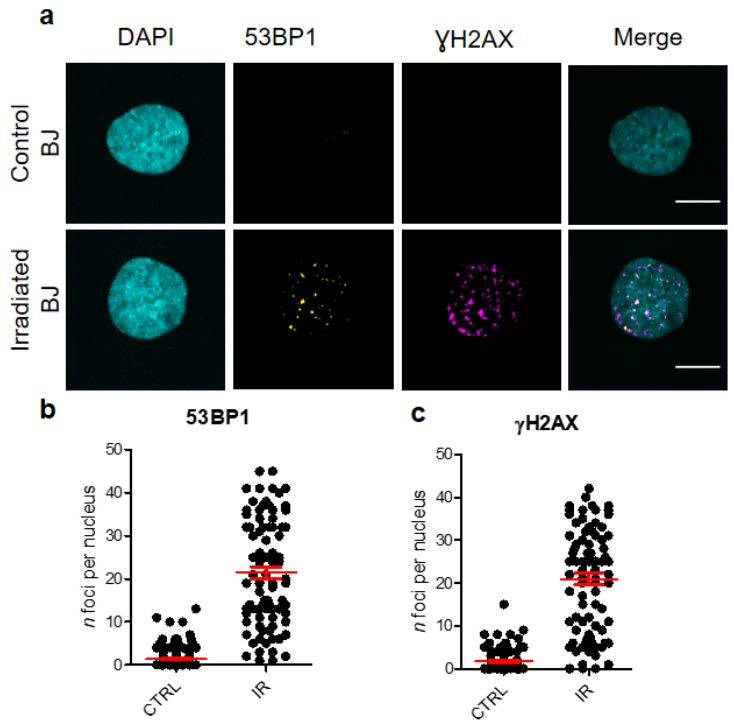

Figure 25 - Immunofluorescence for DDR markers in Irradiated cells.

a. Immunofluorescence for 53BP1 and γH2AX in BJ cells either untreated or irradiated with IR 2Gy and fixed 1 hour after treatment. DNA stained by DAPI. Scale bars: 10 µm. Quantifications are shown in panels **b, c** (n=3)**.**

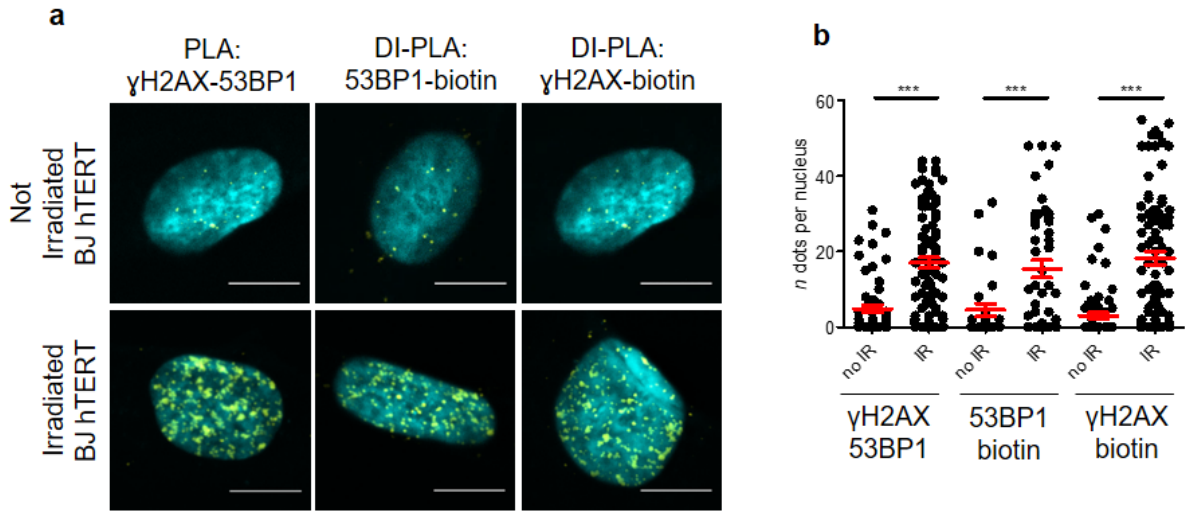

Figure 26 - DI-PLA detects IR-induced DSBs.

a. PLA between γH2AX and 53BP1 or DI-PLA between 53BP1 and biotin or γH2AX and biotin, in not irradiated (No IR) or irradiated (IR) BJ fibroblasts. DNA stained by DAPI. Scale bars: 10µm. Quantifications are shown in panel **b** (n=3).

As expected, I observed DDR foci formation specifically in irradiated cells by immunofluorescence, which were recapitulated by PLA signals detectable only in the

damaged cells. Strikingly, also by DI-PLA I detected signals specifically in the nucleus of irradiated cells, with an efficiency comparable to PLA between 53BP1 and γH2AX and quantitatively similar to the number of foci measured by IF for 53BP1 or γH2AX.

As an additional proof of the robustness of DI-PLA in efficiently detecting heterogenous DSBs, I performed a similar experiment to the one described above, using BJ cells either untreated or treated for 20 minutes with the radiomimetic drug neocarzinostatin (NCS).
Also in this case, I observed similar efficiency in DSB detection between immunofluorescence (Figure 27), PLA between γH2AX and 53BP1 and DI-PLA between biotin and 53BP1 (Figure 28).

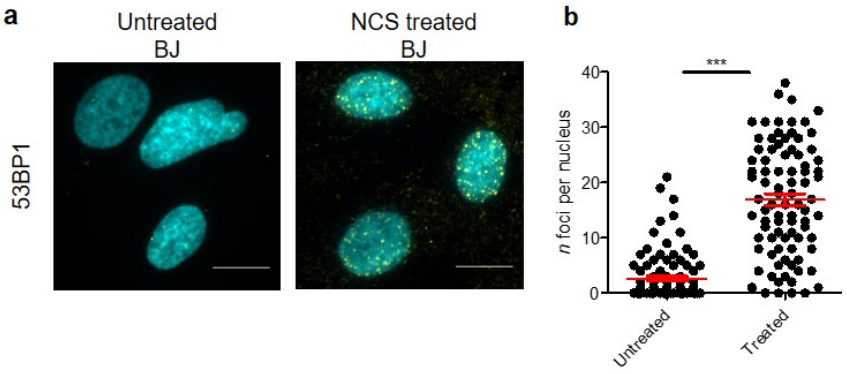

Figure 27 - Immunofluorescence for DDR marker in NCS treated cells.

a. Immunofluorescence for 53BP1 in BJ cells either untreated or treated for 20 minutes with neocarzinostatin (NCS, 50ng/mL). DNA stained by DAPI. Scale bars: 10 µm. Quantifications are shown in panel **b** (n=2).

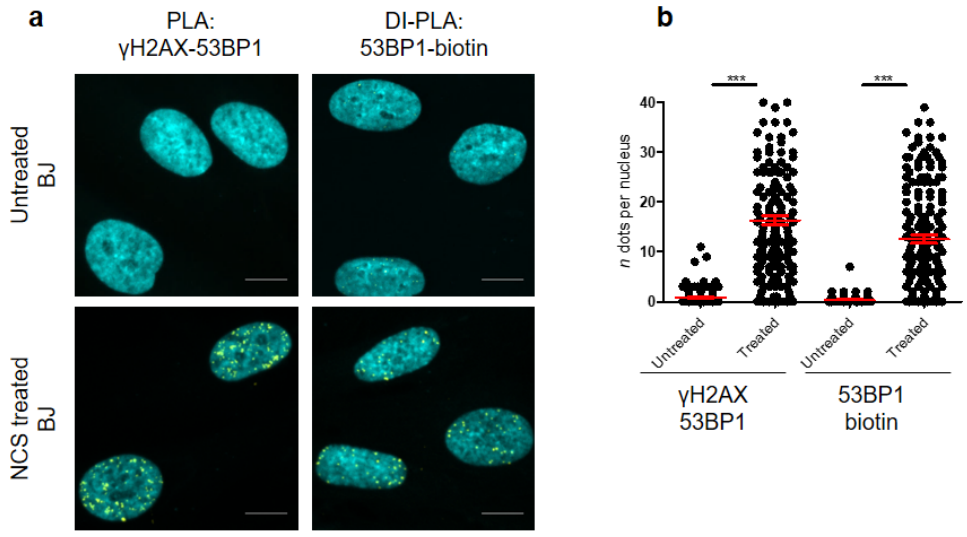

Figure 28 - DI-PLA detects NCS-induced DSBs.

a. PLA between γH2AX and 53BP1 or DI-PLA between 53BP1 and biotin on untreated or NCS treated BJ fibroblasts. DNA stained by DAPI. Scale bars: 10µm. Quantifications are shown in panel **b** (n=3)**.**

Although ionizing radiations and radiomimetic drugs are known to induce DSBs with complex end structures, which might lower the efficiency of DNA ends blunting by T4 DNA polymerase, thus reducing DI-PLA signals, in practice I consistently observed similar results with IF, PLA and DI-PLA in all the conditions I tested. Taken together, these results indicate that DI-PLA reliably detects DSBs generated by different sources, in proximity to an activated DDR marker.

4.2.1.2 DI-PLA signals specificity

To exclude the contribution of antibody binding to unspecific targets that could lead to false positive DI-PLA signals, I repeated DI-PLA on BJ cells fixed 1 hour after irradiation, using linkers not bearing the biotin. As shown in Figure 27, I could clearly observe the lack of any detectable signal by microscopy.

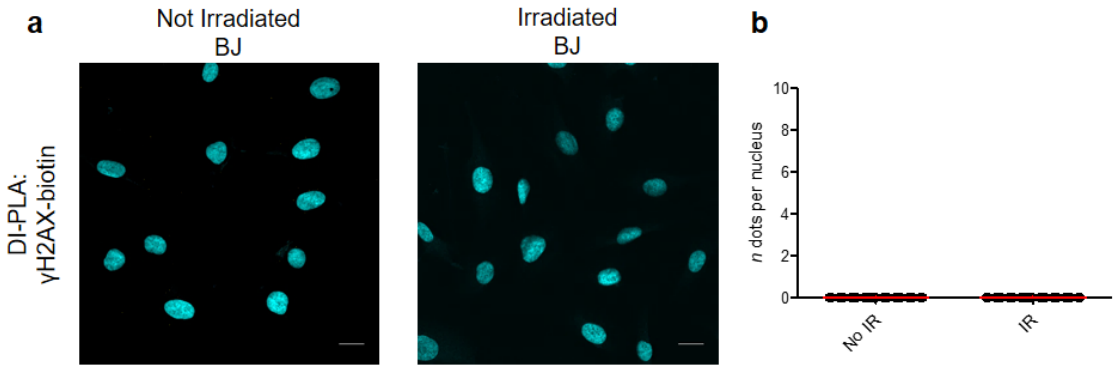

Figure 29 - In the absence of the biotinylated linker DI-PLA does not generate any signal.

a. DI-PLA between γH2AX and biotin in BJ cells either not irradiated (No IR) or irradiated (IR) as in Figure 24, in the presence of a non-biotinylated linker. DNA stained by DAPI. Scale bars: 20µm. Quantifications are shown in panel **b** (n=2).

Another variability that could lead to misinterpretation of DI-PLA data is due to the biotin partner antibodies recognizing DDR factors that are not detectable in the absence of DNA damage. In other words, I asked whether DI-PLA signals increased in DNA damaged cells,

only because they reflect an increase in the DDR markers used as a partner for biotin, rather than the presence of DDR markers in physical proximity of biotin-labeled DSBs. To address this point, I used an antibody against a chromatin component that is unchanged upon DNA damage induction. Thus, I first performed immunofluorescence for the histone H4 on fixed BJ cells either untreated or irradiated (Figure 30).

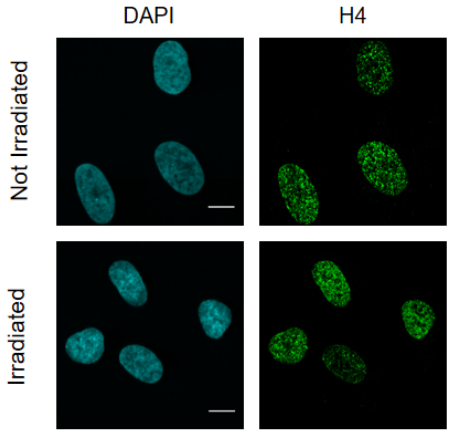

Figure 30 - H4 levels do not change upon IR.

Immunofluorescence for histone H4 in BJ fibroblasts, untreated (-IR) or irradiated (IR) with ionizing radiation (2Gy). DNA stained by DAPI. Scale bars: 10µm.

As expected, the antibody against H4 produced a pan-nuclear staining, that was unchanged upon irradiation. Next, I performed DI-PLA between H4 and biotin, under the same experimental conditions. I observed a low background in untreated cells, and a clear increase of nuclear signals in irradiated cells, similarly to PLA between H4 and γH2AX (Figure 31).

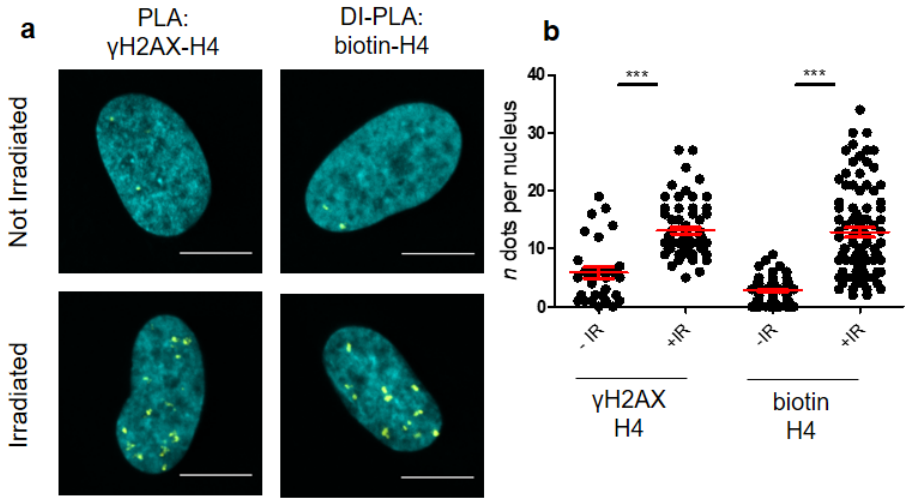

Figure 31 - DI-PLA signals are dependent on biotin-labeled DSBs in proximity to a partner target protein.

a. PLA between γH2AX and H4, and DI-PLA between H4 and biotin, Not Irradiated (-IR) or irradiated (IR) BJ fibroblasts. DNA stained by DAPI. Scale bars: 10μm. Quantifications are shown in panel **b** (n=2).

This result indicates that DI-PLA signals are dependent on biotin-labeled DSBs in proximity to a partner target protein. It also suggests the possibility to use DI-PLA to probe for the presence of DSBs in particular genomic regions that could be characterized by specific chromatin components, such as centromeres or telomeres.

As additional technical control, I asked whether DI-PLA is specific for the distance between biotin and its partner target: I wanted to prove that biotin and the partner protein must be physically close to produce a signal. To answer this question, I performed DI-PLA on irradiated U2OS cells using antibodies against biotin and cyclin A, a protein commonly used as marker of cell cycle phase, which is not recruited at DSBs. To avoid any cell cycle variation (that would result in altered level of Cyclin A), I irradiated BJ fibroblasts (in exponential growth phase) and fixed cells only 15 minutes after IR. As shown in figure 30, I could only observe a low background by DI-PLA between biotin and Cyclin A in both untreated and irradiated cells (Figure 32).

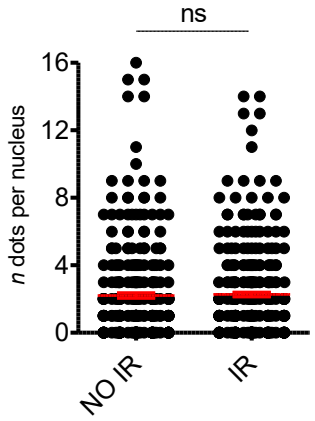

Figure 32 - The partner target protein must be in close proximity to biotin to generate a signal by DI-PLA.

Quantifications of dots per nucleus detected by DI-PLA using antibodies against biotin and Cyclin A on BJ not irradiated or irradiated with 2Gy and fixed 15 minutes after IR (n=2).

This result is an additional proof that the antibody that is paired with the anti-biotin one must be specific for a protein present at the DSBs.

To further test DI-PLA specificity I asked whether the number of signals could be correlated to the dose of DSBs generated in the cell. To investigate this matter, I irradiated BJ cells with different doses of ionizing radiation, fixed and stained them for immunofluorescence for DDR markers (Figure 33) or PLA between γH2AX and DI-PLA between biotin and γH2AX (Figure 34).

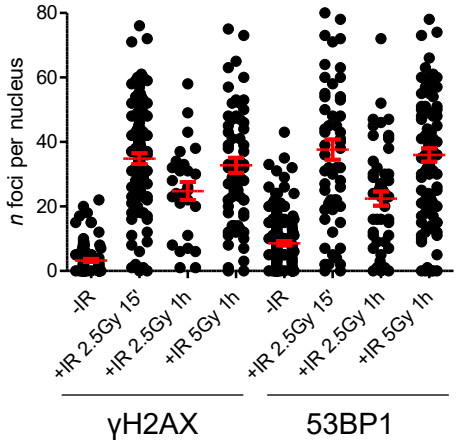

Figure 33 - Immunofluorescence for DDR marker in cells exposed to various doses of IR.

Quantifications of foci per nucleus detected by immunofluorescence using antibodies against γH2AX and 53BP1 on BJ not irradiated or irradiated at different doses and fixed at the indicated time points after irradiation (n=2).

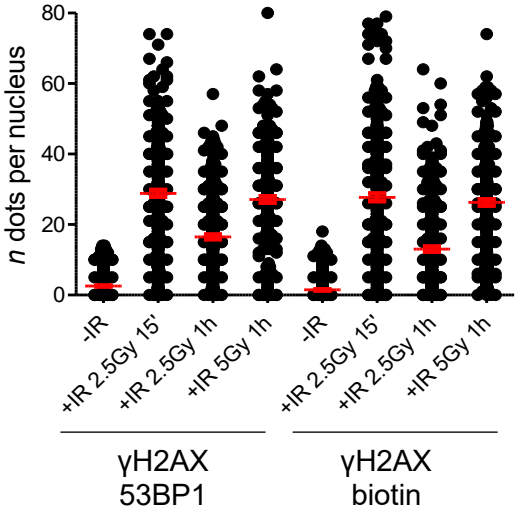

Figure 34 - DIPLA signals depend on the amount of DSBs in the cell.

Quantifications of dots per nucleus generated by PLA using antibodies against γH2AX and 53BP1 or DI-PLA using antibodies against biotin and γH2AX on BJ not irradiated or irradiated at different doses and fixed at the indicated time points after irradiation (n=2).

By DI-PLA I observed a higher number of nuclear signals 15 minutes after IR (Figure 34), compared to 1 hour after IR, while, increasing IR dose from 2.5 Gy to 5 Gy resulted in a 1.5-fold increase in DI-PLA signals, consistently to what I observed by PLA and IF for DDR markers (Figure 33).

To further test DI-PLA sensitivity to the number of DSBs present in the cell, I performed an *in vitro* ligation experiment. I induced U2OS AsiSI cells with tamoxifen, then I fixed with PFA, permeabilized the cells and performed DNA ends blunting and ligation (as the described for DI-PLA), in the absence of any linker: this step should lead to *in vitro* ligation of the available DNA ends. Next, I performed DI-PLA (blunting, ligation with biotinylated linkers and PLA between γH2AX and biotin) and compared with canonical DI-PLA on uninduced U2OS AsiSI cells and induced U2OS AsiSI cells (Figure 35).

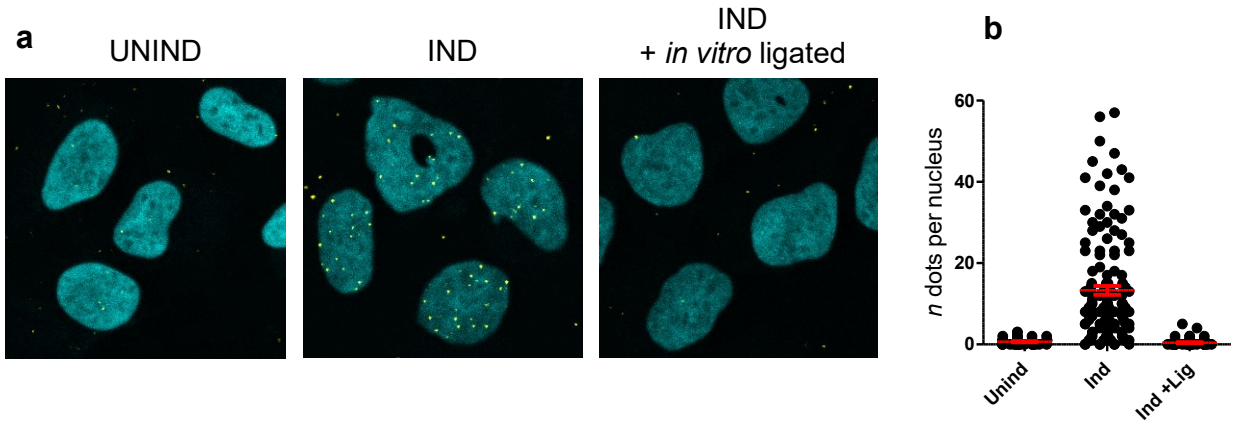

Figure 35 - DI-PLA signals depend on the presence of physical DSBs.

a. DI-PLA between γH2AX and biotin on Uninduced, Induced or Induced *in vitro* Ligated U2OS AsiSI cells. DNA stained by DAPI. Quantifications are shown in panel **b** (n=1).

I could clearly observe, that *in vitro* ligated - induced AsiSI displayed nearly the same very low number of DI-PLA signals as uninduced cells.

This result, together with the experiments with different IR doses, indicates that the number of DI-PLA signals per nucleus directly depends on the amount of DSBs in the cell. Next, I asked whether DI-PLA signals were also spatially specific for DSBs positions.

The easiest way to address this question would be to analyze the co-localization of DI-PLA signals with a DDR marker; this could be achieved using an antibody against a DDR factor, different from the one used as the partner of biotin, which could be detected by immunofluorescence, and then analyze the co-colocalization between the IF signal and DI-PLA. However, this experiment is not simple to perform due to the requirement of having 3 different antibodies raised in 3 different species, with good specificity against their target proteins. Instead, I took advantage of a cell line expressing the DDR marker NBS1 fused to GFP, to achieve direct visualization of the sites of NBS1 recruitment. I induced DNA damage by laser micro-irradiation, then I fixed cells and performed DI-PLA between biotin and γH2AX. As expected, I could clearly observe the sub-cellular recruitment of NBS1 at the site of damage, resulting in bright stripes. As it is shown in Figure 36, I observed almost 80% of DI-PLA signals colocalizing with the NBS1-GFP stripes, clearly indicating a good specificity of DI-PLA signals.

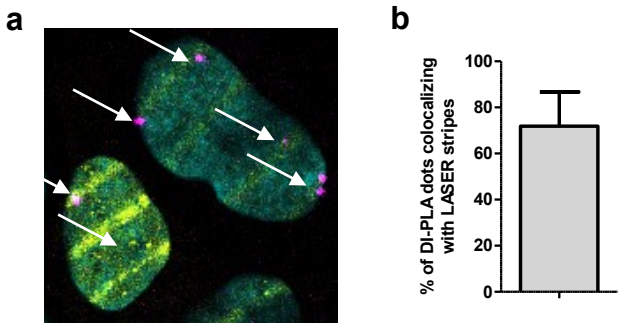

Figure 36 - DI-PLA signals co-localize with DDR marker.

a. DI-PLA for γH2AX and biotin in U2OS NBS1-GFP laser irradiated. GFP is in yellow, DI-PLA signal is magenta. DNA stained by DAPI. Quantifications are shown in panel **b** (250 cells scored)**.**

Collectively, these experiments show that DI-PLA produces detectable signals only in the presence of labeled DSBs in close proximity to the partner factor. Moreover, DI-PLA signals are dependent on the amount of DSBs in the cell and specific for the sub-cellular localization of the DSBs.

4.2.1.3 DI-PLA is suitable to detect DSBs in tissue sections

Having validated the specificity of DI-PLA in detecting DSBs in fixed cells, I asked whether this technique could also be used to investigate DSBs presence in fixed tissue sections. PLA had already been applied in studies on both formalin fixed paraffin embedded (FFPE) and fixed frozen tissues, with minimal modifications to the standard protocol (Leuchowius et al. 2013b, Spears et al. 2012). I used fixed frozen kidney sections from not irradiated and irradiated mice, which I first stained with an antibody against γH2AX by immunofluorescence (Figure 37), and later compared with PLA between γH2AX and 53BP1 and DI-PLA between biotin and γH2AX (Figure 38), without selecting for the cell types.

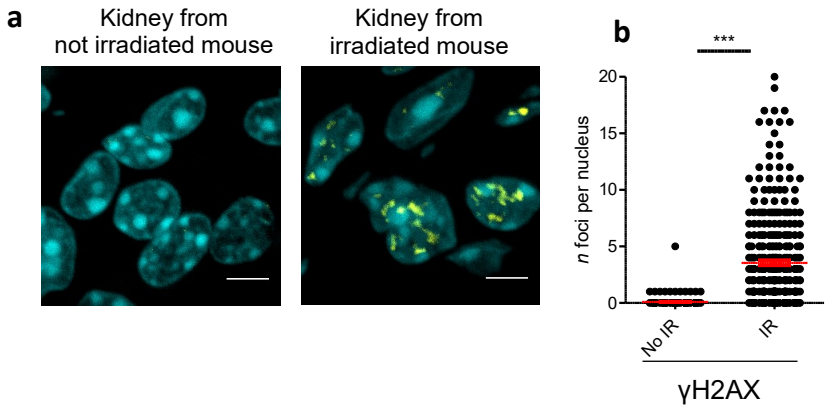

Figure 37 - Immunofluorescence for γH2AX in mouse tissue sections.

a. Immunofluorescence for γH2AX in kidney sections from not irradiated (No IR) or irradiated (IR) with 5Gy TBI and sacrificed 6h after IR. DNA stained by DAPI. Scale bars: 5µm. Quantifications are shown in panel **b** (n=2).

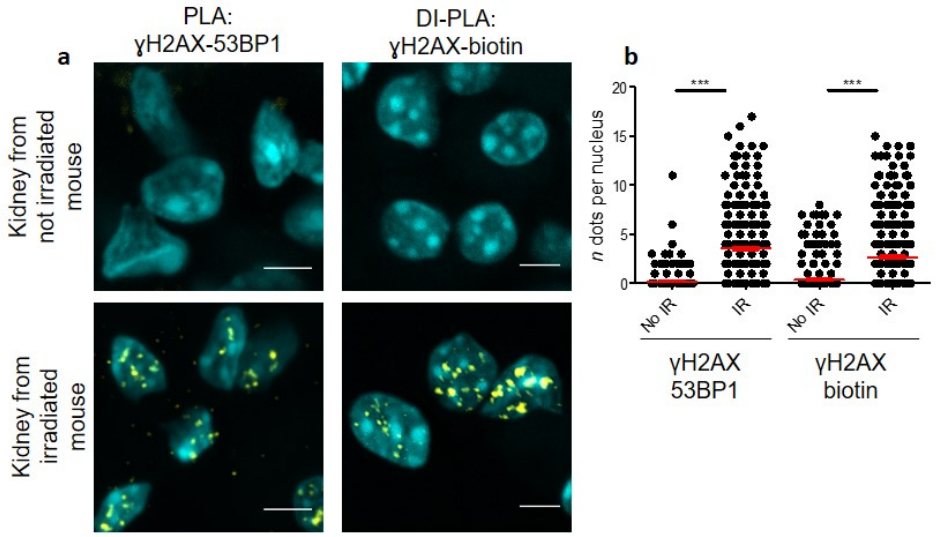

Figure 38 - DIPLA detects DSBs in irradiated mouse tissue sections.

a. DSBs generated by IR are detected by DI-PLA in tissue sections derived from mice. PLA between γH2AX and 53BP1 or DI-PLA between γH2AX and biotin, in kidney sections from not irradiated (No IR) or irradiated (IR) mice (DNA stained by DAPI). Scale bars: 5μm. Quantifications are shown in panel **b** (n=3).

I detected nuclear signals by DI-PLA between biotin and γH2AX only in tissue sections from the irradiated mice, with an efficiency similar to both PLA between 53BP1 and γH2AX and IF for γH2AX, although I occasionally observed unequal staining of the tissue sections, possibly due to the critical thickness of the sections or partial drying of the reaction mixes. Moreover, using the non-biotinylated version of the linker, DI-PLA between biotin and γH2AX did not generate any detectable signal (Figure 39), proving the specificity of DI-PLA signal.

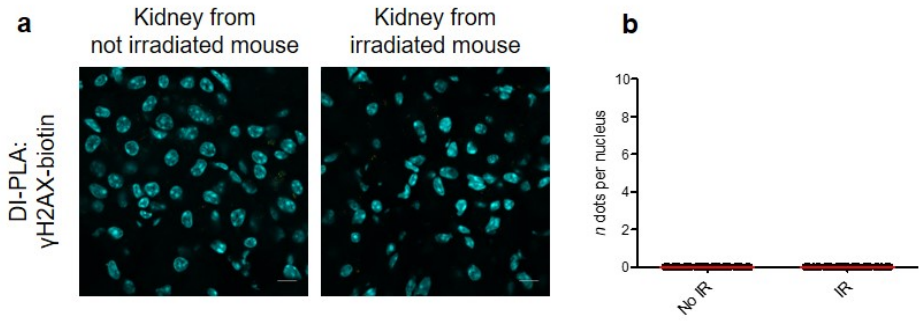

Figure 39 - DSBs are detectable by DI-PLA in tissue sections only in the presence of the biotinylated linker.

a. DI-PLA between γH2AX and biotin, in kidney sections from not irradiated (No IR) or irradiated (IR) mice, using a non-biotinylated linker. DNA stained by DAPI. Quantifications are shown in panel **b** (n=2).

In summary, these results show the feasibility of DI-PLA on fixed frozen tissue sections; instead, I was not able to obtain an efficient staining by DI-PLA of FFPE tissue sections (data not shown).

4.3 Senescent cells accumulate persistent DSBs

When cells are unable to repair DSBs, the unrepaired DNA damage can lead to persistent DDR activation, enforcing a permanent cell-cycle arrest termed cellular senescence (d'Adda

di Fagagna 2008). As discussed in the introduction (section 2.6), senescent cells display persistent DDR foci that are necessary to fuel damage-induced senescence (Rodier et al. 2011). Previously, our lab and others, have proposed that these are persistent DNA lesions in the form of DSBs that resist cell repair activities (Fumagalli et al. 2012, Hewitt et al. 2012). However, others have proposed that such structures might not be sites of damaged DNA per se, but instead stable chromatin alterations resulting from damage (without an underlying lesion), which are necessary to reinforce senescence (DNA-SCARS) (Rodier et al. 2011). So far, whether the persistent DDR foci present in senescent cells correspond to physical DSBs or not has been an open question. However, having previously demonstrated the possibility to detect DSBs in the proximity of an activated DDR marker by DI-PLA, I could finally try to address this matter. Thus, I generated two types of senescent cells and studied them with DI-PLA.

4.3.1.1 Replicative senescent cells display persistent DSBs

First, I compared early with late passage BJ cells: it is well known that late passage fibroblasts undergo replicative senescence, as the result of critically short telomeres that activate a local DDR (Bodnar et al. 1998). Here, I compared fibroblasts at population doubling 30-32 with fibroblasts at population doubling 62-66, that were in senescent state as indicated by senescence-associated β-galactosidase (β-gal) activity (Figure 40) and reduced 5-bromodeoxyuridine (BrdU) incorporation (Figure 41).

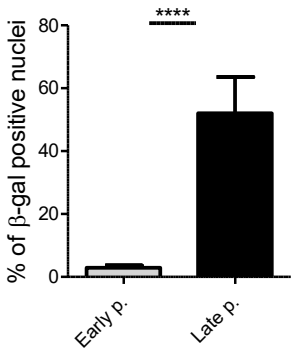

Figure 40 - Quantification of β-gal positive cells.

Early passage (PD 30-32) and late passage (PD 62-66) were compared with the β-gal assay (n=3).

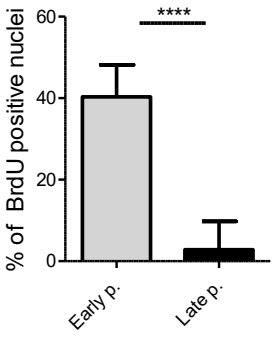

Figure 41 - Quantification of BrdU-positive nuclei.

Early passage (PD 30-32) and late passage (PD 62-66) were incubated for 6h with 5-bromodeoxyuridine, then fixed and stained for BrdU under DNA denaturation condition (Material and methods) (n=3).

.

As expected, most (~ 85%) of late passage BJ cells displayed DDR foci, with a mean of 5 foci per nucleus as determined by immunofluorescent against 53BP1 and γH2AX (Figure 42).

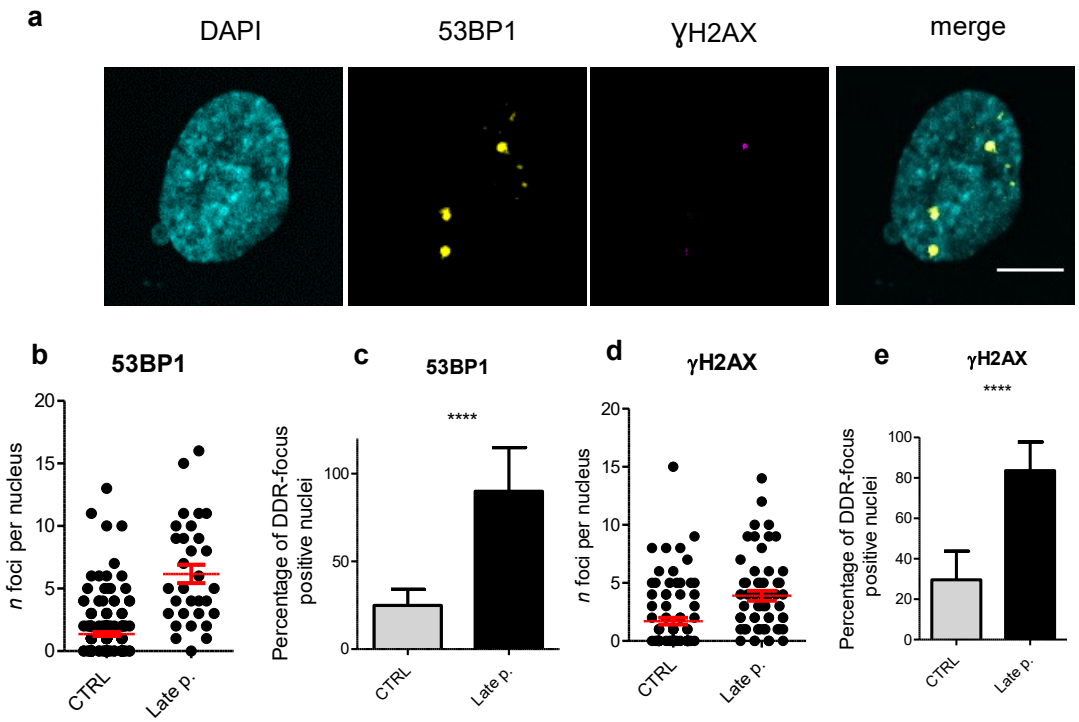

Figure 42 - Immunofluorescence for DDR markers in replicative senescent cells.

a. Immunofluorescence for the DDR markers 53BP1 and γH2AX in late passage BJ cells (PD62-66). DNA stained by DAPI. Quantifications in panels **b-e** (n=3).

Then, on the same cells that I stained by IF, I performed PLA between 53BP1 and γH2AX. Here, consistently with IF results, I observed the accumulation of nuclear dots in about 65%

of nuclei of the senescent cells, with a mean of 5 dots per nucleus; instead, PLA signals could be detected only in a small fraction (20%) of early passage cells, with a mean of 2 dots per nucleus (Figure 43).

Having quantitatively established the presence of persistent DDR activation in replicative senescent cells, in agreement with published data, I next tested for the presence of DSBs at the DDR foci by DI-PLA. Strikingly, DI-PLA between biotin and either 53BP1 or γH2AX, generated a 3-fold increase in average dots per nucleus upon senescence, increasing from 2 in early passage cells to 6 (Figure 43). Overall, I observed that almost 60% of the senescent cells displayed DI-PLA signals, while I could detect nuclear dots in only 20% of the early passage cells (Figure 43).

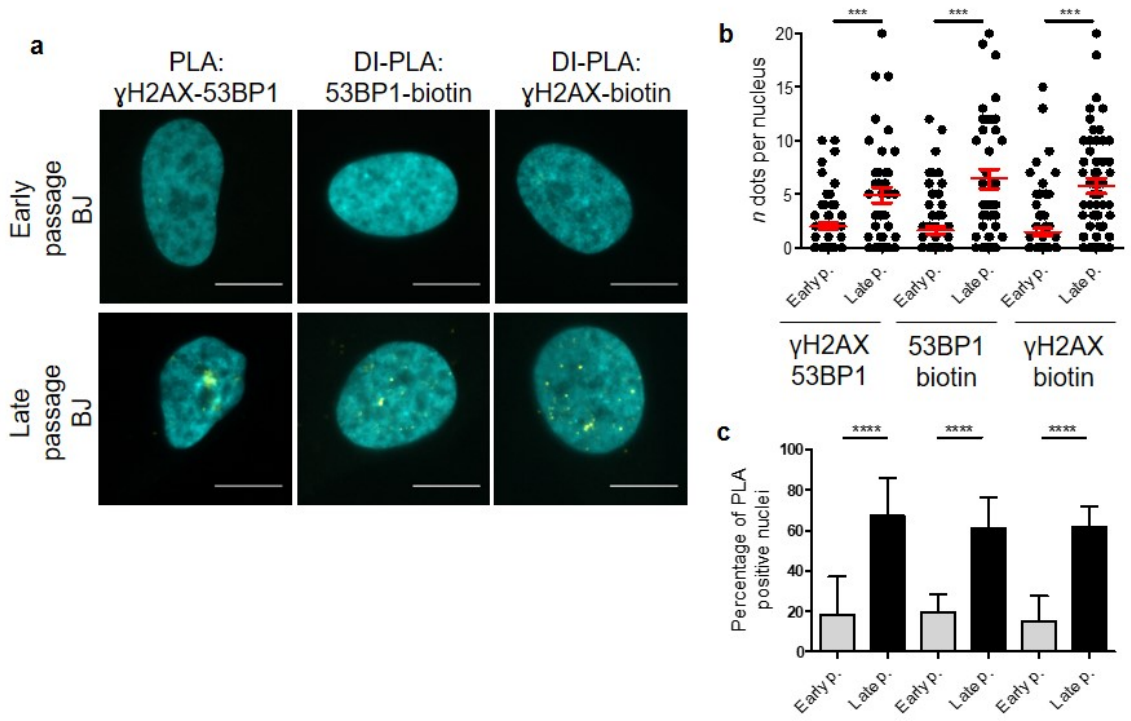

Figure 43 - Replicative senescent cells display unrepaired DSBs as detected by DI-PLA.

a. PLA between γH2AX and 53BP1, and DI-PLA between 53BP1 and biotin or γH2AX and biotin in early passage (Early p.) and senescent (late passage – Late p.) BJ cells. DNA stained by DAPI. Scale bars: 10μm. Quantifications are shown in panels **b,c** (n≥3).

Thus, the consistency of results between DI-PLA, PLA and IF experiments indicate that the persistent DDR foci that enforce cellular senescence correspond to physical DSBs.

4.3.1.2 Irradiation-induced senescent cells display persistent DSBs

To strengthen my observations, I tested whether senescent cells obtained after exposure to a high dose of IR, also displayed persistent DSBs. As previously reported (Fumagalli et al. 2012), BJ hTERT cells (that are immortalized, thus do not undergo telomere erosion and replicative senescence) showed all features of senescent cells 4 weeks after high-dose IR, including β-gal activity (Figure 44), reduced BrdU incorporation (Figure 45) and persistent DDR foci as visualized by IF for 53BP1 and γH2AX (Figure 46), differently from control cells that were not irradiated, but kept in culture for 28 days and underwent quiescence due to contact inhibition.

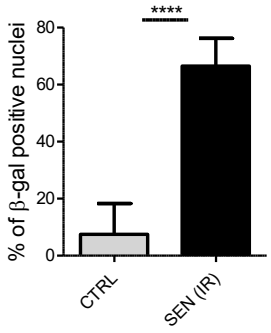

Figure 44 - Quantification of β-gal positive cells.

BJ hTERT cells that were kept in culture for 28 days (CTRL) were compared with BJ hTERT senescent irradiated cells (n=3).

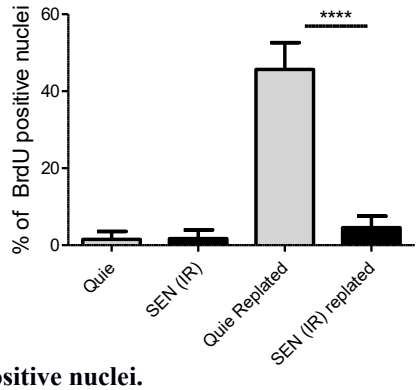

Figure 45 - Quantification of BrdU-positive nuclei.

Quiescent cells do not show BrdU incorporation since they are unable to proliferate due to contact inhibition; however, once re-plated at a lower concentration they are able to restore growth, as indicated by BrdU incorporation. Differently, senescent cells are unable to proliferate, even after re-plating at a lower concentration, as shown by BrdU incorporation rates (n=3).

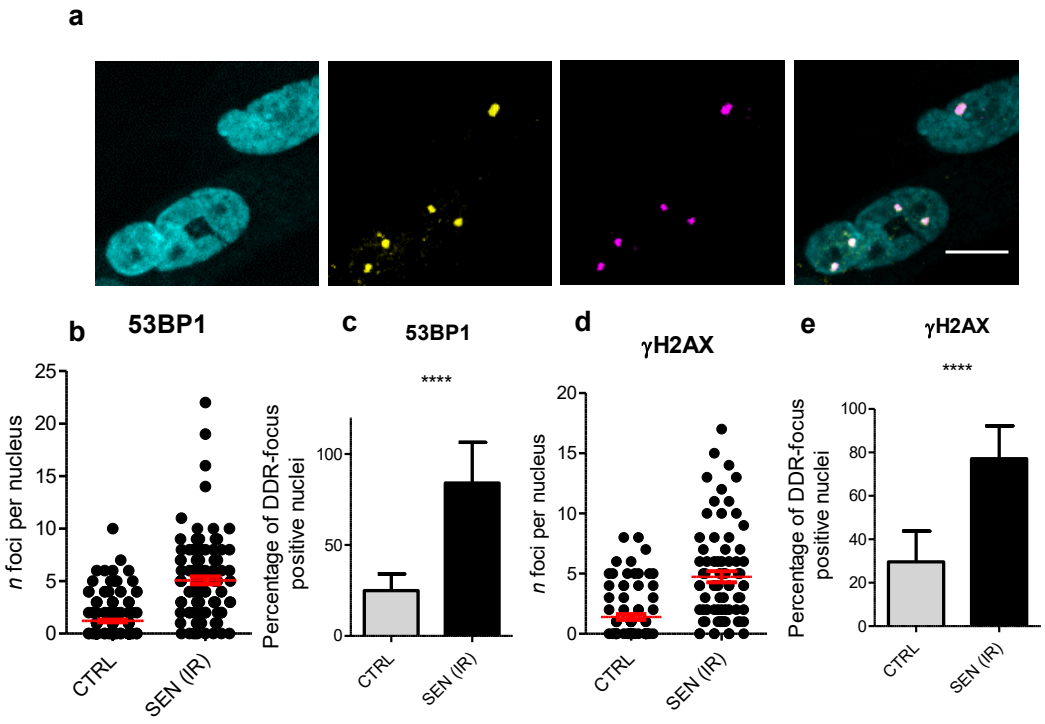

Figure 46 – Immunofluorescence for DDR markers in IR-induced senescent cells.

a. immunofluorescence for the DDR markers 53BP1 and γH2AX in senescent irradiated BJ hTERT cells. DNA stained by DAPI. Quantifications in panels **b-e** (n=3).

Under the same experimental conditions, I performed PLA between 53BP1 and γH2AX and observed that almost 60% of the senescent cells displayed PLA signals with a mean of 5 dots per nucleus, while only 25% of untreated cells were positive for PLA signals, with a mean of 2 dots per nucleus (Figure 47). I also observed similar results with DI-PLA between biotin and either γH2AX or 53BP1, with nearly 3 times more DI-PLA signals in senescent compared to quiescent cells, consistently with the results obtained with the other techniques (Figure 46).

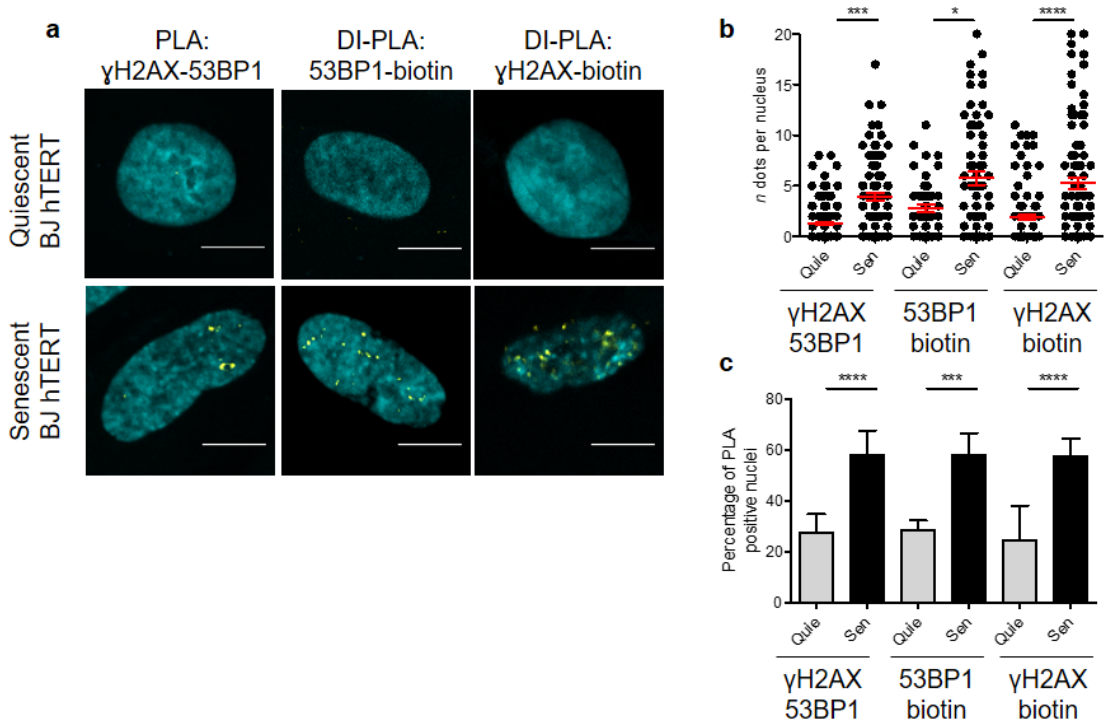

Figure 47 - DI-PLA detects persistent DSBs in IR-induced senescent cells.

a. PLA between γH2AX and 53BP1 or DI-PLA between 53BP1 and biotin or γH2AX and biotin, in Quiescent (Quie) or IR-induced senescent (Sen) BJ hTERT fibroblasts. DNA stained by DAPI. Scale bars: 10µm. Quantifications are shown in panels **b,c** (n≥3).

Altogether, these results, consistent for IF with individual DDR markers, PLA between the 53BP1 and γH2AX and DI-PLA, in both types of senescent cells analyzed, strongly indicate that the persistent DDR foci correspond to physical DSBs.

4.3.1.3 Tissues from aged animals accumulate persistent DSBs

As discussed in the introduction (section 2.6), cellular senescence has also been strongly linked to *in vivo* ageing. Consistently with the observations generated in cell culture, also *in vivo* ageing tissues show accumulation of persistent DDR foci (Fumagalli et al. 2012, López-Otín et al. 2013, White et al. 2015)

Here, having already shown that senescent cells accumulate persistent DSBs, I asked whether the DDR signals that accumulate in aged tissues also correspond to physical DSBs. I first performed PLA between 53BP1 and γH2AX on frontal cortex brain tissue sections

from adult mice (12-14 months old) and old mice (22-24 months); in agreement with data previously reported in literature (Sedelnikova et al. 2004), in the cells of aged tissues I observed a mean of 2 dots per nucleus, with about 50% of the cells displaying at least 1 PLA signal (Figure 48). I did not perform any selection on the cell types used for analyses.

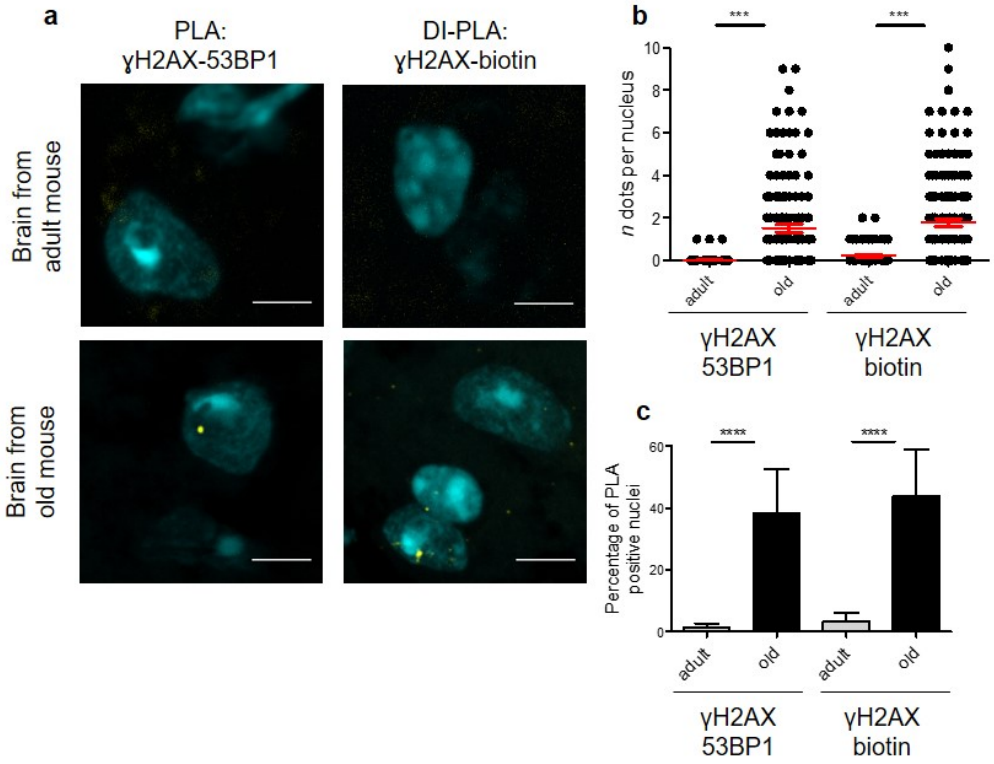

Figure 48 - Aged mammalian tissues display unrepaired DSBs as detected by DI-PLA.

a. PLA between γH2AX and 53BP1 or DI-PLA between γH2AX and biotin in brain sections from adult (12-14 months) or old (22-24 months) mice (DNA stained by DAPI). Scale bars: 5µm. Quantifications are shown in panels **b,c** (n=3).

Consistently, DI-PLA between biotin and γH2AX generated nearly 10 times more signals in frontal cortex sections from old mice (22-24 months) compared to adult mice (12-14 months old), with a mean of 2 DI-PLA dots per nucleus (Figure 48).

To strengthen the results, I extended these analyses to liver sections of the same aged mice and, consistently with the aforementioned results, I measured a statistically significant increase with ageing in the number of signals generated either by PLA between γH2AX and 53BP1 or DI-PLA between biotin and γH2AX, although the absolute numbers of dots per nucleus were overall lower than in the brain (Figure 49).

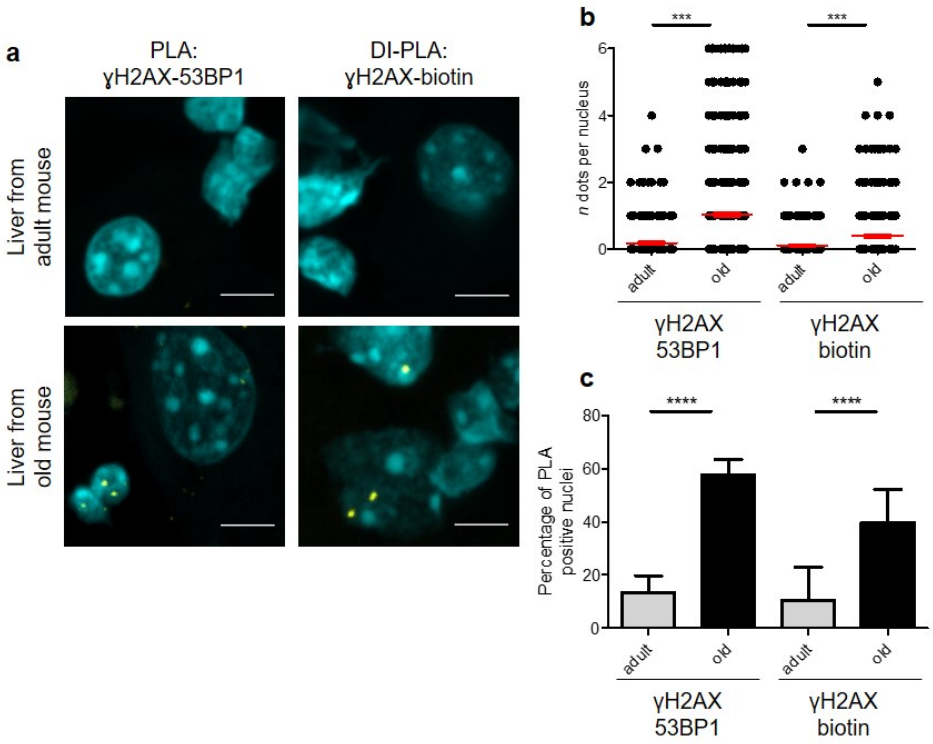

Figure 49 - Aged mice liver accumulate persistent DSBs, detectable by DI-PLA.

a. PLA between γH2AX and 53BP1 or DI-PLA between γH2AX and biotin, in liver sections from adult (12-14 months) or old (22-24 months) mice. DNA stained by DAPI. Scale bars: 5µm. Quantifications are shown in panels **b,c** (n=3).

Overall, the consistent results between PLA and DI-PLA indicate that, in also aged mammalian tissues accumulate senescent cells displaying persistent DSBs.

4.4 Genome-wide accumulation of persistent DSBs

Having demonstrated that persistent DSBs accumulate in senescent cells and tissues, I planned to investigate whether there is any preferential genomic location for the accumulation of DNA damage. It has been proven that telomeric sequences accumulate DNA damage in senescent cells (Fumagalli et al. 2012, Hewitt et al. 2012); however, in the same reports, other regions accumulating γH2AX in senescent cells were observed. Most importantly, the recently developed genome-wide DSBs mapping techniques have never been applied to senescent cells, so I felt that further investigation might reveal new genomic regions accumulating DSBs.

I therefore exposed BJ hTERT cells to a high dose of IR (20Gy). I fixed cells at five different time points after IR: immediately after IR (also called 0 minutes), 60 minutes, 24 hours, 7 days, and 28 days. The last time point was the same at which I validated the presence of persistent DSBs by DI-PLA. As control, I used quiescent BJ hTERT cells that were not irradiated but were kept in culture for 28 days in parallel with the irradiated cells. After cell fixation, I performed BLISS followed by NGS. With this strategy, I aimed to discriminate regions that are repaired quickly after IR and regions that instead accumulate hard-to-repair DSBs till later time points.

In collaboration with our bioinformatician Dr. Iannelli, we, unexpectedly, observed a wide-spread background BLISS signal in not irradiated cells, which represented a problem when trying to infer IR-induced DSBs. Differently from the applications of BLISS that I described in previous paragraphs, here we had to call DSBs *de novo* or, in other words, without *a priori* knowledge of the genomic region where we expected DSB to form. Thus, in order to analyze BLISS data in this particular setting, we set up a collaboration between our group and the one of Prof. Pattini at Politecnico di Milano. I was involved in the development of an algorithm able to identify DSBs in genomic regions of user-defined length (2kbp windows in our analysis) on a genome-wide scale, by processing and analyzing the sequencing output data obtained with BLISS. With this algorithm (see methods, section 3.22), we obtained, for each time point, a list of peaks having significant p-values, representing genomic windows more enriched for reads in the irradiated sample than in the normalized not irradiated control, that we called DSBs. We detected a decreasing number of DSBs at later time points after irradiation (Figure 50a), and we were able to identify 67 DSB sites (defined as 2kbp window), shared between all the time points, excluding repetitive sequences (Figure 50b).

a

IR 0	IR 60	IR 24h	IR 7d	IR 28d
61965	28903	23790	24958	19786

b

	IR 60	IR 24h	IR 7d	IR 28d
IR 0	6850	6569	5964	4136
IR 60		3261	2901	2013
IR 24h			3098	1879
IR 7d				2489
"Hard to Repair" DSBs = 67				

c

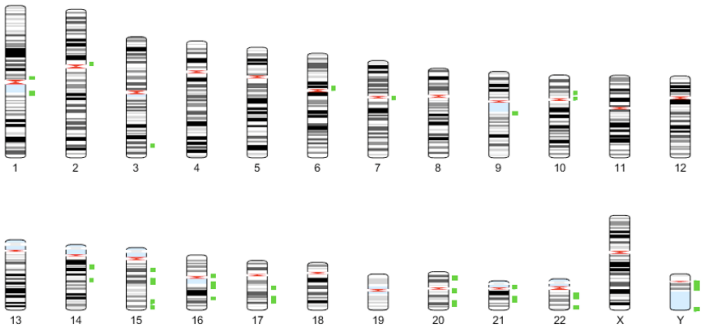

Figure 50 - Genome-wide DSBs accumulation in IR exposed cells, detected by BLISS.

a. DSBs detected by BLISS in BJ hTERT cells exposed to 20Gy IR and fixed at the indicated time point: 0 minutes (immediately after irradiation), 60 minutes, 24 hours, 7 days, 28 days. **b.** Shared DSBs among different time points. "Hard to Repair" DSBs are shared among all time points. **c.** Representation of the genomic location of the "Hard to Repair" DSBs, indicated in green.

To validate these results, I performed a biological replicate followed by BLISS-qPCR on a selected number of sites, comparing quiescent cells with irradiation-induced senescent cells. As shown in Figure 51, I could only observe a partial reproducibility of the expected "hard to repair" sites. In particular, I observed inconsistencies between 2 primer couples matching different sub-regions of the 2kb window detected by our pipeline.

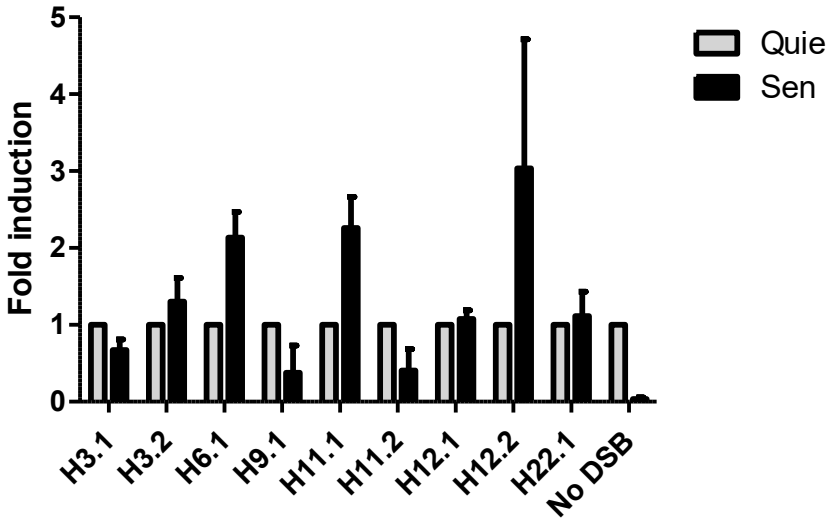

Figure 51 - BLISS-qPCR in IR-induced cells at selected "Hard to repair" sites.

BLISS-qPCR on BJ hTERT cells Quiescent or irradiation-induced senescent (Sen) at different "Hard to repair" sites: .1 or .2 indicate different primer couples in the same 2kb window detected by BLISS sequencing. Bars represent the normalized ratio of % of input for each site in the Induced sample over the Uninduced one. Error bars represent the s.e.m. of 2 replicates.

The inconsistency between BLISS sequencing analysis and BLISS-qPCR could be due to several reasons. First and foremost, it is likely that I was not able to saturate the genome with DSBs when exposing cells to 20 Gy: as further discussed in the Discussion section 5.6, this could result in potentially "hard to repair" regions to never be damaged or damaged in a fraction of cells too low to become detectable by BLISS when cells are pooled. This would also explain the inconsistency of detection between biological replicates. Of course, we cannot rule out the possibility that the pipeline used to analyze BLISS results, is immune from false positive results. In fact, differently from other cases, where we just focused our analysis on selected small regions, and we could simply measure their coverage, in this case we had to develop a pipeline ad hoc to identify DSBs (peaks) *de novo* on the whole genome. In particular, as a proof of principle we tested this pipeline on the AsiSI induced DSBs and we found that the results did not completely overlap (data not shown). Another possibility is that, except for telomers, there are no conserved genomic regions for the accumulation of persistent DSBs in irradiation-induced senescent cells. Before further investigations, I will carry out another round of BLISS followed by NGS on a biological replicate of the first experiment.

4.4.1.1 DSBs accumulate at telomeres in senescent cells

When we performed BLISS analyses, we excluded repetitive sequences, including telomeres, since it would have been impossible to precisely align BLISS reads in those regions, thus our normalization pipeline that counts the number of reads in each 2kb window would not work properly. Moreover, due to their long stretches of repeated sequences, telomeres are prone to sequencing errors. However, it was already known, from data reported in literature by our group and others (Fumagalli et al. 2012, Hewitt et al. 2012) that senescent cells accumulate persistent DDR foci at telomeres (see introduction section 2.6.1), thus I expected to capture telomeric sequences by BLISS in senescent cells. Applying BLISS-qPCR to detect telomeres was also challenging, due to do primer dimers formation or

artefactual amplifications generated when using primers matching the telomeric repeats. However, Cawthon and colleagues (Cawthon 2009) described a strategy to generate fixed length amplicons with telomeric primers containing mismatches, that allow telomere quantification by qPCR. Thus, I used these telomeric primers, to perform BLISS-qPCR on quiescent and senescent cells (BJ hTERT fixed 28 days after IR). Although Cawthon and colleagues developed this strategy to quantify telomere length, here I performed the qPCR on fragmented DNA (where each sample has the same fragment size distribution), so any difference measured by qPCR will be due to a different copy number in telomeres captured by BLISS. Importantly, though, I normalized the BLISS enriched material on the input using different primers, matching a unique genomic locus (in the actin gene body, in this case), since if I used telomeric primers also on the input, the qPCR readout would be dependent not only on the starting material, but also on the telomere length in each sample.

In agreement with data reported in the literature, I observed an increase in captured telomeric regions in senescent cells, compared to quiescent (Figure 52). This value and the background signal obtained in quiescent cells was consistent with the observations reported by Crosetto and colleagues who detected telomeric reads when performing BLESS and BLISS (Crosetto et al. 2013b, Yan et al. 2017).

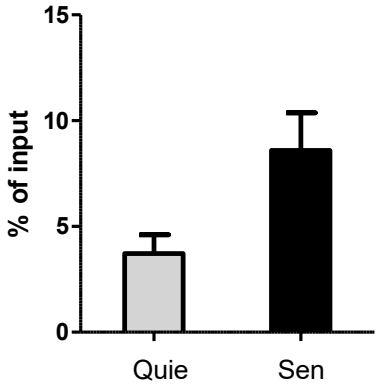

Figure 52 - BLISS-qPCR on Quiescent or irradiation-induced senescent BJ hTERT after 28 day.

BLISS-qPCR was performed on BJ cells either quiescent (Quie) or fixed IR-induced (Sen) after irradiation. Bars represent the % of input for the telomeric primers in each sample (n=2).

To further confirm this result, I performed DI-PLA on the same cells, using an antibody against biotin and a partner antibody against the shelterin protein TRF2, that was observed to be retained at damaged telomeres in IR-induced senescent cells (Fumagalli et al. 2012) (Figure 53).

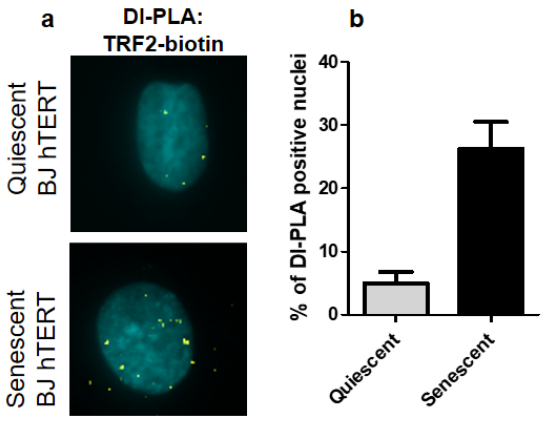

Figure 53 - DI-PLA detects DSBs at telomere in IR-induced senescent cells.

a. DI-PLA between TRF2 and biotin on quiescent or irradiation-induced senescent BJ hTERT. Quantifications are shown in panel **b** (n=2).

I could clearly observe an increased number of signals in senescent cells compared to quiescent, with almost 6-times more positive cells compared to quiescent cells.

The observation that both by DI-PLA and BLISS, I could observe a lower signal in control cells with intact telomeres, compared to irradiated cells is particularly interesting. In fact, it suggests that ligation of the biotinylated linkers is inefficient when telomeres are protected by shelterin proteins. Thus, I thought to exploit this feature to use DI-PLA and BLESS as assays for the telomeric state.

4.4.2 DI-PLA and BLESS can detect dysfunctional telomeres

4.4.2.1 DI-PLA detect uncapped telomeres

Having observed that linkers are not efficiently ligated at functional telomeres, I thought to test the feasibility of using DI-PLA as an assay to probe for telomeres state. I already demonstrated by DI-PLA between TRF2 and biotin that I could detect whether a telomeric

sequence carries a DSB (Figure 53). However, I was interested to test whether I could also use DI-PLA to discriminate between a telomere with a functional shelterin cap and a dysfunctional telomere that has lost the shelterin proteins and its capped state. Although T-loops were first observed *in vitro* almost 20 years ago (Griffith et al. 1999), their detection *in situ* has not been possible until recently (Doksani et al. 2013). However, even if possible, T-loop detection *in situ* requires super-resolution microscopy, thus an assay based on a more accessible technique, would prove valuable for many research laboratories.

To test the feasibility of a DI-PLA based assay to detect uncapped telomeres, I took advantage of *Trf2* conditional knockout mouse embryonic fibroblasts ($Trf2^{F/F}$ MEFs) carrying a Cre-recombinase (*Rosa26-CreERT2*) inducible by 4OHT and constitutively expressing the fusion protein TRF1-GFP (Rossiello et al. 2017). Recombination by Cre robustly induced telomere deprotection and DDR activation at telomeres in the $Trf2^{F/F}$ cell line (Okamoto et al. 2013). Thus, in this cell line, telomeres are detectable by GFP imaging, and telomere uncapping can be induced by adding 4-OHT in cell culture medium.

I performed PLA between γH2AX and GFP (labeling the telomeres) and DI-PLA between biotin and GFP, on uninduced and induced MEFs $Trf2^{F/F}$ TRF1-GFP (Figure 54). As expected, by performing PLA between γH2AX and GFP, I observed an increased number of signals in induced cells, due to DDR activation at uncapped telomeres. Strikingly, I could observe the same trend with DI-PLA between biotin and GFP, indicating that the uncapped telomeres are efficiently labeled by the biotinylated linkers, differently from the protected telomeres.

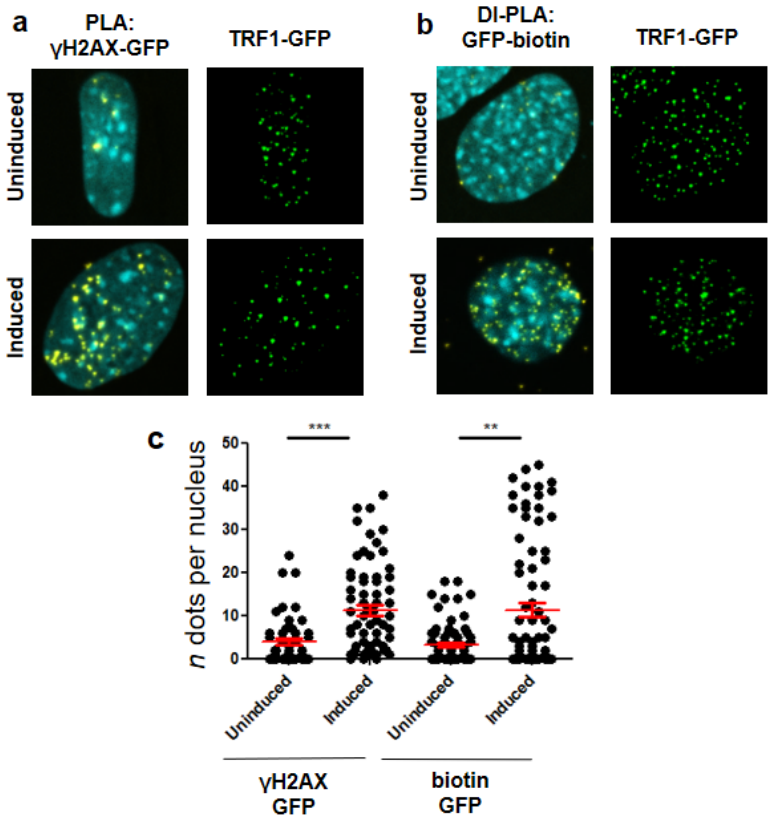

Figure 54 - DI-PLA specifically detects only uncapped telomeres.

a. PLA between γH2AX and GFP and **b**. DI-PLA between GFP and biotin MEF Trf2$^{F/F}$ either uninduced or induced. TRF1-GFP in green. DNA stained by DAPI. Quantifications are shown in panels **c** (n=3).

This intriguing result shows that DI-PLA can be adapted to detect dysfunctional telomeres: either damaged or intact and uncapped.

4.4.2.2 BLESS distinguishes between capped, uncapped and broken telomeres

Based on the observations generated with DI-PLA, I thought to extend the assay to BLESS. Since the technique is based on the same DSB labeling approach by DI-PLA, I expected to measure by BLESS-qPCR an enrichment for telomeric sequences also in the presence of uncapped telomeres.

To first test this hypothesis, I performed BLESS-qPCR with the same telomeric primers used to generate Figure 52, under several conditions: MEFs TRF Trf2$^{F/F}$ either uninduced, as control, or induced with 4OHT for 48h, leading to the telomere uncapping; as positive

control I also used MEFs transfected with a vector coding for the fusion protein TRF1-FokI (Doksani & de Lange 2016) to induce DSBs at telomeres, which I compared with MEF transfected with the same vector coding for the nuclease-dead version of the fusion protein TRF1-FokID405A, to exclude any effect of TRF1 overexpression on telomere detection. As expected, I could observe γH2AX foci by immunofluorescence in induced $Trf2^{F/F}$ MEF and in MEF transfected with TRF1-FokI, but not in uninduced cells or in MEFs transfected with the nuclease-dead version of FokI (Figure 55).

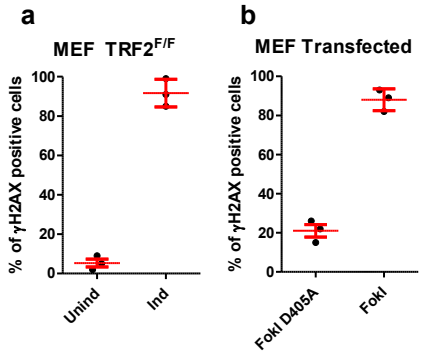

Figure 55 - Induction of telomere uncapping or DSB at telomeres induces DDR activation.

a. Quantification of immunofluorescence for γH2AX in TRF2F/F MEFs either uninduced or induced with 4-OHT for 48h. **b.** Quantification of immunofluorescence for γH2AX in MEFs either transfected with a vector coding for TRF1-FokI or the nuclease-dead version TRF1-FokI D405A (n=3).

Once I validated the experimental conditions, I performed BLESS-qPCR in the same setup described above. To detect telomeres in BLESS captured material, I performed qPCR with the telomeric primers used to generate Figure 52. As shown in Figure 56, I could observe a higher telomeric content in samples containing either uncapped or DSB bearing telomeres, compared to samples with functional telomeres.

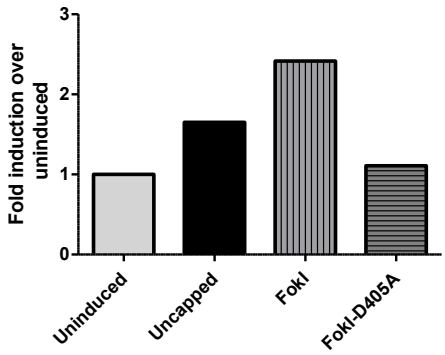

Figure 56 - BLESS-qPCR on MEFs with dysfunctional telomeres.

MEFs TRF2$^{F/F}$ either uninduced or induced with 4-OHT for 48h to induced uncapping, and MEFs transfected with a vector coding for TRF1-FokI or the nuclease dead version TRF1-FokI D405A were fixed and analyzed by BLESS-qPCR using primers matching the telomeric sequences as in Figure 52. Bars represent the normalized ratio of % of input for each site in the Induced sample over the uninduced (n=1).

The higher enrichment of telomeric repeats observed in the FokI transfected cells, compared to the sample with uncapped telomeres, is not completely surprising, because the endonuclease FokI induces several breaks at each telomere, thus providing multiple DNA ends to be captured by BLESS, compared to telomeres uncapped which only have one end to be ligated.

With this strategy qPCR strategy, while being able to discriminate dysfunctional telomeres from intact and functional telomeres, it is not possible to distinguish between DSB bearing telomeres and uncapped telomeres. However, I reasoned that using strand specific primers it could be possible to make this distinction. In particular, using one primer matching the linker sequence and either one primer for the G-rich telomeric repeats or the C-rich telomeric repeats, I could discriminate among intact capped telomeres (that would not be detected by neither of the two primer couples), telomeres containing DSBs (that would be amplified both with G-rich and C-rich primers) and uncapped telomeres that do not bear DSBs (that would only be amplified with a G-rich primer) as depicted in Figure 57.

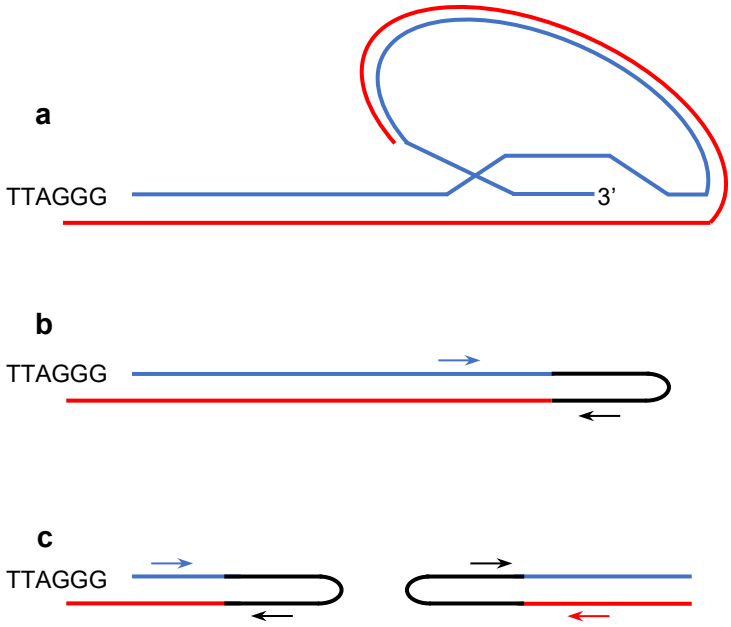

Figure 57 - Scheme of the primers used for telomeric strand-specific BLESS-qPCR.

a. Capped telomeres are folded in a T-loop structure that prevents efficient linker ligation. **b.** Uncapped telomeres have a G-rich 3' end (blue) that can be ligated to the linker (black); PCR amplification with a primer matching the G-rich telomeric sequence (blue arrow) and a primer matching the linker (black arrow) yields detectable amplicons. **c.** DSB bearing telomeres have both a 3' G-rich end (blue) and a 3' C-rich end (red) that can be ligated to the linker (black). PCR amplification with a primer matching the linker (black arrow) and either with a primer matching the G-rich telomeric sequence (blue arrow) or with a primer matching the C-rich telomeric sequence yields detectable amplicons.

Thus, I performed qPCR with strand-specific primer couples on the same samples that I already used to generate Figure 56. The mismatches in the G/C-rich telomeric primers still allowed the specific accumulation of the amplicons generated after the first PCR cycle; however, when used in combination with the primer matching the linker, different amplicons could be generated during the first cycle. To partially prevent this problem, I shortened the amplification step in the qPCR program, to favour specific (short-sized) amplicons generation; indeed, I observed consistent melting temperatures among different samples, indicating the formation of comparable amplicons in all the reactions.

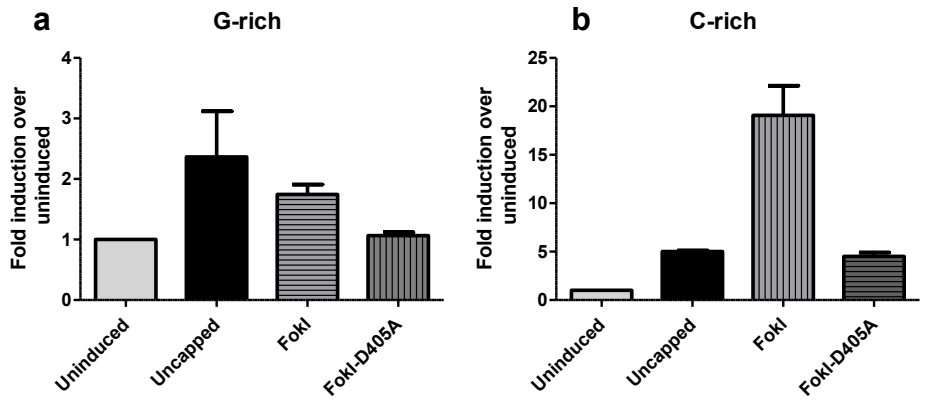

Figure 58 - BLESS-qPCR with strand specific telomeric primers.

BLESS-qPCR on MEFs TRF2F/F either uninduced or induced with 4-OHT for 48h, and MEFs transfected with a vector coding for TRF1-FokI or the nuclease dead version TRF1-FokI D405A. Bars represent the normalized ratio of % of input for each site in the Induced sample over the uninduced (n=2). **a.** The G-rich primer used to generate Figure 56, was used in combination with the primer matching the linker sequence. **b.** The C-rich primer used to generate Figure 56, was used in combination with the primer matching the linker sequence.

As shown in Figure 58, with G-rich primers in combination with the primer matching BLESS linker, I could specifically detect a signal both in uncapped telomeres and broken telomeres. Interestingly, I observed that, while the couple of telomeric primers produced a higher signal in DSB bearing telomeres compared to uncapped telomere (Figure 56), here, using strand-specific qPCR, I detected more G-strand in uncapped telomeres than in broken telomeres. This suggests that the overall higher telomeric signal measured in FokI transfected cells, was due to the sum of G- and C-strand capture by BLESS.

I also detected a higher signal in FokI transfected cells, compared to all other conditions, when using C-rich primers in combination with the primer matching BLESS linker, indicating that the approach is working as expected. However, I observed an increase over the uninduced also in the nuclease dead transfected cells and in cells with uncapped, possibly suggesting a low frequency accumulation of DSB due to the uncapping itself or due to the transfection reagents (as also suggested by γH2AX accumulation in about 20% of FokI D405A transfected cells – Figure 55).

In conclusion, these results show that DI-PLA and BLESS can be used as tools to detect uncapped telomeres, and BLESS followed by strand-specific qPCR can distinguish among 3 different telomeric states: intact, uncapped and broken.

5 Discussion

5.1 BLESS-qPCR is a sensitive method to study DSB accumulation at specific loci

The most used methods to map DNA damage accumulation and DNA repair, both at genome-wide level and in single cells are based on the use of antibodies that recognize DDR markers such as γH2AX. However, a growing body of evidence indicates that this indirect approach to detect DNA damage is not precise. Some groups have reported, or suggested, DDR marker accumulation in the absence of physical DSBs, such as in senescent cells (Rodier et al. 2011), in mitotic cells (Mcmanus & Hendzel 2005, Tu et al. 2013), and in replication stress-induced damage (Rybak et al. 2016b). On the contrary, DNA damage accumulation in the absence of DDR markers is also possible, and it has been reported in astrocytes (Schneider et al. 2012), and in heterochromatic regions (Kim et al. 2007, Lafon-Hughes et al. 2013). Moreover, DNA damage markers spread for several kilobases (up to 1Mb) around the break, preventing precise localization of the DSB position on the genome. A few alternative approaches for direct detection of DNA damage genome-wide have been developed in the last years; they mainly rely on two different approaches, one detecting exposed DNA ends available in a population of cells at a given moment, and a second one tracking the repair of DSBs (see Introduction, section 2.5). Unfortunately, very little data is available in literature comparing the performance different methods, mostly due to the costs associated with reagents and high-throughput sequencing required to test these protocols. The work described in my thesis shows a simple and effective strategy to query by qPCR the DSBs captured by methods that rely on direct DSB labelling and enrichment, such as BLESS (Crosetto et al. 2013b), DSBCapture (Lensing et al. 2016) and BLISS (Yan et al. 2017) (Figures 4-7, 15). The strategy, inspired by the ChIP-qPCR method, requires a primer couple to be designed next to the putative DSB site, then qPCR is performed on both the captured material and on the input (before DSB enrichment), in order to normalize the amount of DNA captured on the starting material, thus allowing comparisons among

different samples. I confirmed the effectiveness of this approach by detecting DSBs in conditions where DNA breaks accumulation was already reported in literature, such as at specific U2OS AsiSI-cleaved sites and in Hela cells transfected with the I-SceI endonuclease that cuts at a single locus in the genome. Further evidence that the approach works reliably came from validation of DSBs detected by NGS analysis of BLISS.

Similar approaches have been described in literature for ligation-mediated PCR (Chailleux et al. 2014), although the recently published protocols developed to map DSBs have not included a qPCR validation step. However, a new protocol, recently published, based on digital droplet PCR, might provide the most sensitive quantification of DSBs accumulating at a specific locus in a population of cells available so far (Rose et al. 2017).

5.2 BLISS performs better than other available methods to measure DSB genome-wide

As mentioned above, very little data is available to compare how well different methods perform. In collaboration with our bioinformatician, Dr. Iannelli, we have compared one of the latest methods developed, BLISS, with two similar approaches (BLESS and DSBCapture) and γH2AX ChIP-seq, the most used technique used to map DNA damage. To have the cleanest experimental setup, I used U2OS cells expressing the AsiSI restriction enzyme, which can potentially cut about 1200 site in the human genome, although, being sensitive to chromatin state and methylation, it cleaves only 10-20% of the putative target loci.

The data that we generated shows that BLISS outperforms both BLESS and DSBCapture, being able to detect the whole array of AsiSI target sites already validated in literature, differently from the other techniques (Figure 11), and it is able to detect a higher absolute number of DSBs. Moreover, target sites detected by BLISS significantly overlap with γH2AX enriched regions (Figure 13), and fall in transcriptionally active regions (Figure 14),

thus in regions where chromatin is open and DNA is likely accessible to the AsiSI enzyme, indicating that BLISS results are reliable. By BLISS, we also detected a number of AsiSI-cleaved sites which were not detected neither by other DSB mapping techniques, nor significantly enriched in γH2AX ChIP-seq. This result suggests a higher sensitivity of BLISS compared to the other available methods, and, while I cannot completely exclude that these represent false positive signals, I could reproducibly detect a subset of these sites in a biological replicate by BLISS-qPCR (Figure 14).

5.3 DSBs lead to transcription inhibition of genes in the surrounding regions

By intersecting the map of DSBs generated by AsiSI induction in U2OS cells with a multilayered expression profiling (including data from RNA-seq, Bru-seq, CAGE and RNA POL II ChIP-seq) we could observe transcription inhibition around the DSB sites (Figure 16, Iannelli et al., 2017). This result shows at unprecedented resolution and at genome-wide level the impact of DSBs in endogenous regions on transcription. Transcription repression following DSB generation is in line with several reports in the literature that show the activation of different mechanisms to prevent aberrant transcript production in the presence of DNA damage, including RNA POL II degradation, chromatin condensation and the recruitment of transcription repressors such as PRC1 (Adam & Polo 2014, Bregman et al. 1996, Shanbhag et al. 2010, Svejstrup 2010). However, there is an apparently contrasting report showing that expression of the I-PpoI endonuclease in mice only induces transcriptional silencing of the genes bearing the damage and not in the surrounding genes (Kim et al. 2016). This discrepancy, could be partially due to the fact that I-PpoI target sites are mainly within ribosomal DNA repeats, while AsiSI targets are in non-repetitive sequences: thus, the different genomic sequences might trigger different mechanisms. Most importantly though, Kim and colleagues, have not validated which subset of I-PpoI sites are

actually cleaved, thus they have probably made an underestimation of DSBs impact on transcription: assuming that I-PpoI cuts only 20% of its putative target sites similarly to AsiSI, the transcription alterations that they observed were masked by 80% of the I-PpoI sites that were not cleaved, thus not associated with any transcriptional perturbation. We observed that the strongest transcription inhibition effect happens in proximity to the DSB, while the repression progressively weaken spreading away from the break site (Iannelli et al. 2017); thus it is likely that Kim and colleagues did not detect transcription inhibition at 10kb or more from the break, just because they did not have enough sensitivity in their analysis.

5.4 Transient DSB formation is involved in LPS-induced enhancer activation

Despite having demonstrated that DSBs induce transcriptional repression, several reports show that transient DSB formation is a mechanism involved in stimuli-specific transcription activation (as discussed in the introduction – section 2.4.3). In agreement with this physiological role for DNA damage, in collaboration with Dr. Vitelli, we probed for the presence of DSBs at the enhancers activated after by LPS stimulation in macrophages and, strikingly, we found that, 5 minutes after exposure of cells to LPS, there is a transient wave of induction of DSBs that are rapidly repaired and disappear after 60 minutes (Figures 17-19). This preliminary observation will be followed by other experiments to understand whether DSBs formation and/or repair is needed for transcription activation and what mechanism leads to the DSB induction in response to LPS recognition (Vitelli, Galbiati et al., in preparation). To prove that DSBs need to be repaired to allow transcription activation we will perform experiments in the absence of Ligase IV; moreover, as proof of concept we will design a guide for an inducible CRISPR-Cas9 to activate transcription in a specific enhancer. Certainly, it will be very interesting to check how the DSB is generated in response

to LPS. At the moment we can speculate that DSBs might be generated by a specific nuclease that is translocated at the enhancer together with factors involved in enhancer activation such as PU1 (Kaikkonen et al. 2014), although experiments will be necessary to prove this hypothesis.

5.5 DI-PLA is a sensitive method to detect DSBs in single-cells

The new method that I have developed and described here, DI-PLA, is a tool to detect by imaging, physical DSBs in proximity of a DDR marker or a chromatin bound factor localized next to the DSB, in single-cells. It allows detection of DSBs induced by several sources, including restriction enzymes, IR and NCS (Figure 24, 26, 28). Although it is difficult to quantitate DI-PLA efficiency in detecting DSBs, the similar results obtained by PLA between two DDR markers and by DI-PLA show that DNA ends generated by different sources are generally available for blunting and ligation reactions. This is also in agreement with several reports using a similar DSB labelling strategy, but followed by NGS (such as BLESS, BLISS, DSBCapture and more), to detect DSB generated by several sources, including restriction enzymes, topoisomerase inhibitors or replication stress (Baranello et al. 2014, Crosetto et al. 2013b, Yan et al. 2016).

I have demonstrated that DI-PLA signals are dependent on the presence of the biotinylated linker (Figure 29), and that the partner antibody used in combination with the anti-biotin one needs to recognize a protein in proximity of a DSB to generate a detectable signal by DI-PLA (Figure 31-32). Interestingly, the partner antibody does not necessarily recognize a DDR marker, opening up the possibility to use DI-PLA to detect DSB at specific loci that are marked by a set of proteins, such as centromeres or telomeres.

Moreover, I have showed that DI-PLA signals are dependent on the number of DSBs present in the cell (Figure 34), they disappear if DSBs are in vitro re-ligated (Figure 35), and DI-

PLA dotted signals co-localize with DSBs positions in the nucleus (Figure 36), strongly supporting the specificity of the assay.

Although most of the DI-PLA validations were performed on adherent cells, I have data showing that DI-PLA can be applied to fixed tissues (Figure 38), albeit I found that section thickness is critical, because I occasionally observed unequal staining efficiency in the sections.

5.6 Senescent cells accumulate persistent DSBs both *in vitro* and *in vivo*

One of the hallmark of cellular senescence is the presence of DDR activation which plays a role both in the initiation and in the maintenance of the senescent state, through activation of the p53/p21 pathway (Munoz-Espin & Serrano 2014). Moreover, following DNA damage induction by several events, including replication stress or exogenous damage, in some cell types, also p16, the other main regulator of senescence, is activated (Mirzayans et al. 2012). Although a DDR-independent mechanism for senescence induction, dependent on the stress-inducible kinase p38MAPK, has been reported, several experiments showed that inactivation of DDR components such as ATM, ATR or CHK2, leads to escape from OIS, replicative senescence and SIPS (Bartkova et al. 2006, Beauséjour et al. 2003, Di Micco et al. 2006, d'adda di Fagagna et al. 2003). However, it has been hypothesized that senescent cells do not retain physical DNA damage, rather stable chromatin alterations resulting from the damage, but without the underlying lesion, which are necessary to reinforce senescence, termed DNA-SCARS (Rodier et al. 2011). Here, by DI-PLA I have showed that both replicative senescent cells (Figure 43) and IR-induced senescent cells (Figure 47) accumulate persistent physical DSBs that are associated with the well-characterized persistent DDR foci. This observation is in agreement with data in the literature showing a preferential accumulation of DDR foci at telomeres (Fumagalli et al. 2012, Hewitt et al.

2012), where DSB repair is physiologically inhibited to prevent chromosome fusions. Interestingly, a recent report showed that DNA repair at telomeres is possible in human proliferating cells, but not in senescent cells (Mao et al. 2016), further supporting the model of persistent physical DSBs fuelling the senescent state.

Cellular senescence associated with DDR activation has also been reported *in vivo*, where it plays a role in the ageing phenotype (as discussed in the introduction – section 2.5.3). Here, I showed that tissues (brain and liver) from aged mice, accumulate persistent DSBs (Figure 48-49). This result is consistent with a recent report showing that chronic DNA damage induction *in vivo*, induces an ageing-like phenotype after only 1 month of treatment, including ageing pathologies, markers of senescence, fused mitochondria and alterations in gene expression profile (White et al. 2015).

It has been well characterized by our group and others that persistent DDR activation in senescent cells is preferentially localized at telomeres (Fumagalli et al. 2012, Hewitt et al. 2012), however we had previously observed that also non-telomeric regions accumulate DNA damage in IR-induced senescent cells. Thus, I applied for the first time a genome-wide single-nucleotide DSB mapping technology, BLISS, to study DNA damage accumulation and repair, over time, following cells exposure to a high dose of IR and during establishment of senescence. However, this is a very challenging experimental setup for several reasons. Firstly, in an ideal setup, the experiment should start by inducing DNA damage at each nucleotide in the genome in all cells. Luckily, since in BLISS analysis we divided the genome in 2kb windows, I only needed to generate 1 DSB every 2kb; this still results in about 1.5milion DSBs. Considering that 2Gy induce roughly 100 DSB per cell (personal observation based on DI-PLA between γH2AX and biotin), 20Gy should induce about 1.000 DSBs per cell, which, in the population of 50.000 cells used for the experiments, exceeds by 30-fold the minimum amount of DSBs (1.5M) that needs to be induced in the ideal experimental setup. While mathematically correct, I cannot exclude that some regions might

be more resistant than others to IR damage, thus resulting in a biased IR-induced damage. Secondly, we unexpectedly found a high background signal in quiescent cells, that led us to use a normalization pipeline (see materials and methods 3.22, and result section 4.4.1.1), that might have masked low-frequency DSB signals; the high-background that we observed in untreated cells might be due to the fact that we kept them in culture for 28 days, thus they have likely been exposed to oxidation stress. Thirdly, *de novo* DSBs detection by BLISS is more challenging than detecting DSBs in specific regions: as reference, the BLISS pipeline that we developed in collaboration with prof. Pattini, detected less than 50% of the U2OS AsiSI-induced DSBs that we detected using a different pipeline that only focuses around AsiSI cleavage sites (Figure 12). For all these reasons, it is likely that we underestimated the number of DSBs generated in this experiment.

As shown if Figure 50, we were able to identify 67 genomic loci that accumulated DSBs at all the time points analysed (but not in the control), that I named "hard to repair". Although some of these sites are falling in pericentromeric or subtelomeric regions, after a preliminary qualitative analysis, I could not observe any shared striking feature among these sites. Most importantly, I was not able to determine whether these sites are biologically relevant, since in a biological replicate analysed by BLISS-qPCR, I did not consistently detect all of them (Figure 51). This inconsistency, might be either due to any of the challenges in the experimental setup and analysis mentioned above, or to an actual lack of conserved genomic regions for DNA damage accumulation in senescent cells, except for telomeric regions. For example, it has been suggested that, in SIPS, non-telomeric DNA damage is short-lived and induced by highly reactive ROS, thus resulting in very low-frequency DSBs that are very hard to detect by BLISS (Hewitt et al. 2012, Passos et al. 2010).

In any case, another round of BLISS followed by NGS will be needed to draw further conclusions.

On the other hand, I was able to detect DSBs accumulating at telomeres both by DI-PLA and by BLISS-qPCR using telomeric primers, exploiting the strategy described by Cawthon and colleagues (Cawthon 2009), thus confirming data available in literature (Figure 52-53).

5.7 DI-PLA and BLESS can be used to study the telomere state

The possibility to detect DSBs accumulation at telomeres in senescence cells by DI-PLA and BLESS (Figures 52-53) led me to think that these two tools could be used to specifically detect dysfunctional telomeres. As proof of concepts experiments I used a cell line where I could induce telomere uncapping, with the addition of tamoxifen to cell culture medium and, indeed, I observed an increase in telomeric signal both by DI-PLA and BLESS (Figures 54-56). Thus, this result suggests the possibility to use these two tools to discriminate between functional and dysfunctional telomeres.

For most of the experiments, however, using DDR markers to check for the presence of damaged or uncapped telomeres is more practical and just as sensitive (if not more, given the low induction measured by BLESS-qPCR at uncapped telomeres, Figure 56) than DI-PLA and BLESS. However, the only way to distinguish between DSBs accumulation at telomeres and T-loop disruption, is by super-resolution imaging (Doksani et al. 2013) or electron microscopy (Griffith et al. 1999). Here, I was able, by using strand specific primers (either C- or G- rich) in combination with a primer matching BLESS linker sequence, to discriminate between three different telomeric states: intact, uncapped and broken (Figure 57-58).

Interestingly, I measured higher enrichments over untreated sample with the C-strand, than with the G-strand, suggesting a higher background coming signal from the G-strand in capped, intact telomeres. This observation is in agreement with data in literature reporting

BLESS capture of telomeric sequences (Crosetto et al. 2013, Zhu et al. 2017). Further analyses will be required to understand why there is a background signal from a population of cells with intact capped telomeres. One possibility is that during S phase, replicating telomeres become available for DSB labelling by ligation with the linker, although this possibility could be ruled out by performing an experiment on quiescent cells. Another possibility is that during cell manipulation the T-loop structure is lost: interestingly very recent data reported by Zhu and colleagues (Zhu et al. 2017) showed that the BLESS crosslinking step and the short proteinase K step used to digest cell membrane prior DNA ends blunting and ligation, are critical for the number of telomeric reads retrieved when performing BLESS followed by NGS. In particular, performing BLESS without cells crosslinking and with a longer proteinase K incubation, yielded 10-fold more telomeric reads compared to the standard BLESS protocol. While this observation suggests that some optimization of the BLESS protocol might be needed to use it as a reliable assay for the telomeric state, it strongly supports the hypothesis that T-loop and shelterin proteins prevent telomere capture by BLESS.

In conclusion, this set of results suggests that by applying BLESS followed by strand specific qPCR is be possible to discriminate between different telomeric states. This approach could be exploited to gain new insights into mechanisms of DDR activation and DNA repair at telomeres.

6 References

Acosta JC, Banito A, Wuestefeld T, Georgilis A, Janich P, et al. 2013. A complex secretory program orchestrated by the inflammasome controls paracrine senescence. *Nat Cell Biol*. 15(8):978–90

Adam S, Polo SE. 2014. Blurring the line between the DNA damage response and transcription: The importance of chromatin dynamics. *Exp. Cell Res.* 329(1):148–53

Aguilera A. 2002. The connection between transcription and genomic instability. *EMBO J.* 21(3):195–201

Ahmed S, Passos JF, Birket MJ, Beckmann T, Brings S, et al. 2008. Telomerase does not counteract telomere shortening but protects mitochondrial function under oxidative stress. *J. Cell Sci.* 121(7):1046 LP-1053

Ancelin K, Bauwens S, Koering C, Brun C, Ricoul M, et al. 2002. Targeting Assay To Study the. *Society*. 22(10):3474–87

Arnoult N, Correia A, Ma J, Merlo A, Garcia-Gomez S, et al. 2017. Regulation of DNA repair pathway choice in S and G2 phases by the NHEJ inhibitor CYREN. *Nature*. advance on:

Aymard F, Bugler B, Schmidt CK, Guillou E, Caron P, et al. 2014a. Transcriptionally active chromatin recruits homologous recombination at DNA double-strand breaks. . (March):

Aymard F, Bugler B, Schmidt CK, Guillou E, Caron P, et al. 2014b. Transcriptionally active chromatin recruits homologous recombination at DNA double-strand breaks. *Nat. Struct. Mol. Biol.* 21(4):366–74

Azzalin CM, Lingner J. 2008. Telomeres: The silence is broken. *Cell Cycle*. 7(9):1161–65

Baar MP, Brandt RMC, Putavet DA, Klein JDD, Derks KWJ, et al. 2017. Targeted Apoptosis of Senescent Cells Restores Tissue Homeostasis in Response to Chemotoxicity and Aging. *Cell*. 169(1):132–147.e16

Bae NS, Baumann P. 2007. A RAP1/TRF2 Complex Inhibits Nonhomologous End-Joining at Human Telomeric DNA Ends. *Mol. Cell*. 26(3):323–34

Baker DJ, Childs BG, Durik M, Wijers ME, Sieben CJ, et al. 2016. Naturally occurring p16Ink4a-positive cells shorten healthy lifespan. *Nature*. 530(7589):184–89

Baker DJ, Wijshake T, Tchkonia T, LeBrasseur NK, Childs BG, et al. 2011. Clearance of p16Ink4a-positive senescent cells delays ageing-associated disorders. *Nature*. 479(7372):232–36

Baner J, Nilsson M, Mendel-Hartvig M, Landegren U. 1998. Signal amplification of padlock probes by rolling circle replication. *Nucleic Acids Res.* 26(22):5073–78

Baranello L, Kouzine F, Wojtowicz D, Cui K, Przytycka TM, et al. 2014. DNA break mapping reveals topoisomerase II activity genome-wide. *Int. J. Mol. Sci.* 15(7):13111–22

Bartek J, Bartkova J, Lukas J. 1996. The retinoblastoma protein pathway and the restriction point. *Curr. Opin. Cell Biol.* 805–14

Bartkova J, Rezaei N, Liontos M, Karakaidos P, Kletsas D, et al. 2006. Oncogene-induced senescence is part of the tumorigenesis barrier imposed by DNA damage checkpoints. *Nature*. 444:633–37

Baumann P, Cech TR. 2001. Pot1, the Putative Telomere End-Binding Protein in Fission Yeast and Humans. *Science (80-.).* 292(5519):1171 LP-1175

Baumann P, Price C. 2011. Pot1 and Telomere Maintenance. . 584(17):3779–84

Beauséjour CM, Krtolica A, Galimi F, Narita M, Lowe SW, et al. 2003. Reversal of human cellular senescence: Roles of the p53 and p16 pathways. *EMBO J.* 22(16):4212–22

Bekker-Jensen S, Lukas C, Melander F, Bartek J, Lukas J. 2005. Dynamic assembly and sustained retention of 53BP1 at the sites of DNA damage are controlled by Mdc1/NFBD1. *J. Cell Biol.* 170(2):201–11

Belotserkovskii BP, Liu R, Tornaletti S, Krasilnikova MM, Mirkin SM, Hanawalt PC. 2010. Mechanisms and implications of transcription blockage by guanine-rich DNA sequences. *Proc. Natl. Acad. Sci.* 107(29):12816–21

Benarroch-Popivker D, Pisano S, Mendez-Bermudez A, Lototska L, Kaur P, et al. 2016. TRF2-Mediated

Control of Telomere DNA Topology as a Mechanism for Chromosome-End Protection. *Mol. Cell*. 61(2):274–86

Benetti R, Garcia-Cao M, Blasco MA. 2007. Telomere length regulates the epigenetic status of mammalian telomeres and subtelomeres. *Nat Genet*. 39(2):243–50

Bennardo N, Cheng A, Huang N, Stark JM. 2008. Alternative-NHEJ is a mechanistically distinct pathway of mammalian chromosome break repair. *PLoS Genet.* 4(6):

Birch J, Anderson RK, Correia-Melo C, Jurk D, Hewitt G, et al. 2015. DNA damage response at telomeres contributes to lung aging and chronic obstructive pulmonary disease. *Am. J. Physiol. - Lung Cell. Mol. Physiol.* 309(10):L1124 LP-L1137

Birch J, Passos JF. 2017. Targeting the SASP to combat ageing: Mitochondria as possible intracellular allies? *BioEssays*. 39(5):1–7

Bodnar AG, Ouellette M, Frolkis M, Holt SE, Chiu CP, et al. 1998. Extension of life-span by introduction of telomerase into normal human cells. *Science*. 279(5349):349–52

Borde V, de Massy B. 2013. Programmed induction of DNA double strand breaks during meiosis: Setting up communication between DNA and the chromosome structure. *Curr. Opin. Genet. Dev.* 23(2):147–55

Branzei D, Foiani M. 2008. Regulation of DNA repair throughout the cell cycle. *Nat. Rev. Mol. Cell Biol.* 9(4):297–308

Bregman DB, Halaban R, van Gool AJ, Henning KA, Friedberg EC, Warren SL. 1996. UV-induced ubiquitination of RNA polymerase II: a novel modification deficient in Cockayne syndrome cells. *Proc. Natl. Acad. Sci. U. S. A.* 93(21):11586–90

Bronner IF, Quail MA, Turner DJ, Swerdlow H. 2013. *Europe PMC Funders Group Improved Protocols for Illumina Sequencing*

Campisi J. 2013. Aging, Cellular Senescence, and Cancer. *Annu Rev Physiol*. 685–705

Canela A, Sridharan S, Sciascia N, Tubbs A, Meltzer P, et al. 2016. DNA Breaks and End Resection Measured Genome- wide by End Sequencing. . 1–14

Capozzo I, Iannelli F, Francia S, d'Adda di Fagagna F. 2017. Express or repress? The transcriptional dilemma of damaged chromatin. *FEBS J.* 284:2133–47

Carpenter AE, Jones TR, Lamprecht MR, Clarke C, Kang IH, et al. 2006. CellProfiler: image analysis software for identifying and quantifying cell phenotypes. *Genome Biol.* 7(10):R100

Cawthon RM. 2009. Telomere length measurement by a novel monochrome multiplex quantitative PCR method. *Nucleic Acids Res.* 37(3):1–7

Cesare AJ, Kaul Z, Cohen SB, Napier CE, Pickett HA, et al. 2009. Spontaneous occurrence of telomeric DNA damage response in the absence of chromosome fusions. *Nat Struct Mol Biol*. 16(12):1244–51

Cesare AJ, Reddel RR. 2010. Alternative lengthening of telomeres: models, mechanisms and implications. *Nat. Rev. Genet.* 11(5):319–30

Chailleux C, Aymard F, Caron P, Daburon V, Courilleau C, et al. 2014. Quantifying DNA double-strand breaks induced by site-specific endonucleases in living cells by ligation-mediated purification. *Nat. Protoc.* 9(3):517–28

Chandra T, Kirschner K, Thuret JY, Pope BD, Ryba T, et al. 2012. Independence of Repressive Histone Marks and Chromatin Compaction during Senescent Heterochromatic Layer Formation. *Mol. Cell*. 47(2):203–14

Chang HHY, Pannunzio NR, Adachi N, Lieber MR. 2017. Non-homologous DNA end joining and alternative pathways to double-strand break repair. *Nat. Rev. Mol. Cell Biol.* 18(8):495–506

Chang J, Wang Y, Shao L, Laberge R-M, Demaria M, et al. 2016. Clearance of senescent cells by ABT263 rejuvenates aged hematopoietic stem cells in mice. *Nat Med*. 22(1):78–83

Chiarle R, Zhang Y, Frock RL, Lewis SM, Molinie B, et al. 2011. Genome-wide translocation sequencing reveals mechanisms of chromosome breaks and rearrangements in B cells. *Cell*. 147(1):107–19

Chow H, Herrup K. 2015. Genomic integrity and the ageing brain. *Nat. Publ. Gr.* 16(11):672–84

Ciccia A, Elledge SJ. 2010. The DNA damage response: making it safe to play with knives. *Mol. Cell*. 40(2):179–204

Clerici M, Mantiero D, Lucchini G, Longhese MP. 2005. The Saccharomyces cerevisiae Sae2 protein promotes resection and bridging of double strand break ends. *J. Biol. Chem.* 280(46):38631–38

Clerici M, Trovesi C, Galbiati A, Lucchini G, Longhese MP. 2014. Mec1/ATR regulates the generation of single-stranded DNA that attenuates Tel1/ATM signaling at DNA ends. *EMBO J.* 33(3):198–216

Cohen SB, Graham ME, Lovrecz GO, Bache N, Robinson PJ, Reddel RR. 2007. Protein Composition of Catalytically Active Human Telomerase from Immortal Cells. *Science (80-.).* 315(5820):1850 LP-1853

Colgin LM, Baran K, Baumann P, Cech TR, Reddel RR. 2003. Human POT1 Facilitates Telomere Elongation by Telomerase. *Curr. Biol.* 13(11):942–46

Coppé J-P, Desprez P, Krtolica A, Campisi J. 2010. The Senescence-Associated Secretory Phenotype: The Dark Side of Tumor Suppression. *Annu. Rev. Pahtology*. (12):3279–88

Coppé J-P, Kauser K, Campisi J, Beauséjour CM. 2006. Secretion of Vascular Endothelial Growth Factor by Primary Human Fibroblasts at Senescence. *J. Biol. Chem.* 281(40):29568–74

Correia-Melo C, Passos JF. 2015. Mitochondria: Are they causal players in cellular senescence? *Biochim. Biophys. Acta - Bioenerg.* 1847(11):1373–79

Correia-Melo C, Marques FD, Anderson R, Hewitt G, Hewitt R, et al. 2016. Mitochondria are required for pro-ageing features of the senescent phenotype. *EMBO J.* 35(7):724–42

Costanzo V, Shechter D, Lupardus PJ, Cimprich KA, Gottesman M, Gautier J. 2003. An ATR- and Cdc7-dependent DNA damage checkpoint that inhibits initiation of DNA replication. *Mol. Cell*. 11(1):203–13

Cowell IG, Sunter NJ, Singh PB, Austin CA, Durkacz BW, Tilby MJ. 2007. γH2AX foci form preferentially in euchromatin after ionising-radiation. *PLoS One*. 2:

Crosetto N, Mitra A, Silva MJ, Bienko M, Dojer N, et al. 2013. Nucleotide-resolution DNA double-strand break mapping by next-generation sequencing. *Nat. Methods*. 10(4):361–65

Crow YJ, Leitch A, Hayward BE, Garner A, Parmar R, et al. 2006. Mutations in genes encoding ribonuclease H2 subunits cause Aicardi-Goutières syndrome and mimic congenital viral brain infection. *Nat. Genet.* 38(8):910–16

Cruz-García A, López-Saavedra A, Huertas P. 2014. BRCA1 accelerates CtIP-ediated DNA-end resection. *Cell Rep.* 9(2):451–59

d'Adda di Fagagna F. 2008. Living on a break: cellular senescence as a DNA-damage response. *Nat. Rev. Cancer*. 8(7):512–22

d'Adda di Fagagna F, Hande MP, Tong W-M, Roth D, Lansdorp PM, et al. 2001. Effects of DNA nonhomologous end-joining factors on telomere length and chromosomal stability in mammalian cells. *Curr. Biol.* 11(15):1192–96

D'Alessandro G, d'Adda di Fagagna F. 2016. Transcription and DNA Damage: Holding Hands or Crossing Swords? *J. Mol. Biol.*

D'Alessandro G, di Fagagna F d'Adda. Transcription and DNA damage: holding hands or crossing swords? *J. Mol. Biol.*

Daley JM, Sung P. 2013. RIF1 in DNA Break Repair Pathway Choice. *Mol. Cell*. 49(5):840–41

Dankort D, Filenova E, Collado M, Serrano M, Jones K, McMahon M. 2007. A new mouse model to explore the initiation , progression , and therapy tumors. *Genes Dev.* 21(415):379–84

David SS, O'Shea VL, Kundu S. 2007. Base-excision repair of oxidative DNA damage. *Nature*. 447(7147):941–50

de Feraudy S, Revet I, Bezrookove V, Feeney L, Cleaver JE. 2010. A minority of foci or pan-nuclear apoptotic staining of gammaH2AX in the S phase after UV damage contain DNA double-strand breaks. *Proc. Natl. Acad. Sci. U. S. A.* 107(15):6870–75

De Magalhães JP, Chainiaux F, Remacle J, Toussaint O. 2002. Stress-induced premature senescence in BJ and hTERT-BJ1 human foreskin fibroblasts. *FEBS Lett.* 523(1–3):157–62

de Silanes IL, Graña O, De Bonis ML, Dominguez O, Pisano DG, Blasco MA. 2014. Identification of TERRA locus unveils a telomere protection role through association to nearly all chromosomes. *Nat. Commun.* 5:4723

Déjardin J, Kingston RE. 2009. Purification of Proteins Associated with Specific Genomic Loci. *Cell*. 136(1):175–86

Demaria M, O'Leary MN, Chang J, Shao L, Liu S, et al. 2016. Cellular senescence promotes adverse effects of chemotherapy and cancer relapse. *Cancer Discov.* 7(2):165–76

Demaria M, Ohtani N, Youssef S, Rodier F, Toussaint W, et al. 2015. An Essential Role for Senescent Cells in Optimal Wound Healing through Secretion of PDGF-AA. . 31(6):722–33

Denchi EL, de Lange T. 2007. Protection of telomeres through independent control of ATM and ATR by TRF2 and POT1. *Nature*. 448(7157):1068–71

Deng Z, Norseen J, Wiedmer A, Riethman H, Paul M. 2010. NIH Public Access. . 35(4):403–13

Deursen JM Van. 2014. The role of senescent cells in aging. . 509(7501):439–46

Di Micco R, Fumagalli M, Cicalese A, Piccinin S, Gasparini P, et al. 2006. Oncogene-induced senescence is a DNA damage response triggered by DNA hyper-replication. *Nature*. 444(7119):638–42

Di Micco R, Fumagalli M, d'Adda di Fagagna F. 2007. Breaking news: high-speed race ends in arrest – how oncogenes induce senescence. *Trends Cell Biol.* 17(11):529–36

Di Micco R, Sulli G, Dobreva M, Liontos M, Botrugno O a, et al. 2011. Interplay between oncogene-induced DNA damage response and heterochromatin in senescence and cancer. *Nat. Cell Biol.* 13(3):292–302

Dimri GP, Lee X, Basile G, Acosta M, Scott G, et al. 1995. A biomarker that identifies senescent human cells in culture and in aging skin in vivo. *Proc. Natl. Acad. Sci.* 92(20):9363–67

Doksani Y, de Lange T. 2016. Telomere-Internal Double-Strand Breaks Are Repaired by Homologous Recombination and PARP1/Lig3-Dependent End-Joining. *Cell Rep.* 17(6):1646–56

Doksani Y, Wu JY, de Lange T, Zhuang X. 2013. Super-Resolution Fluorescence Imaging of Telomeres Reveals TRF2-Dependent T-loop Formation. *Cell*. 155(2):345–56

Dominguez-Sola D, Ying CY, Grandori C, Ruggiero L, Chen B, et al. 2007. Non-transcriptional control of DNA replication by c-Myc. *Nature*. 448(7152):445–51

Dong J, Panchakshari RA, Zhang T, Zhang Y, Hu J, et al. 2015. Orientation-specific joining of AID-initiated DNA breaks promotes antibody class switching. *Nature*. 525:134–39

Duquette ML, Handa P, Vincent JA, Taylor AF, Maizels N. 2004. Intracellular transcription of G-rich DNAs induces formation of G-loops, novel structures containing G4 DNA. *Genes Dev.* 18(13):1618–29

Erusalimsky JD, Kurz DJ. 2005. Cellular senescence in vivo: Its relevance in ageing and cardiovascular disease. *Exp. Gerontol.* 40(8–9):634–42

Evan GI, d'Adda di Fagagna F. 2009. Cellular senescence: hot or what? *Curr. Opin. Genet. Dev.* 19(1):25–31

Fagagna F d'Adda di, Reaper PM, Clay-Farrace L, Fiegler H, Carr P, et al. 2003. A DNA damage checkpoint response in telomere-initiated senescence. *Nature*. 426(6963):194–98

Fernandez-Capetillo O, Mahadevaiah SK, Celeste A, Romanienko PJ, Camerini-Otero RD, et al. 2003. H2AX is required for chromatin remodeling and inactivation of sex chromosomes in male mouse meiosis. *Dev. Cell*. 4(4):497–508

Ferrón S, Mira H, Franco S, Cano-Jaimez M, Bellmunt E, et al. 2004. Telomere shortening and chromosomal instability abrogates proliferation of adult but not embryonic neural stem cells. *Development*. 131(16):4059 LP-4070

Flynn RL, Centore RC, O/'Sullivan RJ, Rai R, Tse A, et al. 2011. TERRA and hnRNPA1 orchestrate an RPA-to-POT1 switch on telomeric single-stranded DNA. *Nature*. 471(7339):532–36

Francia S, Cabrini M, Matti V, Oldani A, d'Adda di Fagagna F. 2016. DICER, DROSHA and DNA damage response RNAs are necessary for the secondary recruitment of DNA damage response factors. *J. Cell Sci.* 129(7):1468–76

Francia S, Michelini F, Saxena A, Tang D, de Hoon M, et al. 2012. Site-specific DICER and DROSHA RNA products control the DNA-damage response. *Nature*. 488(7410):231–35

Frescas D, De Lange T. 2014. Binding of TPP1 protein to TIN2 protein is required for POT1a,b protein-mediated telomere protection. *J. Biol. Chem.* 289(35):24180–87

Fumagalli M, d'Adda di Fagagna F. 2009. SASPense and DDRama in cancer and ageing. *Nat. Cell Biol.* 11(8):921–23

Fumagalli M, Rossiello F, Clerici M, Barozzi S, Cittaro D, et al. 2012. Telomeric DNA damage is irreparable and causes persistent DNA-damage-response activation. *Nat. Cell Biol.* 14(4):355–65

Galbiati A, Beausèjour C, d'Adda di Fagagna F. 2017. A novel single-cell method provides direct evidence of persistent DNA damage in senescent cells and aged mammalian tissues. *Aging Cell*. 16(2):422–27

Gao M, Wei W, Li M-M, Wu Y-S, Ba Z, et al. 2014. Ago2 facilitates Rad51 recruitment and DNA double-strand break repair by homologous recombination. *Cell Res.* 24(5):532–41

Ghezraoui H, Piganeau M, Renouf B, Renaud J-B, Sallmyr A, et al. 2014. Chromosomal Translocations in Human Cells Are Generated by Canonical Nonhomologous End-Joining. *Mol. Cell*. 55(6):829–42

Glass CK, Rosenfeld MG. 2006. Regulated Transcription. . 8888(June):1798–1802

Glück S, Guey B, Gulen MF, Wolter K, Kang T-W, et al. 2017. Innate immune sensing of cytosolic chromatin fragments through cGAS promotes senescence. *Nat. Cell Biol.* 19(9):

Gobbini E, Cesena D, Galbiati A, Lockhart A, Longhese MP. 2013. Interplays between ATM/Tel1 and ATR/Mec1 in sensing and signaling DNA double-strand breaks. *DNA Repair (Amst).* 12(10):791–99

Gomez D, Shankman LS, Nguyen AT, Owens GK. 2013. Detection of histone modifications at specific gene loci in single cells in histological sections. *Nat. Methods*. 10(2):171–77

Gong Y, de Lange T. 2010. A Shld1-Controlled POT1a Provides Support for Repression of ATR Signaling at Telomeres through RPA Exclusion. *Mol. Cell*. 40(3):377–87

Gorbunova V, Seluanov A, Pereira-Smith OM. 2002. Expression of human telomerase (hTERT) does not prevent stress-induced senescence in normal human fibroblasts but protects the cells from stress-induced apoptosis and necrosis. *J. Biol. Chem.* 277(41):38540–49

Grandori C, Wu K, Fernandez P, Ngouenet C, Grim J, et al. 2003. Werner syndrome protein limits MYC-induced cellular senescence service Werner syndrome protein limits MYC-induced cellular senescence. *Genes Dev.* (206):1569–74

Grégoire M-C, Massonneau J, Leduc F, Arguin M, Brazeau M-A, Boissonneault G. 2016. Quantification and genome-wide mapping of DNA double-strand breaks. *DNA Repair (Amst).* 6–11

Greider CW, Blackburn EH. 1987. The telomere terminal transferase of tetrahymena is a ribonucleoprotein enzyme with two kinds of primer specificity. *Cell*. 51(6):887–98

Griffith JD, Comeau L, Rosenfield S, Stansel RM, Bianchi A, et al. 1999. Mammalian Telomeres End in a Large Duplex Loop. *Cell*. 97(4):503–14

Grolimund L, Aeby E, Hamelin R, Armand F, Chiappe D, et al. 2013. A quantitative telomeric chromatin isolation protocol identifies different telomeric states. . 4:2848

Haflick L, Moorhead P. 1961. The serial cultivation of human diploid cell strains. *Exp. Cell Res.* 25:585–621

Hanawalt PC, Spivak G. 2008. Transcription-coupled DNA repair: two decades of progress and surprises. *Nat. Rev. Mol. Cell Biol.* 9(12):958–70

Harding SM, Boiarsky JA, Greenberg RA. 2015. ATM Dependent Silencing Links Nucleolar Chromatin Reorganization to DNA Damage Recognition. *Cell Rep.* 13(2):251–59

Harley CB, Futcher AB, Greider CW. 1990. Telomeres shorten during ageing of human fibroblasts. *Nature*. 345(6274):458–60

Hartung ML, Gruber DC, Koch KN, Grüter L, Rehrauer H, et al. 2015. H. pylori-Induced DNA Strand Breaks Are Introduced by Nucleotide Excision Repair Endonucleases and Promote NF-$κ$B Target Gene Expression. *Cell Rep.* 13(1):70–79

Hayflick L. 1965. The limited in vitro lifetime of human diploid cell strains. *Exp. Cell Res.*

Helmrich A, Ballarino M, Nudler E, Tora L. 2013. Transcription-replication encounters, consequences and genomic instability. *Nat. Struct. Mol. Biol.* 20(4):412–18

Helmrich A, Ballarino M, Tora L. 2011. Collisions between replication and transcription complexes cause common fragile site instability at the longest human genes. *Mol. Cell*. 44(6):966–77

Hemann MT, Strong MA, Hao L-Y, Greider CW. 2001. The Shortest Telomere, Not Average Telomere Length, Is Critical for Cell Viability and Chromosome Stability. *Cell*. 107(1):67–77

Henson JD, Cao Y, Huschtscha LI, Chang AC, Au AYM, et al. 2009. DNA C-circles are specific and quantifiable markers of alternative-lengthening-of-telomeres activity. *Nat Biotech*. 27(12):1181–85

Herbig U, Ferreira M, Condel L, Carey D, Sedivy JM. 2006. Cellular Senescence in Aging Primates. *Science (80-.).* 311(5765):1257 LP-1257

Hernandez-Segura A, de Jong T V, Melov S, Guryev V, Campisi J, Demaria M. 2017. Unmasking Transcriptional Heterogeneity in Senescent Cells. *Curr. Biol.* 27(17):2652–2660.e4

Hewitt G, Jurk D, Marques FDM, Correia-Melo C, Hardy T, et al. 2012. Telomeres are favoured targets of a persistent DNA damage response in ageing and stress-induced senescence. *Nat. Commun.* 3:708

Heyer W-D, Ehmsen KT, Liu J. 2010. Regulation of homologous recombination in eukaryotes. *Annu. Rev. Genet.* 44:113–39

Ho J-N, Lee Y-H, Lee Y-D, Jun W-J, Kim H-K, et al. 2005. Inhibitory effect of Aucubin isolated from Eucommia ulmoides against UVB-induced matrix metalloproteinase-1 production in human skin fibroblasts. *Biosci. Biotechnol. Biochem.* 69(11):2227–31

Hoeijmakers JHJ. 2009. DNA damage, aging, and cancer. *N. Engl. J. Med.* 361(15):1475–85

Hoffman EA, McCulley A, Haarer B, Arnak R, Feng W. 2015. Break-seq reveals hydroxyurea-induced chromosome fragility as a result of unscheduled conflict between DNA replication and transcription. *Genome Res.* 25(3):402–12

Hu J, Meyers RM, Dong J, Panchakshari RA, Alt FW, Frock RL. 2016. Detecting DNA double-stranded breaks

in mammalian genomes by linear amplification-mediated high-throughput genome-wide translocation sequencing. *Nat Protoc.* 11(5):853–71

Hu J, Zhang Y, Zhao L, Frock RL, Du Z, et al. 2015. Chromosomal Loop Domains Direct the Recombination of Antigen Receptor Genes. *Cell*. 163(4):947–59

Iacovoni JS, Caron P, Lassadi I, Nicolas E, Massip L, et al. 2010. High-resolution profiling of γH2AX around DNA double strand breaks in the mammalian genome. *EMBO J.* 29(8):1446–57

Iannelli F, Galbiati A, Capozzo I, Nguyen Q, Magnuson B, et al. 2017. A damaged genome's transcriptional landscape through multilayered expression profiling around in situ -mapped DNA double-strand breaks. . (May):1–7

Ivanov A, Pawlikowski J, Manoharan I, van Tuyn J, Nelson DM, et al. 2013. Lysosome-mediated processing of chromatin in senescence. *J. Cell Biol.* 202(1):129–43

Izhar L, Adamson B, Ciccia A, Lewis J, Pontano-Vaites L, et al. 2015. A Systematic Analysis of Factors Localized to Damaged Chromatin Reveals PARP-Dependent Recruitment of Transcription Factors. *Cell Rep.* 11(9):1486–1500

Jackson SP, Bartek J. 2009. The DNA-damage response in human biology and disease. *Nature*. 461:1071–78

Janzen V, Forkert R, Fleming HE, Saito Y, Waring MT, et al. 2006. Stem-cell ageing modified by the cyclin-dependent kinase inhibitor p16INK4a. *Nature*. 443(7110):421–26

Jarvius M, Paulsson J, Weibrecht I, Leuchowius K-J, Andersson A-C, et al. 2007. In Situ Detection of Phosphorylated Platelet-derived Growth Factor Receptor Using a Generalized Proximity Ligation Method. *Mol. & Cell. Proteomics*. 6(9):1500–1509

Jaskelioff M, Muller FL, Paik J-H, Thomas E, Jiang S, et al. 2011. Telomerase reactivation reverses tissue degeneration in aged telomerase-deficient mice. *Nature*. 469(7328):102–6

Jeon OH, Kim C, Laberge R-M, Demaria M, Rathod S, et al. 2017. Local clearance of senescent cells attenuates the development of post-traumatic osteoarthritis and creates a pro-regenerative environment. *Nat Med*. advance online publication:

Joice R, Nilsson SK, Montgomery J, Dankwa S, Morahan B, et al. 2014. NIH Public Access. . 6(244):1–16

Jurk D, Wang C, Miwa S, Maddick M, Korolchuk V, et al. 2012. Postmitotic neurons develop a p21-dependent senescence-like phenotype driven by a DNA damage response. *Aging Cell*. 11(6):996–1004

Kaikkonen MU, Spann N, Heinz S, Romanoski CE, Karmel A, et al. 2014. Activation Is Coupled To Enhancer Transcription. . 51(3):310–25

Karlseder J, Hoke K, Mirzoeva OK, Bakkenist C, Kastan MB, et al. 2004. The Telomeric Protein TRF2 Binds the ATM Kinase and Can Inhibit the ATM-Dependent DNA Damage Response. *PLOS Biol.* 2(8):e240

Ke R, Nong RY, Fredriksson S, Landegren U, Nilsson M. 2013. Improving Precision of Proximity Ligation Assay by Amplified Single Molecule Detection. *PLoS One*. 8(7):1–5

Kim D, Bae S, Park J, Kim E, Kim S, et al. 2015a. Digenome-seq: genome-wide profiling of CRISPR-Cas9 off-target effects in human cells. *Nat Methods*. 12(3):237–43, 1 p following 243

Kim J, Sturgill D, Tran AD, Sinclair DA, Oberdoerffer P. 2015b. Controlled DNA double-strand break induction in mice reveals post-damage transcriptome stability. *Nucleic Acids Res.* 44(7):1–10

Kim J, Sturgill D, Tran AD, Sinclair DA, Oberdoerffer P. 2016. Controlled DNA double-strand break induction in mice reveals post-damage transcriptome stability. . 1–10

Kim JA, Kruhlak M, Dotiwala F, Nussenzweig A, Haber JE. 2007. Heterochromatin is refractory to γH2AX modification in yeast and mammals. *J. Cell Biol.* 178(2):209–18

Kim SH, Kaminker P, Campisi J, Kim SH, Kaminker P, Campisi J. 1999. TIN2, a new regulator of telomere

length in human cells. *Nat. Genet.* 23(4):405–12

Kramer KM, Brock JA, Bloom K, Moore JK, Haber JE. 1994. Two different types of double-strand breaks in Saccharomyces cerevisiae are repaired by similar RAD52-independent, nonhomologous recombination events. *Mol. Cell. Biol.* 14(2):1293–1301

Kruhlak M, Crouch EE, Orlov M, Montaño C, Gorski SA, et al. 2007. The ATM repair pathway inhibits RNA polymerase I transcription in response to chromosome breaks. *Nature*. 447(7145):730–34

Kunkel TA, Erie DA. 2005. Dna Mismatch Repair *. *Annu. Rev. Biochem*. 74:681–710

Laberge R-M, Awad P, Campisi J, Desprez P-Y. 2012. Epithelial-Mesenchymal Transition Induced by Senescent Fibroblasts. *Cancer Microenviron.* 5(1):39–44

Laberge R-M, Sun Y, Orjalo A V, Patil CK, Freund A, et al. 2015. MTOR regulates the pro-tumorigenic senescence-associated secretory phenotype by promoting IL1A translation. *Nat Cell Biol*. 17(8):1049–61

Lafon-Hughes L, Di Tomaso MV, Liddle P, Toledo A, Reyes-??balos AL, Folle GA. 2013. Preferential localization of γH2AX foci in euchromatin of retina rod cells after DNA damage induction. *Chromosom. Res.* 21:789–803

Larsson C, Grundberg I, Söderberg O, Nilsson M. 2010. In situ detection and genotyping of individual mRNA molecules. *Nat. Methods*. 7(5):395–97

Larsson C, Koch J, Nygren A, Janssen G, Raap AK, et al. 2004. In situ genotyping individual DNA molecules by target-primed rolling-circle amplification of padlock probes. *Nat. Methods*. 1(3):227–32

Lazzerini Denchi E, Attwooll C, Pasini D, Helin K. 2005. Deregulated E2F activity induces hyperplasia and senescence-like features in the mouse pituitary gland. *Mol. Cell. Biol.* 25(7):2660–72

Leduc F, Faucher D, Bikond Nkoma G, Grégoire M-C, Arguin M, et al. 2011. Genome-Wide Mapping of DNA Strand Breaks. *PLoS One*. 6(2):e17353

Lensing S V, Marsico G, Hänsel-Hertsch R, Lam EY, Tannahill D, Balasubramanian S. 2016. DSBCapture: in situ capture and sequencing of DNA breaks. *Nat. Methods*. (August):1–6

Leuchowius K-J, Clausson C-M, Grannas K, Erbilgin Y, Botling J, et al. 2013a. Parallel visualization of multiple protein complexes in individual cells in tumor tissue. *Mol. Cell. Proteomics*. 12(6):1563–71

Leuchowius K-J, Clausson C-M, Grannas K, Erbilgin Y, Botling J, et al. 2013b. Parallel visualization of multiple protein complexes in individual cells in tumor tissue. *Mol. Cell. Proteomics*. 12(6):1563–71

Li H, Handsaker B, Wysoker A, Fennell T, Ruan J, et al. 2009. The Sequence Alignment/Map format and SAMtools. *Bioinformatics*. 25(16):2078–79

Li JSZ, Miralles Fuste J, Simavorian T, Bartocci C, Tsai J, et al. 2017. TZAP: A telomere-associated protein involved in telomere length control. *Science (80-.).*

Lieber MR. 2010. The mechanism of double-strand DNA break repair by the nonhomologous DNA end joining pathway. *Annu. Rev. Biochem.* 79:181

Lindhal T, Barnes DE. 2000. Repair of endogenous DNA damage. *Cold Spring Harb. Symp. Quant. Biol.* 65:127–33

López-Otín C, Blasco MA, Partridge L, Serrano M, Kroemer G. 2013. The hallmarks of aging. *Cell*. 153(6):1194–1217

Lovejoy CA, Li W, Reisenweber S, Thongthip S, Bruno J, et al. 2012. Loss of ATRX, Genome Instability, and an Altered DNA Damage Response Are Hallmarks of the Alternative Lengthening of Telomeres Pathway. *PLOS Genet.* 8(7):e1002772

Lukas C, Falck J, Bartkova J, Bartek J, Lukas J. 2003. Distinct spatiotemporal dynamics of mammalian

checkpoint regulators induced by DNA damage. *Nat. Cell Biol.* 5(3):255–60

Lukas C, Melander F, Stucki M, Falck J, Bekker-Jensen S, et al. 2004. Mdc1 couples DNA double-strand break recognition by Nbs1 with its H2AX-dependent chromatin retention. *EMBO J.* 23(13):2674–83

Lukas J, Lukas C, Bartek J. 2011. More than just a focus: The chromatin response to DNA damage and its role in genome integrity maintenance. *Nat. Cell Biol.* 13(10):1161–69

Lustig AJ, Kurtz S, Shore D. 1990. Involvement of the silencer and UAS binding protein RAP1 in regulation of telomere length. *Science (80-.).* 250(4980):549 LP-553

Madabhushi R, Gao F, Pfenning AR, Pan L, Yamakawa S, et al. 2015. Activity-Induced DNA Breaks Govern the Expression of Neuronal Early-Response Genes. *Cell*. 161(7):1592–1605

Mailand N, Bekker-Jensen S, Faustrup H, Melander F, Bartek J, et al. 2007. RNF8 Ubiquitylates Histones at DNA Double-Strand Breaks and Promotes Assembly of Repair Proteins. *Cell*. 131(5):887–900

Mallette FA, Mattiroli F, Cui G, Young LC, Hendzel MJ, et al. 2012. RNF8- and RNF168-dependent degradation of KDM4A/JMJD2A triggers 53BP1 recruitment to DNA damage sites. *EMBO J.* 31(8):1865–78

Mao P, Liu J, Zhang Z, Zhang H, Liu H, et al. 2016. Homologous recombination-dependent repair of telomeric DSBs in proliferating human cells. . 7:12154

Marteijn J a, Lans H, Vermeulen W, Hoeijmakers JHJ. 2014. Understanding nucleotide excision repair and its roles in cancer and ageing. *Nat. Rev. Mol. Cell Biol.* 15(7):465–81

Martin JA, Buckwalter J. 2003. The role of chondrocyte senescence in the pathogenesis of osteoarthritis and in limiting cartilage repair. *J. Bone Jt. Surgery.*

Martin M, Terradas M, Illiakis G, Tusell L, Genesca A. 2009. Breaks Invisible to the DNA Damage Response Machinery Accumulate in ATM-Deficient Cells. *Genes. Chromosomes Cancer*. 48:745–59

Martinez P, Thanasoula M, Carlos AR, Gómez-López G, Tejera AM, et al. 2010. Mammalian Rap1 controls telomere function and gene expression through binding to telomeric and extratelomeric sites. *Nat. Cell Biol.* 12(8):768–80

Massip L, Caron P, Iacovoni JS, Trouche D, Legube G. 2010. Deciphering the chromatin landscape induced around DNA double strand breaks. *Cell Cycle*. 9(15):2963–72

Mastrocola AS, Kim SH, Trinh AT, Rodenkirch LA, Tibbetts RS. 2013. The RNA-binding protein fused in sarcoma (FUS) functions downstream of poly(ADP-ribose) polymerase (PARP) in response to DNA damage. *J. Biol. Chem.* 288(34):24731–41

Masutomi K, Possemato R, Wong JMY, Currier JL, Tothova Z, et al. 2005. The telomerase reverse transcriptase regulates chromatin state and DNA damage responses. *Proc. Natl. Acad. Sci.* 102(23):8222–27

McCool KW, Miyamoto S. 2012. DNA damage-dependent NF-κB activation: NEMO turns nuclear signaling inside out. *Immunol. Rev.* 246(1):311–26

Mcmanus K, Hendzel M. 2005. ATM-dependent DNA damage-independent mitotic phosphorylation of H2AX in normally growing mammalian cells. *Mol Cell Biol*

Meerang M, Ritz D, Paliwal S, Garajova Z, Bosshard M, et al. 2011. The ubiquitin-selective segregase VCP/p97 orchestrates the response to DNA double-strand breaks. *Nat. Cell Biol.* 13(11):1376–82

Mellon I, Bohr VA, Smith CA, Hanawalt PC. 1986. Preferential {DNA} repair of an active gene in human cells. *Proc. Natl. Acad. Sci. U. S. A.* 83(23):8878–82

Meng FL, Du Z, Federation A, Hu J, Wang Q, et al. 2014. Convergent transcription at intragenic super-enhancers targets AID-initiated genomic instability. *Cell*. 159(7):1538–48

Michaloglou C, Vredeveld LCW, Soengas MS, Denoyelle C, Kuilman T, et al. 2005. BRAFE600-associated senescence-like cell cycle arrest of human naevi. *Nature*. 436(7051):720–24

Mimitou EP, Symington LS. 2008. Sae2, Exo1 and Sgs1 collaborate in DNA double-strand break processing. *Nature*. 455(7214):770–74

Mirzayans R, Andrais B, Hansen G, Murray D. 2012. Role of p16 INK4A in replicative senescence and DNA damage-induced premature senescence in p53-deficient human cells. *Biochem. Res. Int.* 2012:

Mishina Y, Duguid EM, He C. 2006. Direct reversal of DNA alkylation damage. *Chem. Rev.* 106(2):215–32

Mitchell JR, Wood E, Collins K. 1999. A telomerase component is defective in the human disease dyskeratosis congenita. *Nature*. 402(6761):551–55

Molofsky A V, Slutsky SG, Joseph NM, He S, Pardal R, et al. 2006. Increasing p16INK4a expression decreases forebrain progenitors and neurogenesis during ageing. *Nature*. 443(7110):448–52

Monnat Jr RJ, Hackmann AFM, Cantrell MA. 1999. Generation of Highly Site-Specific DNA Double-Strand Breaks in Human Cells by the Homing Endonucleases I-PpoI and I-CreI. *Biochem. Biophys. Res. Commun.* 255(1):88–93

Morrison AJ, Highland J, Krogan NJ, Arbel-Eden A, Greenblatt JF, et al. 2004. INO80 and γ-H2AX interaction links ATP-dependent chromatin remodeling to DNA damage repair. *Cell*. 119(6):767–75

Mosteiro L, Pantoja C, Alcazar N, Marión RM, Chondronasiou D, et al. 2016. Tissue damage and senescence provide critical signals for cellular reprogramming in vivo. *Science (80-.).* 354(6315):aaf4445

Munoz-Espin D, Serrano M. 2014. Cellular senescence: from physiology to pathology. *Nat Rev Mol Cell Biol*. 15(7):482–96

Muñoz-Espìn D, Cañamero M, Maraver A, Gòmez-Lòpez G, Contreras J, et al. 2013. Programmed cell senescence during mammalian embryonic development. *Cell*. 155(5):

Narita M, Nũnez S, Heard E, Narita M, Lin AW, et al. 2003. Rb-mediated heterochromatin formation and silencing of E2F target genes during cellular senescence. *Cell*. 113(6):703–16

Nergadze SG, Farnung BO, Wischnewski H, Khoriauli L, Vitelli V, et al. 2009. CpG-island promoters drive transcription of human telomeres. *RNA*. 15(12):2186–94

Noureddine H, Gary-Bobo G, Alifano M, Marcos E, Saker M, et al. 2011. Pulmonary artery smooth muscle cell senescence is a pathogenic mechanism for pulmonary hypertension in chronic lung disease. *Circ. Res.* 109(5):543–53

O'Sullivan RJ, Karlseder J. 2010. Telomeres: protecting chromosomes against genome instability. *Nat. Rev. Mol. Cell Biol.* 11(mARCH):

Okamoto K, Bartocci C, Ouzounov I, K.Diedrich J, Ill JRY, Denchi EL. 2013. A two-step mechanism for TRF2-mediated chromosome end protection. *Nature*. 494(7438):502–5

Olive PL, Banath JP. 2006. The comet assay: a method to measure DNA damage in individual cells. *Nat. Protoc.* 1(1):23–29

Olive PL, Wlodek D, Banáth JP. 1991. DNA Double-Strand Breaks Measured in Individual Cells Subjected to Gel Electrophoresis DNA Double-Strand Breaks Measured in Individual Cells Subjected to Gel. . 4671–76

Ostuni R, Piccolo V, Barozzi I, Polletti S, Termanini A, et al. 2013. Latent enhancers activated by stimulation in differentiated cells. *Cell*. 152(1–2):157–71

Palm W, de Lange T. 2008. How Shelterin Protects Mammalian Telomeres. *Annu. Rev. Genet.* 42(1):301–34

Panier S, Boulton SJ. 2014. Double-strand break repair: 53BP1 comes into focus. *Nat. Rev. Mol. Cell Biol.* 15:7–18

Panier S, Ichijima Y, Fradet-Turcotte A, Leung CCY, Kaustov L, et al. 2012. Tandem Protein Interaction Modules Organize the Ubiquitin-Dependent Response to DNA Double-Strand Breaks. *Mol. Cell*. 47(3):383–95

Pankotai T, Bonhomme C, Chen D, Soutoglou E. 2012. DNAPKcs-dependent arrest of RNA polymerase II transcription in the presence of DNA breaks. *Nat. Struct. Mol. Biol.* 19(3):276–82

Park J-I, Venteicher AS, Hong JY, Choi J, Jun S, et al. 2009. Telomerase modulates Wnt signalling by association with target gene chromatin. *Nature*. 460(7251):66–72

Parrilla-Castellar ER, Arlander SJH, Karnitz L. 2004. Dial 9–1–1 for DNA damage: the Rad9–Hus1–Rad1 (9–1–1) clamp complex. *DNA Repair (Amst).* 3(8–9):1009–14

Parrinello S, Samper E, Krtolica A, Goldstein J, Melov S, Campisi J. 2003. Oxygen sensitivity severely limits the replicative lifespan of murine fibroblasts. *Nat Cell Biol*. 5(8):741–47

Passos JF, Nelson G, Wang C, Richter T, Simillion C, et al. 2010. Feedback between p21 and reactive oxygen production is necessary for cell senescence. *Mol. Syst. Biol.* 6(347):1–14

Paulsen MT, Veloso A, Prasad J, Bedi K, Ljungman EA, et al. 2014. Use of Bru-Seq and BruChase-Seq for genome-wide assessment of the synthesis and stability of RNA. *Methods*. 67(1):45–54

Periyasamy M, Patel H, Lai CF, Nguyen VTM, Nevedomskaya E, et al. 2015. APOBEC3B-Mediated Cytidine Deamination Is Required for Estrogen Receptor Action in Breast Cancer. *Cell Rep.* 13(1):108–21

Petruk S, Fenstermaker TK, Black KL, Brock HW, Mazo A. 2016. Detection of RNA-DNA association by a proximity ligation-based method. *Sci. Rep.* 6:27313

Petruska J, Arnheim N, Goodman MF. 1996. Stability of intrastrand hairpin structures formed by the CAG/CTG class of DNA triplet repeats associated with neurological diseases. *Nucleic Acids Res.* 24(11):1992

Polo SE, Jackson SP. 2011. Dynamics of DNA damage response proteins at DNA breaks: a focus on protein modifications. *Genes Dev.* 25(5):409–33

Porro A, Feuerhahn S, Delafontaine J, Riethman H, Rougemont J, Lingner J. 2014. Functional characterization of the TERRA transcriptome at damaged telomeres. *Nat. Commun.* 5:5379

Porro a, Feuerhahn S, Reichenbach P, Lingner J. 2010. Molecular dissection of telomeric repeat-containing RNA biogenesis unveils the presence of distinct and multiple regulatory pathways. *Mol Cell Biol*. 30(20):4808–17

Price JS, Waters JG, Darrah C, Pennington C, Edwards DR, et al. 2002. The role of chondrocyte senescence in osteoarthritis. *Aging Cell*. 1(1):57–65

Puc J, Kozbial P, Aggarwal AK, Rosenfeld MG, Puc J, et al. 2015a. Ligand-Dependent Enhancer Activation Regulated by Topoisomerase-I Activity Article Ligand-Dependent Enhancer Activation Regulated by Topoisomerase-I Activity. *Cell*. 160(3):367–80

Puc J, Kozbial P, Aggarwal AK, Rosenfeld MG, Puc J, et al. 2015b. Ligand-Dependent Enhancer Activation Regulated by Topoisomerase-I Activity. *Cell*. 160(3):367–80

Quinlan AR, Hall IM. 2010. BEDTools: A flexible suite of utilities for comparing genomic features. *Bioinformatics*. 26(6):841–42

Rassoolzadeh H, Coucoravas C, Farnebo M. 2015. The proximity ligation assay reveals that at DNA double-strand breaks WRAP53β associates with γH2AX and controls interactions between RNF8 and MDC1. *Nucleus*. 6(5):417–24

Reaban ME, Lebowitz J, Griffin JA. 1994. Transcription induces the formation of a stable RNA·DNA hybrid in the immunoglobulin α switch region. *J. Biol. Chem.* 269(34):21850–57

Redon S, Reichenbach P, Lingner J. 2010. The non-coding RNA TERRA is a natural ligand and direct inhibitor of human telomerase. *Nucleic Acids Res.* 38(17):5797–5806

Riley T, Sontag E, Chen P, Levine A. 2008. Transcriptional control of human p53-regulated genes. *Nat. Rev. Mol. Cell Biol.* 9:402–12

Rodier F, Coppé J-P, Patil CK, Hoeijmakers WAM, Muñoz DP, et al. 2009. Persistent DNA damage signalling triggers senescence-associated inflammatory cytokine secretion. *Nat. Cell Biol.* 11(8):973–79

Rodier F, Muñoz DP, Teachenor R, Chu V, Le O, et al. 2011. DNA-SCARS: distinct nuclear structures that sustain damage-induced senescence growth arrest and inflammatory cytokine secretion. *J. Cell Sci.* 124(Pt 1):68–81

Rogakou EP. 1998. DNA Double-stranded Breaks Induce Histone H2AX Phosphorylation on Serine 139. *J. Biol. Chem.* 273(10):5858–68

Rose JC, Stephany JJ, Valente WJ, Trevillian BM, Dang H V, et al. 2017. Rapidly inducible Cas9 and DSB-ddPCR to probe editing kinetics. *Nat Meth*. 14(9):891–96

Rossiello F, Aguado J, Sepe S, Iannelli F, Nguyen Q, et al. 2017. DNA damage response inhibition at dysfunctional telomeres by modulation of telomeric DNA damage response RNAs. *Nat. Commun.* 8(May 2016):13980

Rossiello F, Herbig U, Longhese MP, Fumagalli M, d'Adda di Fagagna F. 2014. Irreparable telomeric DNA damage and persistent DDR signalling as a shared causative mechanism of cellular senescence and ageing. *Curr. Opin. Genet. Dev.* 26C:89–95

Rudolph KL, Chang S, Lee H-W, Blasco M, Gottlieb GJ, et al. 1999. Longevity, Stress Response, and Cancer in Aging Telomerase-Deficient Mice. *Cell*. 96(5):701–12

Rybak P, Hoang A, Bujnowicz L, Bernas T, Zarębski M, et al. 2016a. Low level phosphorylation of histone H2AX on serine 139 (γH2AX) is not associated with DNA double-strand breaks. *Oncotarget*. 139(31):1–7

Rybak P, Hoang A, Bujnowicz L, Bernas T, Zarębski M, et al. 2016b. Low level phosphorylation of histone H2AX on serine 139 (γH2AX) is not associated with DNA double-strand breaks. . 139:

Sadaie M, Salama R, Carroll T, Tomimatsu K, Chandra T, et al. 2013. Redistribution of the Lamin B1 genomic binding profile affects rearrangement of heterochromatic domains and SAHF formation during senescence. *Genes Dev.* 27(16):1800–1808

San Filippo J, Sung P, Klein H. 2008. Mechanism of eukaryotic homologous recombination. *Annu. Rev. Biochem.* 77:229–57

Sancar A, Lindsey-Boltz LA, Ünsal-Kaçmaz K, Linn S. 2004. Molecular Mechanisms of Mammalian DNA Repair and the DNA Damage Checkpoints. *Annu. Rev. Biochem.* 73(1):39–85

Saretzki G, Murphy MP, Zglinicki T Von. 2003. MitoQ counteracts telomere shortening and elongates lifespan of fibroblasts under mild oxidative stress. *Aging Cell*. 2(2):141–43

Sartori AA, Lukas C, Coates J, Mistrik M, Fu S, et al. 2007. Human CtIP promotes DNA end resection. *Nature*. 450(7169):509–14

Satyanarayana A, Greenberg RA, Schaetzlein S, Buer J, Masutomi K, et al. 2004. Mitogen Stimulation Cooperates with Telomere Shortening To Activate DNA Damage Responses and Senescence Signaling Mitogen Stimulation Cooperates with Telomere Shortening To Activate DNA Damage Responses and Senescence Signaling. . 24(12):5459–74

Schafer MJ, White TA, Iijima K, Haak AJ, Ligresti G, et al. 2017. Cellular senescence mediates fibrotic pulmonary disease. *Nat. Commun.* 8:14532

Schmitt CA. 2003. Senescence, apoptosis and therapy — cutting the lifelines of cancer. *Nat Rev Cancer*. 3(4):286–95

Schneider L, Fumagalli M, d'Adda di Fagagna F. 2012. Terminally differentiated astrocytes lack DNA damage response signaling and are radioresistant but retain DNA repair proficiency. *Cell Death Differ.* 19(4):582–91

Schoeftner S, Blasco MA. 2008. Developmentally regulated transcription of mammalian telomeres by DNA-dependent RNA polymerase II. *Nat Cell Biol*. 10(2):228–36

Schwer B, Wei P-C, Chang AN, Kao J, Du Z, et al. 2016. Transcription-associated processes cause DNA double-strand breaks and translocations in neural stem/progenitor cells. *Proc. Natl. Acad. Sci.* 113(8):201525564

Sedelnikova O a, Horikawa I, Zimonjic DB, Popescu NC, Bonner WM, Barrett JC. 2004. Senescing human cells and ageing mice accumulate DNA lesions with unrepairable double-strand breaks. *Nat. Cell Biol.* 6(2):168–70

Serrano M, Lin AW, McCurrach ME, Beach D, Lowe SW. 1997. Oncogenic ras provokes premature cell senescence associated with accumulation of p53 and p16(INK4a). *Cell*. 88:593–602

Sfeir A, de Lange T. 2012. Removal of Shelterin Reveals the Telomere End-Protection Problem. *Science (80-.).* 336(6081):593 LP-597

Sfeir A, Kosiyatrakul ST, Hockemeyer D, MacRae SL, Karlseder J, et al. 2009. Mammalian Telomeres Resemble Fragile Sites and Require TRF1 for Efficient Replication. *Cell*. 138(1):90–103

Shanbhag NM, Rafalska-Metcalf IU, Balane-Bolivar C, Janicki SM, Greenberg RA. 2010. ATM-Dependent chromatin changes silence transcription in cis to dna double-strand breaks. *Cell*. 141(6):970–81

Shandilya J, Roberts SGE. 2012. The transcription cycle in eukaryotes: From productive initiation to RNA polymerase II recycling. *Biochim. Biophys. Acta - Gene Regul. Mech.* 1819(5):391–400

Sharma V, Misteli T. 2013. Non-coding RNAs in DNA damage and repair. *FEBS Lett.* 587(13):1832–39

Shi L, Tang X, Tang G. 2016. GUIDE-Seq to Detect Genome-wide Double-Stranded Breaks in Plants. *Trends Plant Sci.* 21(10):815–18

Shiloh Y. 2006. The ATM-mediated DNA-damage response: taking shape

Shiraki T, Kondo S, Katayama S, Waki K, Kasukawa T, et al. 2003. Cap analysis gene expression for high-throughput analysis of transcriptional starting point and identification of promoter usage. *Proc. Natl. Acad. Sci. U. S. A.* 100(26):15776–81

Shmuel a. 1992. Identification of Programmed Cell Death In Situ. *Cell*. 119(3):493–501

Smith S, de Lange T. 2000. Tankyrase promotes telomere elongation in human cells. *Curr. Biol.* 10(20):1299–1302

Smogorzewska A, van Steensel B, Bianchi A, Oelmann S, Schaefer MR, et al. 2000. Control of human telomere length by TRF1 and TRF2. *Mol Cell Biol*. 20(5):1659–68

Söderberg O, Gullberg M, Jarvius M, Ridderstråle K, Leuchowius K-J, et al. 2006. Direct observation of individual endogenous protein complexes in situ by proximity ligation. *Nat. Methods*. 3(12):995–1000

Soto-Gamez A, Demaria M. 2017. Therapeutic interventions for aging: the case of cellular senescence. *Drug Discov. Today*. 22(5):786–95

Spears M, Taylor KJ, Munro AF, Cunningham CA, Mallon EA, et al. 2012. In situ detection of HER2:HER2 and HER2:HER3 protein-protein interactions demonstrates prognostic significance in early breast cancer. *Breast Cancer Res. Treat.* 132(2):463–70

Spycher C, Miller ES, Townsend K, Pavic L, Morrice NA, et al. 2008. Constitutive phosphorylation of MDC1

physically links the MRE11-RAD50-NBS1 complex to damaged chromatin. *J. Cell Biol.* 181(2):227–40

Sulli G, Di Micco R, d'Adda di Fagagna F. 2012. Crosstalk between chromatin state and DNA damage response in cellular senescence and cancer. *Nat. Rev. Cancer*. 12(10):709–20

Sun Y, Jiang X, Chen S, Fernandes N, Price BD. 2005. A role for the Tip60 histone acetyltransferase in the acetylation and activation of ATM. *Proc. Natl. Acad. Sci. U. S. A.* 102(37):13182–87

Svejstrup JQ. 2010. The interface between transcription and mechanisms maintaining genome integrity. *Trends Biochem. Sci.* 35(6):333–38

Symington LS, Gautier J. 2011. Double-Strand Break End Resection and Repair Pathway Choice. *Annu. Rev. Genet.* 45(1):247–71

Takai H, Smogorzewska A, de Lange T. 2003. DNA Damage Foci at Dysfunctional Telomeres. *Curr. Biol.* 13(17):1549–56

Tomás-Loba A, Flores I, Fernández-Marcos PJ, Cayuela ML, Maraver A, et al. 2008. Telomerase Reverse Transcriptase Delays Aging in Cancer-Resistant Mice. *Cell*. 135(4):609–22

Toussaint O, Medrano EE, von Zglinicki T. 2000. Cellular and molecular mechanisms of stress-induced premature senescence (SIPS) of human diploid fibroblasts and melanocytes. *Exp. Gerontol.* 35(8):927–45

Tsai SQ, Zheng Z, Nguyen NT, Liebers M, Topkar V V, et al. 2014. GUIDE-seq enables genome-wide profiling of off-target cleavage by CRISPR-Cas nucleases. *Nat. Biotechnol.* 33(2):187–97

Tu WZ, Li B, Huang B, Wang Y, Liu XD, et al. 2013. γH2AX foci formation in the absence of DNA damage: Mitotic H2AX phosphorylation is mediated by the DNA-PKcs/CHK2 pathway. *FEBS Lett.* 587(21):3437–43

Tümpel S, Rudolph KL. 2012. The role of telomere shortening in somatic stem cells and tissue aging: Lessons from telomerase model systems. *Ann. N. Y. Acad. Sci.* 1266(1):28–39

van Steensel B, de Lange T. 1997. Control of telomere length by the human telomeric protein TRF1. *Nature*. 385(6618):740–43

van Steensel B, Smogorzewska A, de Lange T. 1998. TRF2 Protects Human Telomeres from End-to-End Fusions. *Cell*. 92(3):401–13

Venteicher AS, Abreu EB, Meng Z, McCann KE, Terns RM, et al. 2009. A Human Telomerase Holoenzyme Protein Required for Cajal Body Localization and Telomere Synthesis. *Science (80-.).* 323(5914):644 LP-648

Veres A, Gosis BS, Ding Q, Collins R, Ragavendran A, et al. 2014. Low incidence of Off-target mutations in individual CRISPR-Cas9 and TALEN targeted human stem cell clones detected by whole-genome sequencing. *Cell Stem Cell*. 15(1):27–30

Vitelli V, Galbiati A, Iannelli F, Pessina F, Sharma S, d'Adda di Fagagna F. 2017. Recent Advancements in DNA Damage Transcription Crosstalk and High-Resolution Mapping of DNA Breaks. *Annu. Rev. Genomics Hum. Genet.* 18:87–113

von Zglinicki T, Saretzki G, Döcke W, Lotze C. 1995. Mild Hyperoxia Shortens Telomeres and Inhibits Proliferation of Fibroblasts: A Model for Senescence? *Exp. Cell Res.* 220(1):186–93

Wang B, Elledge SJ. 2007. Ubc13/Rnf8 ubiquitin ligases control foci formation of the Rap80/Abraxas/Brca1/Brcc36 complex in response to DNA damage. *Proc. Natl. Acad. Sci. U. S. A.* 104(52):20759–63

Wang W-Y, Pan L, Su SC, Quinn EJ, Sasaki M, et al. 2013. Interaction of FUS and HDAC1 regulates DNA damage response and repair in neurons. *Nat. Neurosci.* 16(10):1383–91

Wang X, Chien Y, Scuoppo C, Wang X, Fang X, et al. 2011. Control of the senescence-associated secretory phenotype by NF-kappaB promotes senescence and enhances Control of the senescence-associated secretory phenotype by NF- k B promotes senescence and enhances chemosensitivi. *Genes Dev.* (February):2125–36

Wang X, Wang Y, Wu X, Wang J, Wang Y, et al. 2015. Unbiased detection of off-target cleavage by CRISPR-Cas9 and TALENs using integrase-defective lentiviral vectors. *Nat. Biotechnol.* 33(2):175–78

Wang Z, Gerstein M, Snyder M. 2009. RNA-Seq: a revolutionary tool for transcriptomics. *Nat. Rev. Genet.* 10(1):57–63

Waters LS, Minesinger BK, Wiltrout ME, D'Souza S, Woodruff R V, Walker GC. 2009. Eukaryotic translesion polymerases and their roles and regulation in DNA damage tolerance. *Microbiol. Mol. Biol. Rev.* 73(1):134–54

Wei W, Ba Z, Gao M, Wu Y, Ma Y, et al. 2012. A role for small RNAs in DNA double-strand break repair. *Cell*. 149(1):101–12

White CI, Haber JE. 1990. Intermediates of recombination during mating type switching in Saccharomyces cerevisiae. *EMBO J.* 9(3):663–73

White RR, Milholland B, de Bruin A, Curran S, Laberge R-M, et al. 2015. Controlled induction of DNA double-strand breaks in the mouse liver induces features of tissue ageing. *Nat. Commun.* 6:6790

Wright WE, Piatyszek M, Rainey W, Byrd W, Shay JW. 1996. Telomerase activity in human germline and embryonic tissues and cells. *Dev. Genet.* 18(2):173–79

Wu P, Takai H, de Lange T. 2012. Telomeric 3′ overhangs derive from resection by Exo1 and Apollo and fill-in by POT1b-associated CST. *Cell*. 150(1):39–52

Yan WX, Mirzazadeh R, Garnerone S, Scott DA, Schneider MW, et al. 2016. BLISS: quantitative and versatile genome-wide profiling of DNA breaks in situ. *bioRxiv*

Yan WX, Mirzazadeh R, Garnerone S, Scott D, Schneider MW, et al. 2017. BLISS is a versatile and quantitative method for genome-wide profiling of DNA double-strand breaks. *Nat. Commun.* 8(May):15058

Yarden RI, Pardo-Reoyo S, Sgagias M, Cowan KH, Brody LC. 2002. BRCA1 regulates the G2/M checkpoint by activating Chk1 kinase upon DNA damage. *Nat. Genet.* 30(3):285–89

Ye JZS, Donigian JR, Van Overbeek M, Loayza D, Luo Y, et al. 2004a. TIN2 binds TRF1 and TRF2 simultaneously and stabilizes the TRF2 complex on telomeres. *J. Biol. Chem.* 279(45):47264–71

Ye JZS, Hockemeyer D, Krutchinsky AN, Loayza D, Hooper SM, et al. 2004b. POT1-interaction protein PIP1: A telomere length regulator that recruits POT1 to the TIN2/TRF1 complex. *Genes Dev.* 18(14):1649–54

Yun MH, Davaapil H, Brockes JP. 2015. Recurrent turnover of senescent cells during regeneration of a complex structure. *Elife*. 4(MAY):1–16

Zhang R, Chen W, Adams PD. 2007. Molecular Dissection of Formation of Senescence-Associated Heterochromatin Foci. *Mol. Cell. Biol.* 27(6):2343–58

Zhao X-N, Usdin K. 2015. The repeat expansion diseases: the dark side of DNA repair. *DNA Repair (Amst).* 32:96–105

Zhu Y, Dojer N, Biernacka A, Pardo B, Forey R, et al. 2017. Quantitative DSB sequencing (qDSB-Seq): a method for genome-wide accurate estimation of absolute DNA double-strand break frequencies per cell

Zhu Y, Tchkonia T, Pirtskhalava T, Gower AC, Ding H, et al. 2015. The Achilles' heel of senescent cells: from transcriptome to senolytic drugs. *Aging Cell*. 14(4):644–58

Acknowledgments

I would like to thank several people that supported me during my PhD.

My supervisor, Dr. Fabrizio d'Adda di Fagagna, for giving me the possibility to join his group, and for his support throughout my PhD.

Prof. Gioacchino Natoli and Prof. Jan Hoejimakers, for taking time out from their busy schedules to serve as my internal and external co-supervisors, respectively.

Dr Joao Passos and Dr. Vincenzo Costanzo, for accepting to be my examiners and for reading my thesis.

The IFOM-IEO-Campus facilities, in particular the Genomics, Cell Culture, and the Imaging, and the Kitchen units, for their important help in my work.

The FDA people for making work time a fun time, but also for providing good advices and support when needed.

iFabio, for the great help he gave me at the beginning and throughout all my PhD, and for always being ready to give me a useful advice on any matter I asked.

All the new friends I have met during my PhD, in particular Corey and Valentina, and also the ones that were not here, but kept a connection with me, for making these years a lot of fun.

Giusy, for supporting me when I didn't ask for it, and for being an inspiration of how a passionate researcher is.

Il ringraziamento più sentito va alla mia famiglia, per avermi dato la possibilità di arrivare fin qui, dandomi un punto di riferimento solido a cui appoggiarmi e dandomi la serenità per affrontare tutte le piccole sfide di questo percorso.